Experiments and Analysis on Wood Gasification in an Open Top Downdraft Gasifier

A Thesis submitted for the Degree of
Doctor of Philosophy
in the Faculty of Engineering

by

Sadhan Mahapatra

Centre for Sustainable Technologies
Indian Institute of Science
Bangalore, India

March 2016

dedicated
to all my teachers
from
School,
Visva-Bharati,
Jadavpur University and
Indian Institute of Science

Acknowledgement

"Gratitude is the memory of the heart"

-Jean Massieu

At the outset, I would like to acknowledge Tezpur University for permitting me to take up my PhD research at Indian Institute of Science. I am indebted to Prof. S Dasappa for being kind enough to take me as a student at Centre for Sustainable Technologies, imparting his understanding, knowledge and guiding me in biomass gasification research. He encouraged me to complete my work during the most critical phase of my life and provided excellent facilities at Combustion, Gasification and Propulsion Laboratory of the Institute. I will cherish the freedom I had working at the laboratory and it is an experience for lifetime. I am also indebted to late Prof. P J Paul, who was also one of my supervisor and his suggestions towards the analysis of results were of great help.

I would like to take the opportunity to thank the past and present Chairman and faculty members of the Centre for Sustainable Technologies for their constant support and encouragement during my stay at the Centre.

I wish to acknowledge the support received from HV Sridhar, G Sridhar, V Gayathri, DN Subbukrishna and KC Suresh during my stay at laboratory, with whom I had many fruitful discussions, academic and non-academic. I would like to acknowledge technicians Mallaiah, Anil, Shankar, Anantha and Channakeshava who were an essential support during the experimental work. I have received help in many ways from SD Ravi, Srinath and all other project assistants at the laboratory, which I would like to acknowledge greatly. My special thanks to all my friends Asha, Shiva, Sarita, Snehesh, Sandeep, Anand, Arvinda, Abhishek, Varun, Gnanendra, Ashutosh, Ambrish, Ravi, Rakesh and above all, to all my students of Tezpur University at IISc/Bangalore. I thank them for scientific and non-scientific discussion, which helped me in

becoming a well informed person. Tea sessions at the canteen of the Institute and the outing on the weekends with them are some of the most memorable times spent at the Institute. Special thanks to Snehesh for all the logistic support and Sandeep for patient listening of all kinds of wisdom. Late night long discussions, in the Students' room/Tea Board have been an enlightening experience. Whether it was the discussion in itself that was enlightening or was the ambience, will forever remains a mystery. I had the privilege of having many memorable interactions with all the friends of CST and CGPL.

Special thanks to my friends Debashish, Gazi, Chandan, Bhim, Rabin, Wasefer, Sonatan, Sudipa; Dr Biren Das, and other colleagues at Tezpur, my students Indra, Manoj, Pallabi, Bhaskar and all others. Special mention JKS, Boby, Babu and my family members for all kinds of support and encouragement for so long years. I would also like to thank all those who have directly or indirectly helped me in these long years and provided moral support to complete the work in a lively and cheerful manner.

Publications

- **Sadhan Mahapatra, Sandeep Kumar, S Dasappa**. Gasification of wood particles in a co-current packed bed: Experiments and model analysis. *Fuel Processing Technology* 2016; 145: 76-89.

- **Sadhan Mahapatra, S Dasappa**. Experiments and analysis of propagation front under gasification regimes in a packed bed. *Fuel Processing Technology* 2014; 121: 83-90.

- **Sadhan Mahapatra, S Dasappa**. Influence of surface area to volume ratio of fuel particles on gasification process in a fixed bed. *Energy for Sustainable Development* 2014; 19: 122-129.

- **Sadhan Mahapatra, S Dasappa**. Rural electrification: optimising the choice between decentralised renewable energy sources and grid extension. *Energy for Sustainable Development* 2012; 16 (2): 146-154.

- **Sadhan Mahapatra, HN Chanakya, S Dasappa**. Evaluation of various energy devices for domestic lighting in India: technology, economics and CO_2 emissions. *Energy for Sustainable Development* 2009; 13(4): 271-279.

- **Sadhan Mahapatra, S Dasappa**. Off-grid biomass gasification based rural electrification in lieu of grid extension. Proc. *19th European Biomass Conference and Exhibition*, pp 2203-2208, Berlin, Germany, 6-10 June 2011.

Table of Contents

Chapter II Experiments: Materials and methods

Chapter III Influence of particle size and residence time on gasification process

Chapter IV Propagation front under gasification regimes in packed bed

Chapter V Mathematical model for packed bed analysis

Chapter VI Results and discussion on Packed bed analysis

Chapter VII Conclusions and future work

Appendix A   Access to electricity through biomass gasification system

References

List of Figures

List of Tables

Nomenclature

Capital Letters

A_c	cross-sectional area of the reactor, m^2
A_s	particle surface area, m^2
A_{sr}	surface area of the reactor, m^2
C_P	specific heat, kJ/(kg-K)
D	diffusivity, m^2/s
D_e	effective diffusivity, m^2/s
D_p	particle diameter, mm
H	enthalpy of reaction, kJ/kg
H_C	enthalpy of carbon (summation of $C+CO_2$, $C+O_2$ and $C+H_2O$ reactions), kJ/kg
H_R	heat generation due to reaction per unit volume due to gas phase reaction, kJ/m^3
H_R''	radiative heat transfer, kJ/m^2
K_D	mass transfer coefficient, kg/s
L	length of the reactor, m
M_g	molecular mass of the mixture of gases, kg/kmol
M_i	molecular mass of the ith species, kg/kmol
Q	total radiative flux incident on the surface, W/m^2
T	temperature, K
T_{gas}	gas temperature, K
T_∞	ambient temperature, K
T_S	particle surface temperature, K
T_j	temperature of latitude section, K
V	volume of the biomass/char particle, m^3
V_a	air flow rate, m^3/s
Y_i	mass fraction of i_{th} species
$Y_{i,s}$	i_{th} species concentration at gas film surrounded the particle surface

Lowercase Letters

f_j	view factor
h	heat loss coefficient, $W/(m^2 K)$
h_l	reactor heat loss coefficient, $W/(m^2 K)$
t	time , s
$\dot{m}$	mass flow rate, kg/s
$\dot{m}_p$	gasification rate of one particle, kg/s
$\dot{m}''$	mass flux, kg/m^2 s
n	number of particles per unit volume
r	particle radius, m

r_p	pore radius of wood char, m
v_{pm}	flame front propagation velocity, mm/s
v	fluid velocity, m/s

Greek symbols

α	absorptivity (or emissivity) of the surface
ϵ	particle porosity
ϵ_b	bed porosity
κ	thermal conductivity, W/(m-K)
$\dot{\varpi}_i'''$	volumetric reaction rate of i_{th} specie, kg/(m^3-s)
$\dot{\varpi}_c'''$	volumetric char reaction rate, kg/(m^3-s)
ρ	density, kg/m^3
$\bar{\rho}$	average particle density, kg/m^3
ρ_a	density of air, kg/m^3
ρ_c	density of wood char, kg/m^3
σ	Stefan–Boltzmann constant, W/m^2 K^4
τ	tortuosity factor
μ	air viscosity, Pa-s
Δt	time required to reach the reference temperature between two thermocouples, s
Δx	distance between two thermocouples, mm

Subscripts

i	Species CO, CO_2, H_2, H_2O and N_2
s	Surface
∞	Free stream

Abstract

The thesis, through experimental and numerical investigations reports on the work related to packed bed reactors in co-current configuration for biomass gasification. This study has extensively focused on the gasification operating regimes and addressing the issues of presence of tar, an undesirable component for engine application.

Systematically, the influence of fuel properties on the gasification process has been studied using single particle analysis and also in packed bed reactors. Studies related to the effect of fuel properties - size, surface area volume ratio and density on the reactor performance are addressed. The influence of these parameters on the propagation rate which indirectly influences the residence time, tar generation, gas compositions is explicitly elucidated. Most of the reported work in literature primarily focuses on counter-current configurations and analysis on propagation flame front/ignition mass flux and temperature profiles mostly under the combustion regime. In this work, flame propagation front movement, bed movement and effective movement for a co-current packed bed reactor of different reactor capacities and a generalized approach towards establishing *'effective propagation rate'* has been proposed. The work also reports on the importance of particle size and sharing of air from the top and through nozzles on tar generation in the open top down draft reactor configuration.

Firstly, pyrolysis, an important component of the thermo-chemical conversion process has been studied using the flaming time for different biomass samples having varying size, shape and density. The elaborate experiments on the single particle study provides an insight into the reasons for high tar generation for wood flakes/coconut shells and also identifies the importance of the fuel particle geometry related to surface area and volume ratio. Effect of density by comparing the flaming rate of wood flakes and coconut shells with the wood sphere for an equivalent

diameter is highlighted. It is observed that the tar level in the raw gas is about 80% higher in the case of wood flakes and similar values for coconut shells compared with wood pieces. The analysis suggests that the time for pyrolysis is lower with a higher surface area particle and is subjected to nearly fast pyrolysis process resulting in higher tar fraction with low char yield. Similarly, time for pyrolysis increases with density as observed from the experimental measurements by using coconut shells and wood flakes and concludes the influence on the performance of packed bed reactors. Studies on co-current reactor under various operating conditions from closed top reactor to open top reburn configuration suggests improved residence time reduces tar generation. This study establishes, increased residence time with staged air flow has a better control on residence time and yields lower tar in the raw gas.

Studies on the influence of air mass flux on the propagation rate, peak temperature, and gas quality, establishes the need to consider bed movement in the case of co-current packed bed reactor. It is also observed that flame front propagation rate initially increases as the air mass flux is increased, reaches a peak and subsequently decreases. With increase in air mass flux, fuel consumption increases and thereby the bed movement. The importance of bed movement and its effect on the propagation front movement has been established. To account for variation in the fuel density, normalized propagation rate or the ignition mass flux is a better way to present the result. The peak flame front propagation rates are 0.089 mm/s for 10 % moist wood at an air mas flux of 0.130 kg/m^2-s and while 0.095 mm/s for bone-dry wood at an air mass flux of 0.134 kg/m^2-s. These peak propagation rates occur with the air mass flux in the range of 0.130 to 0.134 kg/m^2-s. The present results compare well with those available in the literature on the effective propagation rate with the variation of air mass flux, and deviations are linked to fuel properties. The propagation rate correlates with mass flux as $\dot{m}''^{0.883}$ during the increasing regime of the front movement. The extinction of flame propagation or the front receding has been established both experimentally supported from the model analysis and is found to

be at an air mass flux of 0.235 kg/m^2-s. The volume fraction of various gaseous species at the reactor exits obtained from the experiment is 14.89±0.28 % CO_2, 15.75±0.43 % CO and 11.09±1.99 % H_2 respectively with the balance being CH_4 and N_2.

The model analysis using an in-house program developed for packed bed reactor provide a comprehensive understanding with respect to the performance of packed bed reactor under gasification conditions. The model addresses the dependence on air mass flux on gas composition and propagation rate and is used to validate the experimental results. Based on the energy balance in the reaction front, the analysis clearly identifies the reasons for stable propagation front and receding front in a co-current reactor. From the experiments and modelling studies, it is evident that turn-down ratio of a downdraft gasification system is scientifically established. Both the experimental and the numerical studies presented in the current work establishes that the physical properties of the fuel have an impact on the performance of the co-current reactor and for the first time, the importance of bed movement on the propagation rate is identified.

CHAPTER I

Introduction and Literature Review

1.0 Introduction

With growing demand for clean energy and declining reserves of fossils fuels, search for alternative energy sources has been initiated which can replace fossil fuel based economy (Kucuk and Demirbas, 1997). Carbon dioxide and other greenhouse gases emissions due to excessive use of fossils fuels lead to global warming resulting in climate change. Different renewable energy technologies based on solar, hydro, wind, biomass resources are considered to be clean, sustainable and most importantly less harmful towards nature. Biomass has been a major source of energy after fossil fuels such as coal and petroleum, supplying about 14% of the primary energy of the world (Kucuk and Demirbas, 1997). In developing countries, 35% of total energy is derived from biomass out of which 90% is used in the form of traditional fuel, e.g. fuel wood for cooking (Kucuk and Demirbas, 1997). According to Renewable 2014 Global Status Report, total primary energy consumption of biomass reached approximately about 57 EJ in 2013, out of which almost 60% was traditional biomass, and the rest was modern bio-energy (solid, gaseous, and liquid fuels) (REN 21, 2014). It has also been recognized as an ideal energy resource that can be used for the decentralized energy systems. Renewable sources contributed approximately 22.1% of total electricity production, out of which 1.8% share is from biomass energy in the world (REN 21, 2014). Presently, thermo-chemical conversion and biological conversion are largely complimentary technologies, which are widely accepted for efficient utilization of biomass as a source of modern energy.

Biomass is a natural product, which stores solar energy as chemical energy by the process of photosynthesis in the presence of sunlight. Biomass largely contains cellulose (about 50%), hemicellulose (about 25%) and lignin (25%) having an average chemical composition of $CH_{1.4}O_{0.6}$, with slight variations (Mukunda, 2011).

There has been an increasing interest in the thermo-chemical conversion of biomass and urban wastes for upgrading the energy in terms of more easily handled fuels, namely gases, liquids, and bio-char. Biomass gasification, a thermo-chemical conversion process, has been extensively used during World War II (SERI, 1979). However, later (i) due to the availability of oil and (ii) availability of fossil fuel technology, use of biomass gasification technology has decreased substantially. However, researchers revisited the gasification research from the early eighties due to (i) increased oil price, (ii) climate change related issues and (iii) energy access to remote areas (Kucuk and Demirbas, 1997).

Biomass gasification process involves complex chemical reactions that convert solid biomass into combustible gaseous fuel, water vapor, char (solid carbon) and tar (aromatic higher hydrocarbons) (SERI, 1979). Air is widely used as a gasifying medium for generating producer gas (a mixture of CO, H_2, CO_2, CH_4, and N_2) that can be used both for power and thermal applications. Reactor operating parameters like gasification agents/medium, gasification temperature, equivalence ratio and fuel properties need optimization based on the end use of the gaseous fuel. However, it must be noted, that the desired characteristics of producer gas for two applications, viz. power generation and synthetic liquid fuel production are different (Buragohain *et al.* 2010). In the former case, optimizing the operating conditions to generate producer gas with maximum calorific value is important, while in the latter situation; the H_2/CO ratio (along with the actual content of H_2 and CO in terms of moles) is important (Buragohain *et al.* 2010).

1.1 Biomass gasification process

Biomass gasification is a thermochemical process that converts carbonaceous materials like biomass into useful, convenient gaseous fuels or chemical feedstock. In the case of complete combustion, the theoretical amount of air of 6 to 6.5 kg is required for per kg of biomass (stoichiometric air to fuel ratio) and the end products are CO_2 and H_2O (SERI, 1979). In the case of gasification process, biomass is

subjected to partial oxidation under sub-stoichiometric condition with the air quantity being limited to 1.4 to 1.8 kg per kg of biomass. The equivalence ratio for gasification is close to 0.25. The resultant mixture of gases produce during gasification process is called producer gas, which contains carbon monoxide (20-22%)), hydrogen (20 to 22%), carbon-dioxide (12-14%), methane (1-2%), water vapour and the rest is nitrogen (CGPL, 2015). The product gas also contains higher molecular weight compounds identified as "tar" and particulate matter which is carbon/residual ash. The product gas has a calorific value of 4.5 to 5 MJ/kg with conversion efficiencies of the gasification process in the range of 60% to 80% (Mukunda, 2011).

1.2 Gasification process zones

The gasification process is a combination of four major thermal processes: *drying, pyrolysis, oxidation or combustion and reduction.* Figure 1.1 represents the different processes occurring in the gasification process.
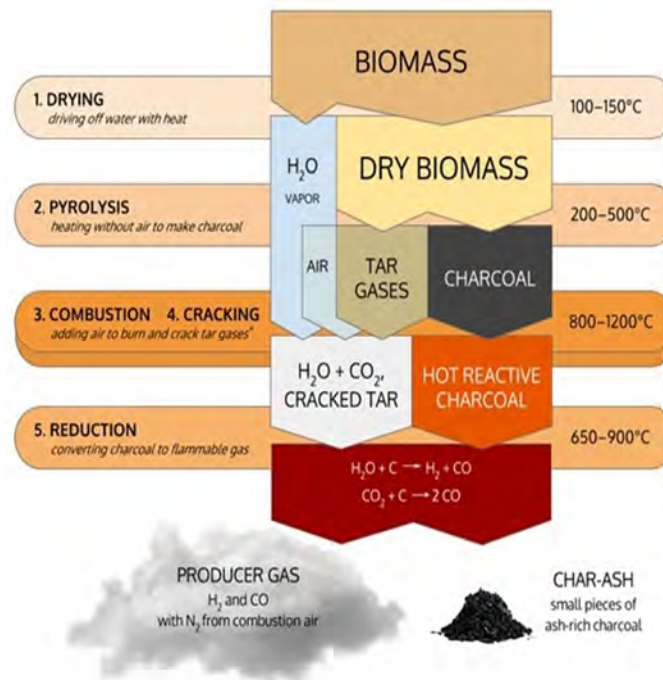
Fig 1.1 Biomass gasification processes *(Gasification, 2015)*

1.2.1 Drying

The main process of drying zone is the drying of the biomass (wood). In general, the wood used in the gasifier has a moisture content of 10-30%. Various experiments reveal that less than 15% moisture in wood is suitable for gasification purpose (CGPL, 2015). In this process, the physical moisture present in the wood evaporates and the rate depends on the prevailing temperature in this zone. Some organic acids are also products, during the drying process.

1.2.2 Pyrolysis

Pyrolysis is the application of heat to raw biomass in the absence of air. In this process, biomass breaks down into char, various gases and liquids. This process is also known as devolatilization, where volatiles are released. The products of pyrolysis depend upon temperature, pressure, residence time and heat losses. Pyrolysis, which takes place between 280 to 500 ^oC, produces gases containing carbon dioxide and tars. The gases and liquids produce during low temperature (low heating rate) pyrolysis, also known as slow pyrolysis. The products are complex H, C and O molecules bonding identified as volatiles. The volatiles are reactive and in other sense, are less strongly bonded in the biomass than the fixed carbon, which is the direct C-C bond. The outputs from this process are tar (liquid, sticky substances) and fixed carbon, known as char.

1.2.3 Oxidation or combustion

Apart from gaseous species under going oxidation, large complex molecules such as tar breaks down into lighter gases during exposure to heat. The combustion reaction being exothermic yields a theoretical oxidation temperature of 1450 ^oC.

1.2.4 Reduction

In a gasifier, the products of partial combustion (water, carbon dioxide and un-combusted partially cracked pyrolysis products) pass through a red hot charcoal bed, where the following reduction reaction takes places.

$$C + CO_2 \rightarrow 2CO - 164.9 \text{ MJ/kg mole} \qquad (1.1)$$
$$C + H_2O \rightarrow CO + H_2 - 122.6 \text{ MJ/kg mole} \qquad (1.2)$$
$$CO + H_2O \rightarrow CO_2 + H_2 + 42 \text{ MJ/kg mole} \qquad (1.3)$$
$$C + 2H_2 \rightarrow CH_4 + 75 \text{ MJ/kg mole} \qquad (1.4)$$
$$CO_2 + H_2 \rightarrow CO + H_2O - 42.3 \text{ MJ/kg mole} \qquad (1.5)$$
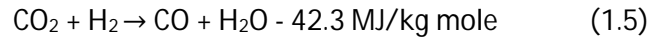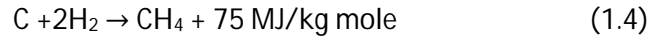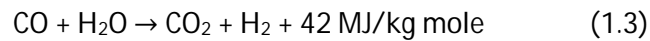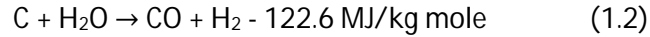
Conversion is effected through set of reaction 1.1 to 1.5 in the reduction zone. Fig 1.2 presents the schematic of the reduction reactions. The reaction 1.1 and 1.2 are the main reduction reactions and these reactions being endothermic reduce the bed temperature. The temperatures in the reduction zone are normally 800 - 1000 ^{0}C. Lower the reduction zone temperature (~ 700 - 800 ^{0}C), lower is the calorific value of the gas and higher is the tar content. Here a CO_2 molecule is reduced by carbon to produce two CO molecules, and H_2O is reduced by carbon to produce H_2 and CO. Hence, the output combustible gases from the exit of the gasifier are H_2, CO and CH_4.
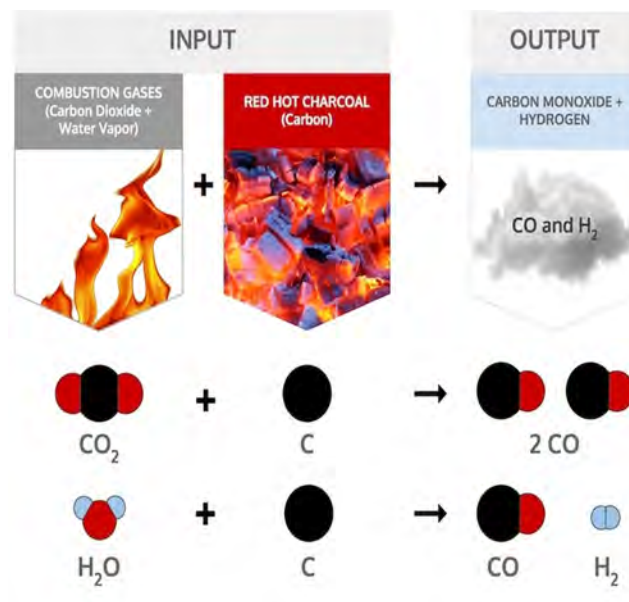
Fig 1.2 Reduction reactions in biomass gasifier *(Gasification, 2015)*

1.3 Gasification technologies

Major reactors being commercial practices for biomass are updraft, downdraft, cross-draft and fluidized bed gasifier. Fixed bed gasifiers (updraft, downdraft or

cross-draft) are typically simpler, less expensive and produce lower heat content producer gas (Gasification, 2015; Mukunda, 2011). Fluidized bed gasifiers adapted from the fluidized bed combustion are relatively complicated due to dynamic adjustment of equivalence ratio for gasification and also generate a gas with high tar content (Knoef, 2012). As the present study focuses on fixed bed gasification additional details regarding them are discussed in the following sections.

1.3.1 Updraft or counter-current gasifier

The oldest and simplest type of gasifier is the updraft or counter-current gasifier as indicated in Fig 1.3. The air intake is at the bottom near the grate and the product gas leaves from the top of the gasifier. Near the grate area, the combustion reactions occur, and other processes like reduction reactions, pyrolysis occurs above the grate. The tars and volatiles produced during this process are carried in the gas stream. Ash is removed from the bottom of the gasifier. The major advantages of this type of gasifier is its simplicity, better carbon conversion and internal heat exchange leading to low gas exit temperatures and high system efficiency, as well as the possibility of operation with various types of feedstock. The major drawback is high tar content in the output gas and the cleaning of output gas. This type of gasifier is used for direct heat application in which tar is simply burnt.
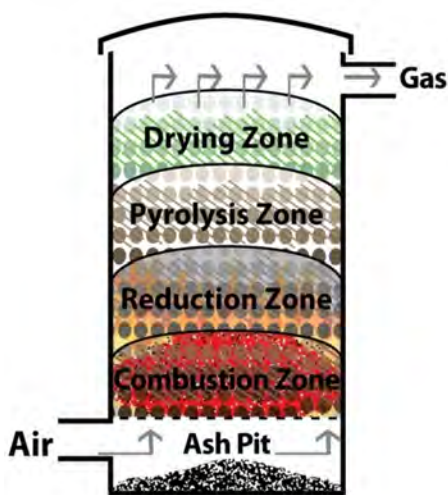
Fig 1.3 Updraft or counter-current gasifier
(Gasification, 2015)
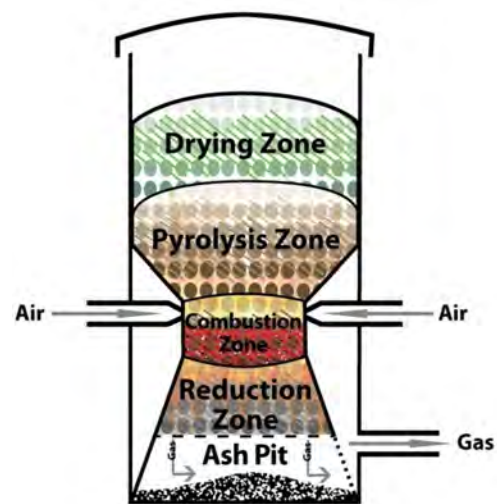
Fig 1.4 Downdraft or co-current gasifier
(Gasification, 2015)

1.3.2 Downdraft or co-current gasifier

A solution to the problem of tar in the exit gas is overcome by designing co-current or downdraft gasifiers, in which primary gasification air is introduced at or above the oxidation zone in the gasifier. The producer gas comes out from bottom of the gasifier, so that fuel and gas move in the same direction, as schematically shown in Fig 1.4. The products released during pyrolysis process pass through a red hot char bed and are converted into gases like hydrogen, carbon dioxide, carbon monoxide and methane. Depending on the temperature of the hot zone and the residence time of the tarry vapor in this zone, a more or less complete breakdown of the tars occurs. The main advantage of downdraft gasifiers is the possibility of producing low tar output gas suitable for engine applications. In practice, however, a tar-free gas is very difficult over the whole operating range of the gasifier. The major drawback of downdraft systems lies in its inability to operate on a number of unprocessed fuels. In particular, fluffy, low density materials give rise to flow problems and excessive pressure drop, and the loose solid fuel must be pelletized or briquette before use. Downdraft gasifiers also suffer from problems associated with high ash content fuels and sometime clinkers are formed due to ash fusion at a higher temperature. The efficiency of downdraft gasifier is lower than the updraft gasifier due to lack of internal heat exchange as well as the lower heating value of the gas.

1.3.3 Cross draft gasifier

Cross draft gasifier schematically illustrated in Figure 1.5 is an adaptation for the use of charcoal. Charcoal gasification results in very high temperatures (more than 1500 °C) in the oxidation zone which can lead to material problems. In cross draft gasifiers, insulation against these high temperatures is provided by the fuel (charcoal) itself. Advantage of the system rests in the very small scale at which it can be operated. The disadvantage of cross draft gasifiers is their minimal tar converting capabilities and the consequent need for high quality (low volatile content) charcoal.
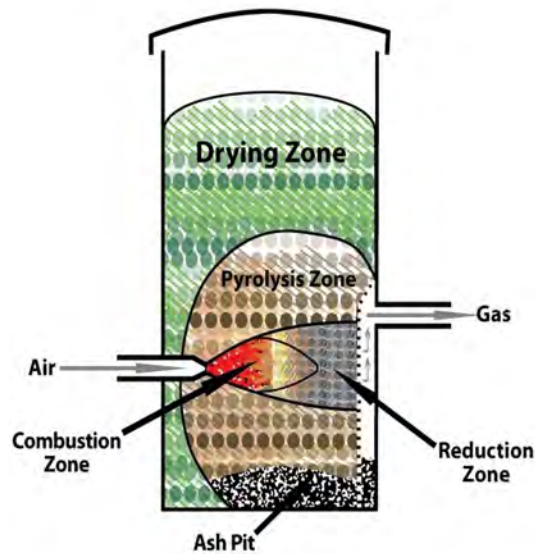
Fig 1.5 Cross draft gasifier *(Gasification, 2015)*

1.4 Open top down draft reburn gasifier

The open top twin air entry gasification system developed at the Indian Institute of Science (IISc), Bangalore is unique in terms of generating superior quality producer gas (Dasappa et al. 1989, 1994, 2004). The biomass gasification system consists of a reactor, gas cooling and cleaning system. Fig 1.6 represents the schematic diagram of this kind of gasification system.
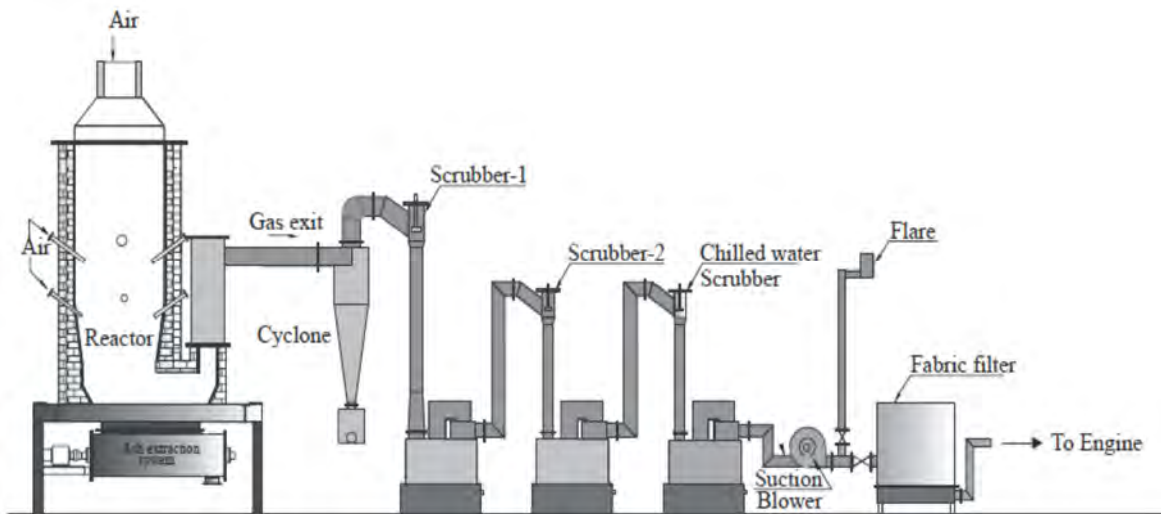
Fig 1.6 Open top downdraft gasification system *(CGPL, 2015)*

This system design has a long cylindrical reactor with air entry both from the top and through the air nozzle point i.e. the oxidation zone. This gasification system has air flow shared between the top and the nozzle to stabilize the flame front. There are two advantages resulting from sharing of air supply from top and nozzles. The advantages are (a) increasing the char consumption and (b) helping in re-burning the higher molecular weight compound released during pyrolysis. The principal feature of the design is related to the high residence time of the reacting species in the reactor by providing sufficiently thick reduction zone resulting in low tar content at the output gas. This is achieved by the combustible gases generated in the oxidation zone located around the side air nozzles re-burnt before passing through a bottom section of hot char bed. In this situation, the reacting mixture is allowed to stay in the high temperature environment along with reactive char for such duration that ensures cracking of higher molecular weight compounds (tar).

Measurements show that the fraction of higher molecular weight compounds in the hot gas from this gasifier design is lower than a closed top design. The cracking of the tars also improves the overall gasification efficiency. The superior reactor design also improves the energy content of the output gases. The cold gas efficiency has been reported in the range of 75% for a capacity of 75kg/hr gasifier (Mukunda et al. 1994). These results are among the best of conversion efficiency reported in the literature. The temperature of the exit gas from the reactor is about 350- 550 ^{0}C, with contaminants in the form of particulate matter (1000 mg/Nm^3) and tar (150 mg/Nm^3). The hot gas is further processed in the gas cooling and cleaning system in order to condition the gas to a level that is acceptable for engine operations. Typical composition of the gas after cooling to ambient temperature is about 18-20% H_2, 18-20% CO, 2-3% CH_4, 12% CO_2, 2.5% H_2O and the rest being N_2. The lower calorific value of the gas is in the range of about 4.5 to 5.0 MJ/kg (CGPL, 2015). The gas cooling and cleaning system provides cooled producer gas with tar and particulate matter level in the range of ppb levels. Measurements show that the tar and particulate matter level is less than 5 mg/Nm^3. The particle size measurement at the

cyclone exist of the gasifier in Switzerland, based on IISc design indicated that majority of the particles (> 95 %) are well below 0.5 μm (CGPL, 2015). Towards consolidating the literature regarding the sub-processes involved in the packed bed reactors, following sections briefly highlight the relevant literature on the subject.

1.5 Literature review on the gasification process

The main objectives of the present work are experiments and analysis towards establishing the effect of air mass flux on thermal profile moving into virgin fuel bed, bed temperature, gas composition, and related aspects under sub-stoichiometric operating conditions of a co-current gasification system. Hence, the work reported in the area of single particle combustion, flaming and glowing combustion, tar generation, effect of physical properties of biomass sample on gasification process, propagation front in packed bed, and model analysis on biomass gasification are explored in the literature and presented in the following sections.

1.5.1 Single particle combustion

Mukunda *et al.* (1984) studied the combustion characteristics of wooden spheres of various diameters for understanding their role in wood gas generators. This study presents a comprehensive analysis of wood spheres combustion related to weight loss, particle diameter shrinkage, temperature at the surface and core of the particle during flaming (time taken during oxidation pyrolysis) and glowing time (time taken for char oxidation). It is observed that in case of flaming combustion, particle sphere diameter decreases by about 10% and weight losses is about 75-80%. This reduction is due to the loss of volatiles from the wood particles. The study reported that the glowing zone combustion involves the remaining weight loss of 20-25%, and diameter variation follows the d^2 law. Simmons and Ragland (1986) studied the burning rate for millimeter sized wood particles in a convective flow furnace. The experiments are carried out by varying the furnace temperatures, oxygen concentration, Reynolds number, moisture content and particle size to address the influence of these parameters on the burning rate. The study concluded that devolatilization phase is distinct from char combustion. It is observed that the

percentage of mass loss in the devolatilization stage is 80-90% and the burning time of this stage is 50% of the total burning time. The study reported that the devolatilization rate of a given particle is influenced by the surrounding temperature, Reynolds number, and oxygen concentration. It is also observed that with the reduction of particle size, burning rate per unit mass increases linearly and moisture content of the particles played a crucial role in burning rate in the devolatilization stage. The char burn phase is controlled by the rate of diffusion of oxygen to the char surface.

Yang *et al.* (2008) studied both experimentally and mathematically the combustion characteristics of a single biomass particle of varying size. In this study, different sub-processes such as moisture evaporation, devolatilization, tar cracking, gas-phase reactions, and char gasification are examined, and the sensitivity to the variation in model parameters, especially the particle size and heating rate are investigated. It is found that the radiation heat transfer is the major heat transfer mode between the fuel particles and its surrounding. Lu *et al.* (2008) studied the combustion process in an entrained flow reactor with poplar biomass particles with varying sizes and presented an one-dimensional particle model that simulated the drying, rapid pyrolysis, gasification and char oxidation processes of particles with different shapes (sphere, cylinder, and flat plate). It is reported that the model can be used to simulate the combustion process of biomass particles of any shape (particle aspect ratio, volume, and surface area). Lu *et al.* (2008) concluded that the temperature gradients in particles strongly influence the predicted and measured rates of temperature rise and combustion process, which also depends upon surface area and the temperature exposed on the particles surface. Varunkumar *et al.* (2011) studied the single particle combustion using experiment and model analysis to observe the mass loss rate in the flaming and char glowing combustion phase and also the effect of particle density on the same. The study reported that char combustion rate closely follows the d^2 law and ignition time for a wood sphere (10-15 sec) is less than for pellets (25 sec); as pellets have high thermal inertia compared to the wood sphere. A co-relation has

also been derived between the burn time, char density, Reynolds number, and Grashoff number.

Momeni *et al.* (2013a) investigated the ignition, devolatilization and burnout time of single biomass particles of various shapes and sizes. It is found that for similar volume (mass) of various shape biomass particles, mass loss for cylindrical particles (aspect ratio: 6) is faster than the spherical particles (aspect ratio: 1) and burn time decreases with the increase of particle aspect ratio (length/diameter). Spherical particles have faster conversion time due to higher surface area/volume ratio (ratio is 2) and in the case of cylindrical particles of different length; the conversion characteristics are more or less same due to similar surface area/volume ratio (ratio is 1.5). It is concluded that the gas temperature and oxygen concentration had a significant effect on all the sub-processes during biomass combustion. The effect of the oxygen concentration in the reactant mixture on char oxidation is more pronounced at low ambient temperature compared to higher temperatures. Momeni *et al.* (2013b) investigated both experimentally and numerically the ignition and burn time of pine wood particles (millimeters in size) in the hot ambient gas stream (1473–1873 K) with oxygen concentration (5–20%) in a single particle combustion reactor rig. The study concluded that a large temperature gradient inside the particles play an important role in the ignition process. The process conditions had significant effect on ignition and burn time of the samples.

Riaza *et al.* (2014) studied the combustion behaviors of single particles of four different pulverized biomass in a drop-tube furnace at a temperature of 1400 K in both air and O_2/CO_2 atmospheres. The study reported that the volatile flames of biomass particles are much less sooty than the coal particles of same size and char combustion duration is also shorter. It is also observed that combustion intensity of biomass is stronger in the air (O_2:21% and N_2: 79%) than the oxy-fuel conditions (O_2:21% and CO_2:79%). Fatehi and Bai (2014) presented a comprehensive mathematical model for biomass combustion by considering the different thermo-

chemical process of biomass combustion viz., moisture evaporation, pyrolysis, heterogeneous char reactions and intra-particle heat and mass transfer. The study identified two stages in temperature rise. In the first case, the temperature in the center of the particle rises slowly due to moisture presence in the particle. Later as the pyrolysis starts the temperature reaches around 700K at a relatively faster rate and at the end of pyrolysis, the temperature quickly increases to 1700K due to char combustion. Mason *et al.* (2015) studied combustion behavior of pine, eucalyptus and willow with varying particle size, moisture content and aspect ratio. An empirical expression is arrived at towards the relationship between particle mass and ignition delay, volatile flame duration and char burn duration. The simple comparison of burn time on the density of different sample shows no clear correlation. However, as the aspect ratio increase, volatile release increases and hence burn time enhances. This is due to the higher heat transfer per unit of mass for higher aspect ratio leading to faster devolatilization. It is also observed that as the density of the particle increases, char burn time increases. Wan *et al.* (2015) investigated experimentally and numerically the pyrolysis characteristics of coal, biomass (straw), and coal–biomass blends of 8 mm diameter spherical particles. The study observed the devolatilization characteristics of the particles at different temperatures using a single particle reactor system. It is found from the study that for coal samples, the maximum yield at pyrolysis occurs at 1100K and beyond this volatile yields do not enhance much.

Sharma *et al.* (2015) investigated the flaming and glowing combustion of biomass and different types of coal samples with a particle size of diameter between 5 to 20 mm. In the case of coal, char burning is important as it has a higher percentage of carbon unlike biomass and the char conversion time is also much longer than biomass. It is found that the ignition time increases with the increase in particle diameter and for coal it is higher than the biomass. This is due to the higher thermal inertia of the coal particle than the biomass (coal has four times higher external and internal resistance than biomass). It is observed that flaming time of biomass

samples is higher than coal sample due to higher volatile matter in the biomass. Higher glowing time i.e. char combustion in case of coal samples suggest that the heterogeneous char reaction is slower than the flaming process. The normalized flaming time for same equivalent diameter is nearly same for all the fuel samples. The conversion time during flaming varies with diameter index 1.5 to 1.8, and it varies between 1.7 to 2.0 for glowing.

In summary, various researchers have addressed the single particle study of wood/biomass under various ambient conditions towards addressing the pyrolysis process and the char conversion time. Most of the studies clearly identify the process being diffusion limited and follows the d^2 law. With the increase in heat flux on the particle, it is evident that the pyrolysis process shifts from slow to fast, with changes in the volatile and char yields. The literature clearly indicates the importance of the single particle combustion study while addressing the packed bed of particles. The properties of the fuel size, shape, density, surface area to volume ratio, etc. plays an important role in the overall pyrolysis gas yield, flaming and char burn time etc.

1.5.2 Reaction front in packed bed

The investigation into the combustion front propagation in packed bed gasifiers has been generally restricted to charcoal, coke, polyurethane and a few studies related to biomass. A number of authors have examined the combustion front (reaction or ignition front) propagation rate in the combustion regime against the air stream through a packed bed of solids such as foam, char and wood assuming the combustion front propagation to be one-dimensional. The primary emphasis in all these studies has been to predict the flame spread through the porous media. However, very few attempts have been made to study the combustion front propagation using fuels with different physical conditions. The process that occurs in a typical wood gasifier is heterogeneous reactions in a packed bed with homogeneous heat release in the gas phase coupled with the devolatilization of the solid fuel.

Ohlemiller *et al.* (1979) formulated a one-dimensional model for smoldering combustion for flexible polyurethane foam assuming thermal equilibrium between gas and solid phases and neglecting the gas phase reactions. It is observed that if the ignition mass flux (propagation rate in kg/m^2-s or mm/s) is too low, solid will not reach a position to start the reaction and somewhat longer irradiation time is necessary to achieve the self-sustaining smolder. The study concludes that the heat generation goes up when the flux terminates and as the flux increases the heat generation decreases. Heat transfer process by conduction and convection dictates the smolder propagation rate and heat release rate and the smolder velocity is dependent on the rate of oxygen supply (air supply rate). Reed and Markson (1982) have done a detailed study on gasification reaction velocities under various conditions in a downdraft gasifier. This study concludes that as biomass is pyrolyzed, the gases and vapors mix with incoming air, forming a combustible mixture. The reaction velocities depend on the stoichiometric of the fuel vapours and oxidisers. The flame propagates upwards at relatively higher velocity than the downward velocity of biomass.

Fatehi and Kavinay (1994) analyze the downward propagation of the combustion front in a packed bed of wood particles, where the air is supplied from below. In this study, the incoming air flows in a direction opposite to that of the reaction front. During the pyrolysis process, the output product is char and volatiles in gas phase. The gas phase kinetics is assumed to be much faster than char oxidation for surface heterogeneous reactions. The speed at which the burning front propagates is primarily controlled by gas flow rate and the initial concentrations of the oxidant. The front speed, adiabatic temperature and the extent of solid consumption are determined as functions of entering air velocity. This study also examined the oxygen-limited and fuel-limited regimes. It can be observed from Fig 1.7 that at low air flow rate, the bed will not ignite defining lower flammability limit and at a higher flow rate, fluidization of bed has occurs. It is observed that in the oxygen limited regime, adiabatic temperature increases as the air flow rate increases. As the air flow

increases, consumption of fuel and front speed also increases. In the fuel limited regime, the adiabatic temperature is lower than the stoichiometric condition as the air flow rate increases and front speed also reduces. In this regime, the upper extinction limit has reached beyond which flame front would not propagate through the medium due to excessive cooling of the reaction front. A lower extinction regime is also identified for the self-sustained propagation of the reaction front, below this, the amount of solid burn is too small, or cannot produce sufficient heat required for initiating the reactions.
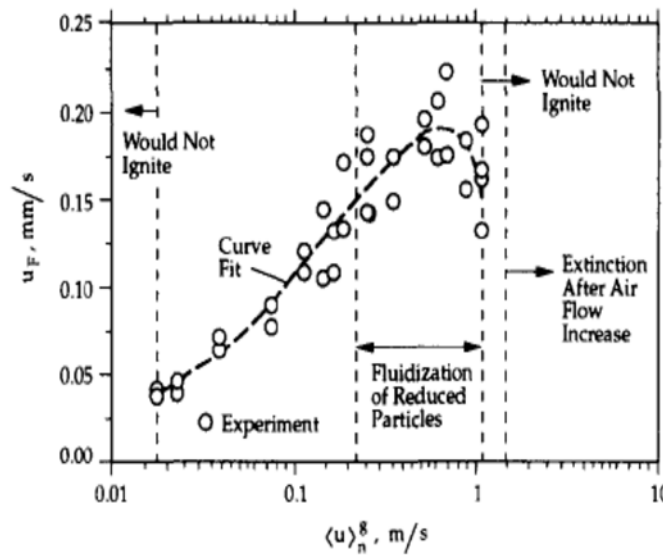
Fig 1.7 Propagation of burning front with respect to air velocity
(adapted from Fatehi and Kavinay, 1994)

Gort (1995) explores the effect of moisture, particle size, and volatile components of wood particles, coke and municipal solid wastes in a batch-type grate furnace. It is reported that the ignition rate decreases with increase in fuel moisture content, and the peak ignition rate is shifted towards the lower air mass flux with the increase in moisture content of the fuel. This study shows that the ignition rate has a weak dependence on the particle size of wood particles, whereas it changes strongly with the size of coke particles. Shin and Choi (2000) observed that the flame propagation rate depends on the air supply rate, calorific value and particle size of the fuel. This study identified oxygen-limited and reaction-limited regimes based on the

availability of oxygen. Further as the air flow rate increases, flame extinction is observed due to excessive convective cooling and as the particle size increases (surface area per unit mass decreases) flame propagation speed decreases. Saastamoinen *et al.* (2000) investigated the ignition front propagation in a fixed bed of wooden particles and explored the effects of physical properties of the particles, air flow rate on the ignition front speed through experiment and modeling. It is observed that ignition front speed and bed temperature is maximum at a particular air flow rate. It is also found that with increase in moisture content of the fuel ignition front speed decreases. However, for a range of moisture content used in this study has no significant effect on the peak bed temperature. The study did not notice any effect of particle size on the ignition front speed. However, larger particles increase the peak temperature of the bed to some extent. The study observed that the propagation front speed is inversely proportional to the density of the fuel samples.

Horttanainen *et al.* (2000) studied the ignition front propagation against the air flow using experiments and modeling. It is found that the primary factors affecting the propagation rate are the fuel moisture, volatile content, air mass flux through the packed bed and the physical properties of the fuel samples like shape, size and bulk and particle density. The experimental study shows that the increase of moisture of the fuel particle decreases the reaction front propagation rate, as vaporization of the moisture consumes certain energy and lowers the temperature. It is found that the ignition front speed increases with the decrease in bed density and as the surface area/volume increase, the front propagation is faster. This is due to the fact that small particles need less energy than the larger size particles. This study concluded that the ignited mass flow rate of the fuels per unit area of the bed (front velocity × bed density) is the important parameter while designing combustion equipment. Gort and Brouwers (2001) analyzed theoretically the propagation of a reaction front in a packed bed. The study concludes that the reaction front depends on the temperature, which influences the reaction rate. Dasappa and Paul (2001)

investigated the combustion front propagation rate in a wood-char packed bed reactor (open top down draft gasifier). Fig 1.8 represents the measured propagation rate and peak temperature in a packed char bed. The peak propagation rate is found to be 0.25 mm/s at an air mass flux of 0.06 kg/m²-s and the peak temperature of the bed at this air mass flux is 1100 K. It is observed that the flame front moves upwards, towards the top from where the air is drawn, and eventually the front reaches the top. The front movement varies with the air mass flux and with the increase in air mass flux, the front velocity increases initially, reaches a peak at certain air mass flux and then gradually reduces. With further increases in air mass flux, the flame front ceases to propagate and finally quenches.
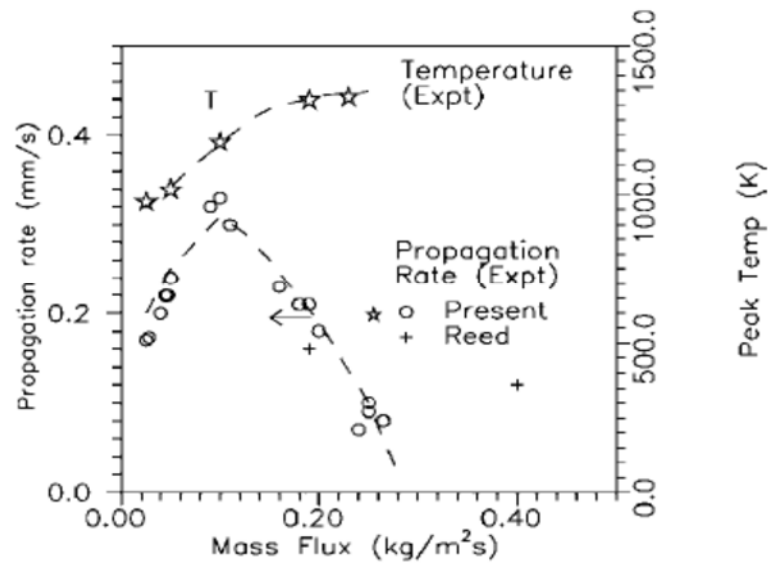
Fig 1.8 Propagation rate and peak temperature in a packed char bed
(adapted from Dasappa and Paul, 2001)

Rönnbäck *et al.* (2001) investigated experimentally the influence of air flow rate and fuel samples properties on the ignition front. It is found that the ignition front moves opposite to the air flow, and ignition rate, ignition front temperature (bed temperature) are strongly dependants on the air flow rate. As the air flow rate increases, flame propagation speed also increases and it is limited by the reaction rate of the fuel. However, at higher air flow rate, flame propagation movement is extinct due to convective cooling of the bed, reduces the bed temperature. It is also

observed from the study that the ignition rate is higher for larger particles at lower air flow rate. Thunman and Leckner (2001) studied the reaction front propagation in cross-current bed combustion of wet biomass samples. It is observed that front propagation depends on the airflow rate and moisture content of the fuel samples. As the moisture content of the fuel increase, the reaction front propagation slows down. Friberg and Blasiak (2002) present the experimental results on the effect of mass flux in a packed bed of solid biomass fuel combustion. This study concludes that the specific surface area of the wood particle is the determinant parameter for rate of conversion to gas and independent of the type and shape of the wood particle. Horttanainen *et al.* (2002) investigated the ignition front propagation of various wood fuels. It is found that the ignition mass fluxes for thin wood chips and mixture of wood chips and sawdust are higher. The moisture content decreases the propagation rate. The study reported that the optimal air flow rate, at which the propagation rate is maximum, is lower for small size particles as surface area unit volume is higher. It is observed that the maximum propagation rates are achieved under fuel rich conditions. Thin wood chips propagation rate is higher than pellets due to the difference in density of these two samples. However, this effect is not observed in the case of all other fuels. It is also found that the ignition mass flux increases with the increase of the porosity of the bed and sphericity of the particles.

Thunman and Leckner (2003) developed a model for the combustion of solid fuel both for co-current and counter-current combustion in a fixed bed on a grate. It is found from the study that the total conversion time of the fuel samples is shorter in the case of co-current in compare to the counter-current case. In the case of a co-current system, oxygen is consumed by the char combustion, whereas, in the case of the counter-current configuration, large extent is consumed by the volatiles and this postpones char combustion. Yang *et al.* (2004) experimentally and through mathematical model assessed the effect of air flow and moisture on the combustion of wood chips in a stationery bed. It is observed that the reaction zone thickness in the bed increases as the combustion proceeds and becomes very hot before the

combustion ends. The burning rate increases as the air flow rate increases until a peak point is reached, beyond which further increase in the air flow rate reduces the burning rate. It is also reported that the burning rate is inversely proportional to the moisture content of the fuel. However, the air flow rate at which the burning rate is maximum is shifted to a higher value for drier fuel. It is also observed that the flame temperature increases as the air flow rate increase. Yang *et al.* (2005) studied the particle size effect on Pinewood combustion in stationery packed bed. This study experimentally measured the mass loss rate, temperature profile, gas composition at fixed air flow rate for the different sizes of the particle. It is observed that smaller particle takes lesser time to ignite, has higher burning rate and the reaction zone is thinner as compared to larger particle size. It is concluded that burning rate is inversely proportional to fuel particle size. However, the larger particle produces higher bed temperature. Thunman and Leckner (2005) study observed that the particle size has a significant effect on the conversion in a packed bed, and the density of fuel has limited influence on the conversion rate. However, front propagation speed is higher in the case of low density fuel as compared to high density fuel.

Yang *et al.* (2006) has reported mathematical simulation results of biomass and municipal solid waste sub-stoichiometric conversions with fixed bed and moving bed. This study concludes that char conversion rate is significantly lower than devolatilization rate. It is found that the char conversion process occupies half and devolatilization occupies one-third of the total bed length. It is also found that the devolatilization rate for biomass is twice higher than that of municipal solid waste due to less moisture and ash content. Ryu *et al.* (2006) experimentally studied four different types of biomass samples in a fixed bed reactor and evaluated the effect of particle size, bulk density and air flow rate on the combustion characteristics. It is observed from the study that ignition front speed and burning rate increases as the air flow rate increases. However, ignition front speed is inversely proportional to the bulk density of the fuel samples. The small particles have higher ignition front speed

as compared to large size particles. This is due to the slow devolatilization of the large size particle being thermally thick. Tinaut *et al.* (2008) investigated the biomass gasification process through a one-dimensional model and experiments in a small scale biomass gasifier. This study evaluates the effect of biomass particle size and air flow rate on the propagation rate. It is observed that biomass particle size does not have a clear influence on the maximum temperature. The model enables to study the effect of fuel samples physical properties on the gasification process and agrees well with the experimental results.

Porteiro *et al.* (2010) experimentally studied the ignition front in the counter-current process for different biomass fuels and concluded that the air mass flow rate is one of the parameter that has influence on ignition front propagation velocity. It is observed that the maximum front velocity is achieved at sub-stoichiometric conditions, as the cooling effect due to excess air is minimum. This study reveals that the ignition front does not depend much on the bulk density beyond 400 kg/m^3. The propagation rate for small particles (pine shavings) is higher than the large particles (RDF). The reason is likely due to the highest surface to volume ratio (in the case of pine shavings) which enhanced the inter-particle heat transfer inside the bed and increased the ignition mass flux. It is concluded that there is a clear dependence of ignition mass flux on the moisture content of fuel particle. Hernández *et al.* (2010) studied the effect of particle size and residence time on gasifier performance in an entrained flow gasifier using three different types of biomass. This study concludes that fuel conversion increases (57.5% for 8 mm diameter particles) when the fuel particle size reduces and it leads to an improvement in gasification performance. It is observed that smaller the fuel particle size, heat and mass transfer is more effective, as the surface area per unit volume is higher. As the particle size decreases, the release of volatiles during pyrolysis and char combustion gradually increases. It concludes that higher residence time inside the reactor improves the gasification process. The higher reaction temperature and higher residence time together improves the gas composition and leads to higher gasification efficiency.

Luo *et al.* (2010) have studied the pyrolysis and gasification of a municipal solid waste of different size in a fixed bed reactor. It is found that higher temperature inside the reactor resulted in higher gas output with less tar and char, and smaller size particle produce more H_2 and CO gaseous products with less char and tar. Plis and Wilk (2011) investigated the syngas composition from a fixed bed biomass gasifier by using theoretical equilibrium calculations and experiments, and the results are compared. This study experimentally evaluates the effects of excess air, different biomass samples (wood pellets and oats husk pellets) and moisture content of biomass samples on the syngas composition. It is observed that CO mole fraction is higher in the case of dry fuels and CO_2 fraction increases as the moisture content of fuel increases. It is found that at lower excess air ratio, CO mole fraction increases and reach it maximum and further increment of excess air ratio leads to decrease in CO mole fraction.

Yin *et al.* (2012) studied the particle size effect on the gasification performance in a downdraft fixed bed gasifier using different size of peach trees pruning. Larger particle has lower biomass consumption than the smaller particle at a given air flow rate. This study concluded that as the particle size increases, the gas yield increases while the tar and dust content decreases. Pérez *et al.* (2012) have reported experimental studies on biomass gasification in a packed bed and evaluate the effect of biomass particle size and air mass flux on the flame front velocity. It is observed that increase in superficial air velocity increases the flame front velocity. This study observed that as the equivalence (fuel/air) ratio decreases, the thermo-chemical process moves from gasification regime (fuel rich) to the combustion (fuel lean) regime. It is also found that the reactor diameter does not have a significant effect on the propagation rate. However, as the reactor diameter increases, heat loss reduces due to surface area to reactor capacity ratio and propagation rate or producer gas quality improves slightly. This study concluded that particle size increase, means effective surface area available for reaction reduces, resulted in the reduction of

mass and heat transfer in the thermo-chemical process, leading to lower biomass consumption, maximum bed temperatures, and lower flame front velocity.

Gnanendra *et al.* (2012) investigated the propagation rate of reaction front in a packed bed of pellets in a reverse downdraft configuration. It is found that the front velocity initially increases and then decreases with the increase in air mass flux. This increase or decrease in propagation front is related to the heat release and heat loss from the system. The peak temperature increases as the air mass flux increase and the peak temperature is found in the range of 1450K±75K. This study concludes that at low air mass flux, the peak bed temperature is below the ash fusion temperatures and at higher air mass flux; higher reaction front temperature leads to ash fusion temperature and formation of clinkers in the reactor.

1.5.2.1 Reactor configurations in packed bed

It is evident from the reported literature corresponding to packed bed configuration that propagation front rate is the most important parameter. Propagation front in a packed bed can be classified as counter-current and co-current propagation relative to the direction of the air and solid fuel movement. In the case of counter-current propagation, flame front propagates in a direction opposite to that of air flow. In the case of a co-current (downdraft) configuration, apart from the flame front moving upwards into the fresh fuel bed, the bed moves (contributed by size reduction during pyrolysis and fuel consumption) downward direction.

Fig 1.9 presents the schematic diagram of different reactor configurations. In the case of updraft or counter-current as well as reverse down draft configurations, air is in contact with the fuel where both pyrolysis as well as char combustion occurs in the reaction/combustion zone. Most of the packed bed configurations studied here are the reverse downdraft type (Table 1.1) where the top fuel layer is ignited initially, and the propagation front moves downwards into the virgin fuel bed, and

the oxidiser (air) comes in contact with fuel in the combustion zone as in the case of the updraft gasifier.
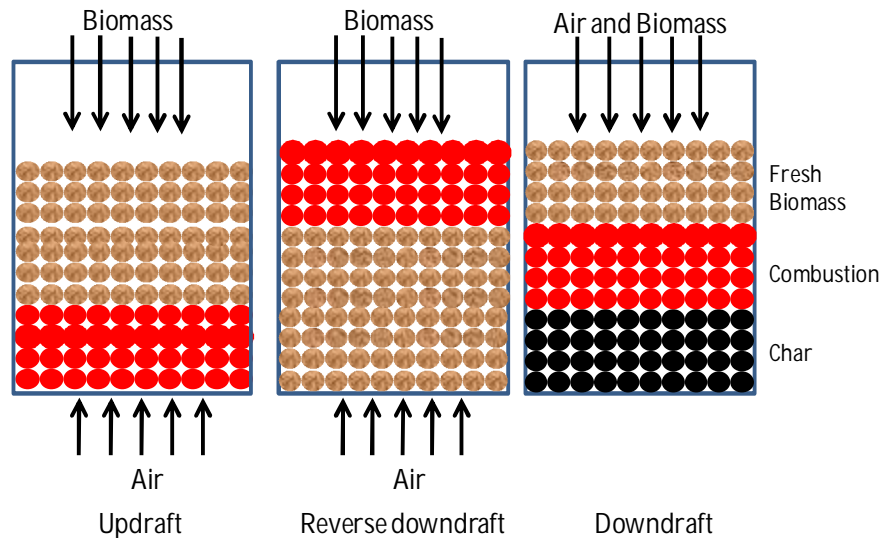
Fig 1.9 Different reactor configurations

The front movement in reverse downdraft configuration is directly linked to the oxidiser and fuel vapor combustion zone movement. In both the above cases, there is no fuel (bed) movement which affects the propagation front. In the case of downdraft configuration, fuel and air both moves downwards direction. With the flame front moving into the fresh fuel, the effective or overall propagation rate is dependent on the reaction zone movement (upward) and also the bed movement (downward) due to fuel consumption within the bed. Thus, it is important to address the effective propagation, a combination of flame front movement and the bed movement. In the case of reverse downdraft configuration, the bed movement is zero and the flame front movement, or ignition mass flux is identified as effective bed movement.

Table 1.1 Fuel properties and reactor configurations summary from literature

Fuel sample	Dimension (mm)	Equivalent radius (mm)	Surface area / volume (mm^{-1})	Sphericity	Density (kg/m^3)		Void fraction	Moisture (%)	Heating value (MJ/kg)	Reactor configuration	Reference
					Bulk	Particle					
Not available	6.4	3.2	0.94	0.998	300	663	0.60	Not available	14.0	Reverse Downdraft/ Counter-current	Fatehi and Kaviany, 1994[1]
	10	5	0.60	0.999	200	500	0.55	10	18		Gort, 1995[2]
Wood chips	5-20	3	1.89	0.561	157	500	0.69	10.8			Horttanainen et al. 2000[3]
Pine	8	4	0.75	0.999	307	579	0.47	9.1	19.3		Rönnbäck et al. 2001[4]
Wood pellets	3.8	3.8	0.79	0.999	690	1180	0.42	6.2	16.3		Porteiro et al. 2010[5]
RDF pellets	7.4	7.4	0.41	0.999	340	560	0.39	17.9	14.6		
Pine shavings	1.3	1.3	2.31	0.998	150	530	0.72	8.5	17.5		

---

[1] *Wood particle diameter is 6.4 mm, bulk density is calculated by considering the void fraction to be 0.6.*

[2] *In this study, 10 mm diameter wood particles are used and the density of the particle is considered to be 500 kg/m^3.*

[3] *Wood chips are 5-20 mm, the average size 12.5x5x1.5 mm is considered for surface area per unit volume calculation.*

[4] *Diameter of the wood particle is 8 mm.*

[5] *In this study, the fuel particle size is given in equivalent radius.*

Most of the experiments and models reported in the literature are focused on counter-current gasification system. In the study, of Fatehi and Kaviany (1994), Horttanainen *et al.* (2000), Rönnbäck *et al.* (2001) and Porteiro *et al.* (2010), fixed bed reactor is used, where solid fuel does not move. The air flows from the bottom (upward) where the bed is ignited and flame moves in the downward and is termed as counter-current (Porteiro *et al.* 2010). However, in the present study, solid fuel moves downward along with air flow, and flame moves against the air flow and is termed as co-current (reference to fuel and air flow). In the case of co-current configuration (open top downdraft gasification system), bed movement (contributed by fuel particle size reduction during pyrolysis and fuel consumption) is in the downward direction and the flame movement in the fuel bed is in the upward direction against the fuel and air flow.

1.5.3 Effect of fuel properties and gasification operation on tar generation

Biomass gasification essentially yields producer gas, condensable tars, particulate or dust, char, and ash. Tars are loosely defined as organic condensable (at room temperature) compounds formed during thermo-chemical reactions. The major tar species derived from biomass gasification range from single-ring to five-ring aromatic hydrocarbons (Kinoshita *et al.* 1994). Tar formation in the final product gas is one of the major concerns with biomass gasification systems. It is necessary to understand the scientific implications of the influence of fuel properties (particle size) on the gas quality. Various authors have reported on tar formation in various gasification systems at different operating conditions, the effect of fuel samples physical properties, the composition of tars, and mechanism of reduction of tar at the output gas.

Kinoshita *et al.* (1994) have done detailed parametric tests on tar formation at varying temperature, equivalence ratio and residence time in a fluidized bed gasifier. It is observed that benzene and naphthalene are the major species under most of the experiments. This study concludes that the temperature and equivalence ratio have

significant effects on tar yield and tar composition. Tar yield decreases with increase in temperature or equivalence ratio. However, actual concentration of particulate and tar in the gas also depend upon the reactor design, properties of the feedstock and operating conditions. Hasler and Nussbaumer (1999) have reported the tar and particle collection efficiencies of various methods in fixed bed gasifiers. The study concluded that 90% particle removal is easier as compared to 90% tar removal, and none of the available methods can reduce the tar content beyond 90%. Hence, some operational problems in the IC engine occur due to the tar present in the output gas even after gas cleaning. Hasler and Nussbaumer (2000) have developed a sampling method to measure the tar components and tested at different gasifier installations. The gas quality for successful internal combustion engine operation has been found as below 50 mg/m^3 for particulates and less than 100 mg/m^3 for tars in the case of naturally aspirated engines. This study also concludes that the composition of tars (heavy tars, PAH, phenols, water-soluble organic residue) and its cleaning is different for every application of the producer gas and hence the distinction between these is required for cleaning purpose. Abatzoglou *et al.* (2000) have formulated the tar sampling method that includes both gravimetric and chromatographic determinations. The method consists of iso-kinetic probe for sample extraction, heated filter for particulate collection, water condenser and cooled solvent to collect the tar present in the output gas. Dogru *et al.* (2002) observed that zone temperature is constant at air-fuel ratio 1.40-1.45 Nm^3/kg in the case of downdraft gasifier operation with hazelnut shell. The study found that at this air-fuel ratio, gasifier performance is optimum and produces high calorific value gas and optimum tar output is found as 0.023 kg/h of operation.

Devi *et al.* (2003) reported that hot gas cleaning after the gasifier and the treatment inside the gasifier are the major techniques for tar removal. It is important to optimize the gasifier operating parameters, use of catalyst or gasifier design modification to reduce the tar level in the output gas. This study observed that the operating parameters such as the bed temperature, equivalence ratio, and residence time play

an important role in the formation and decomposition of tar. It is also found that two stage gasification or secondary air input in the gasifier can also reduce tar in the output gas. Hence, to obtain the best quality gas output, the gasifier performance needs to be optimized by its design and operation practices. It is also desirable to achieve a high carbon conversion of biomass and low tar content in the resultant product gas by having higher operating temperature (above 1073K) in the gasifier to crack the higher molecular weight compounds. Nunes *et al.* (2008) reported that tar concentration in the output gas reduces with the increase of bed temperature, a decrease in particle size and increase in residence time. It is concluded that complete removal of tar is not an easy task; it requires the optimal design and reactor parameters and also dependant to some extent on the feedstock properties. Han and Kim (2008) reviewed the different mechanism for tar reduction during the thermochemical conversion of biomass gasification and pyrolysis. It is found that tar reduction by various methods varied from 40-99%. The selection of better gasifier, optimizing operating parameters not only reduces the tar but also convert the tar into useful gases. It is found that the bed temperature needs to be high for thermal cracking of the tar. Catalyst cracking, plasma technology are also effective means to reduce the tar levels in the output gas. Namioka *et al.* (2009) reported a simple method for gravimetric tar analysis and concluded that gravimetric tar generation decreases with the increase in thermal cracking temperature.

Hernández *et al.* (2010) have done experimental tests of three different fuel samples in an entrained flow gasifier to evaluate the effect of biomass particle size and residence time on the producer gas quality. It is found that fuel conversion increases (57.5% for 8 mm diameter particles) when reducing the fuel particle size, reaching a value as high as 91.4% for 0.5 mm diameter. The smaller the fuel particle size, more effective is the mass and heat transfer since the particle external surface area/volume is higher. This study concluded that combined effect of higher reaction temperature and residence time has a positive effect on the output gas quality. Phuphuakrat *et al.* (2010) experimentally reported tar yield in a downdraft gasification system. This

study observed that as the equivalence ratio increases from 0.30 to 0.32, temperature slightly increases from 995 to 1014 °C, whereas tar content in the syngas decreases sharply from 11.8 to 6.56 g/m^3. With the increase of equivalence ratio, oxidation zone temperature increases because air promoted the combustion reaction. Higher temperature enhanced the cracking and combustion of tar. However, it is also found that tar cannot be eliminated by the influence of air supply alone.

Luo *et al.* (2010) reported that the particle size and the temperature have integrated effects on product yield and composition in steam gasification process in a fixed bed reactor. As the temperature increases (600 to 900 °C), gas yield increases and tar and char decreases for all particle sizes. This increase at higher temperature is mainly due to tar and char decomposition which is converted to gas through Boudouard reactions and thermal cracking reaction. It is found that larger particle due to greater heat transfer resistance led to incomplete pyrolysis and resulted in a large amount of residual char. However, the particle size effect is not significant towards pyrolysis and gasification performance at higher temperature. Feng *et al.* (2011) reported that with the increase in particle size, gas production increases. However, in a packed bed, with the increase in particle size, pressure drop decreases, resulting in an increase in gas flow rate. Anis and Zainal (2011) has reviewed different types of methods to reduce the tar formation in biomass gasification systems. This study observed that reduction of the amount of tar in the producer gas is important not only on the quantity of tars but also the composition of tars.

Ueki *et al.* (2011) reported that the amount of tar generated in continuous running mode under updraft and downdraft conditions are 132.4 and 32.3 g/m^3 respectively. Tar compounds in syngas under downdraft conditions are lower than those under updraft conditions. This is because tars are cracked as the output gases pass through char conversion section at high temperature. Yin *et al.* (2012) studied downdraft fixed bed gasifier performance using different sizes of peach tree pruning. This study observed that as the particle size increases, the gas yield increases and tar and dust

content decreases. It is found that tar and dust concentration reduces from 550 to 14.43 mg/Nm^3 as the particle size increases from below 1 cm to 6-8 cm. Pérez *et al.* (2012) experimental studies concluded that higher process temperatures lead to volatile reforming reactions with higher reaction rates, which in turn results in the lower tar production. This study also concludes that as the equivalence air/fuel ratio increases, the thermo-chemical process moves from gasification (fuel rich) to combustion (fuel lean) regimes. It is found that the tar concentration reduces with increase in superficial air velocity.

Hernández *et al.* (2013) studied the effect of gasifier operating conditions like fuel /air ratio, gasification medium and reaction temperature on the tar production in a small scale drop-tube gasifier. It is observed that an increase in the relative fuel/air ratio leads to increase in tar generation. This is due to the fact that increase of fuel/air ratio decrease the available oxygen in the fuel bed to oxidize the volatile matter released from the fuel. It is also found that as the bed temperature increases tar generation decreases. Yu *et al.* (2014) studied the tar content and composition characteristics for cellulose, hemi-cellulose and lignin components of biomass in the gasification system. It is found that as the temperature increases from 800 to 1100 ^{0}C, tar yields reduced from 1.93 mg/g, 1.85 mg/g and 1.99 mg/g to 0.20 mg/g, 0.27 mg/g and 0.82 mg/g for cellulose, hemi-cellulose and lignin respectively. The study observed that tar reduction with increase of temperature and in case of lignin the temperature effect is less in compared to other components, indicating tar product from lignin to be thermally more stable. Pattanotai *et al.* (2015) experimentally studied the effect of particle aspect ratio (length/diameter) on pyrolysis and gasification process of a wood sample. It is found that tar generation from pyrolysis decreases with increase in aspect ratio. High aspect ratio increases the residence time for intra-particle tar decomposition, leading to low tar yields. Char reactivity during gasification increases with decrease in aspect ratio. High aspect ratio increases the residence time for intra-particle tar decomposition, leading to low tar yields.

The highlights of the literature clearly suggests the importance of the fuel properties and operating conditions for low tar generation from gasification systems. Surface area per unit volume of the particle in packed bed influences the flaming time and also generation of higher molecular weight compound. These understanding support the effect of physical properties of fuel samples on the gasification process which helps to fix the operating regimes of the gasifier to produce consistently good quality producer gas with low tar content.

1.5.4 Modeling and analysis of packed bed

Modeling of biomass gasification involves the representation of chemical and physical phenomena constituting pyrolysis, combustion, reduction processes occurs inside the biomass gasifier reactor. Typically, there are two approaches for modeling viz. thermodynamic equilibrium and kinetic. These models are used to understand the complex biomass gasification process simulation and gasifier design optimization. Thermodynamic equilibrium models are further classified into two types as (i) stoichiometric models and (ii) non-stoichiometric models. Numerous authors have used stoichiometric and non-stoichiometric equilibrium models to study the gasification process under various operating conditions. It is found that the thermodynamic models are useful for preliminary comparison and process studies on the influence of process parameters. However, kinetic based models on the other hand provide better results but are computationally intensive. Biomass gasification process depends on a number of complex chemical reactions like pyrolysis, partial oxidation of pyrolysis products, gasification of the resulting char, conversion of tar and lower hydrocarbons, and the water gas shift reaction. The biomass gasification model needs to have sub-models for the pyrolysis and char reactions with O_2, CO_2 and H_2O couple with heat and mass transfer process among the particles and bed. A brief review of available literature on modeling and simulations of biomass gasification systems is presented in the following section.

Mukunda *et al.* (1984) developed a model to understand the glowing combustion of porous char particle and compared with the experimental results. The study concluded that the model results for both flaming and glowing combustion brought out the weight loss and diameter variations, and variation of temperature at surface and core closely agrees with experimental results. Koufopanos *et al.* (1989) studied the kinetics of pyrolysis process of ligno-cellulosic materials. It is observed that kinetic rates control the process for the particle size of below 1 mm. However, for larger size particles, both kinetic and heat and mass transfer control the process. Wang and Kinoshita (1993) developed a kinetic model to describe the biomass gasification process. The model results are also validated with experimental findings. It is observed that the reactions are very fast during first 20 s and after that the reactions proceed relatively slowly. The reaction rates are controlled by the char particle size. As the particle size increases, reaction rate reduces, leading to longer residence time for the same conversion ratio. It is also observed that temperature influences the reaction rate, equilibrium constant and residence time. The study concluded that biomass gasification process depends on the gasifying medium, temperature, residence time, char particle size, equivalence ratio and moisture. Dasappa *et al.* (1994) modeled the char sphere gasification in CO_2-N_2 mixtures. This model is based on conservation equations with reaction-diffusion considerations and this model can explain the conversion time vs. diameter, conversion vs. composition, etc. It is observed that the conversion time follows tc~$d^{1.03}$ for the larger particle. However, the conversion time for diffusion limited cases follows tc~d^2. It is also found that conversion time varied inversely with the initial char density.

Dasappa *et al.* (1998) have developed a model using one-dimensional species and energy conservation equations for wood-char gasification for a single particle and packed bed. The process is modeled with char reacting with different reactants, diffusion and convection of species and energy in the porous medium and heterogeneous reaction between species and char. The propagation front against the air flow is estimated by using this model and compared with the experimental results.

It is observed that the reaction front velocity initially increases and then decreases with an increase in air mass flux, indicating heat balance in the system. Dasappa and Paul (2001) modeled the packed char bed and validated the results with the experimental findings. The simulation results show that peak temperature in case of no heat loss from the reactor is 170 K higher than the heat loss consideration. Similarly, the peak propagation rate for no heat loss case is 0.53 mm/s and for heat loss consideration, it is 0.30 mm/s. The higher peak propagation rate is due to higher bed temperature and higher heat transfer between the particles. It is found that around 7 percent of the fuel heat value can be considered as heat loss from the reactor. Heat release in the reaction zone increases with the increase in oxygen fraction in the ambient, and propagation front can be sustained in this situation. This study concludes that the extinction occurs when all the energy released in the reaction zone is taken away by the incoming reactants at higher air mass flux.

Bryden and Hagge (2003) modeled the pyrolysis process of moist and shrinking biomass particle. This study focused on the effect of moisture and shrinking on the pyrolysis of single biomass particle that experiences external constant radiant heat flux. It is observed that pyrolysis process is different for three different regimes such as thermally thin, thermally thick, and thermal wave. This study observed that pyrolysis time increases with the increase in moisture, and decreases with the increase in shrinkage. Babu and Chaurasia (2003) described a mathematical model for single wood particle pyrolysis considering the heat transfer and chemical kinetics equations. It is found that as the particle size increases, the pyrolysis time also increases. This study concludes that in the case of pyrolysis modeling of the single wood particle, both heat transfer and kinetics equations must be considered together. Babu and Chaurasia (2004a) used a numerical model to study the pyrolysis of biomass particles and the effect of shrinkage on particle size, pyrolysis time, product yields, specific heat capacity and Biot number. It is observed that shrinkage has an effect on pyrolysis time and yield for the thermally thick regime and negligible effect on the thermally thin regime. In the case of larger particle size, ash layer is formed on the

surface of the particle. As the particle shrinks, the insulating effect of char layer reduces and heat transfer to the unreacted core also reduces. This study observed that higher heat transfer rate of the shrinking particle reduce the pyrolysis time. It is also found that the shrinkage reduces the residence time of gases within the particle. Babu and Chaurasia (2004b) study observed that spherical particles have lesser conversion time as compared to slab shape particle, due to higher surface/volume ratio. The study observed that the product yield (volatiles and gases) of the pyrolysis process is more for the sphere as compared to slab shape particle. However, the char yield is more for slab and low for the sphere shape particle.

Di Blasi (2004) developed a one-dimensional model for fixed bed counter-current gasifier to understand the reaction front and gasification behavior. This model considers the heat and mass transport with wood drying, devolatilization, char gasification and combustion of both char and gas species. The study indicates the existence of a regime of decreasing temperature and propagation speed of the combustion front at near extinct conditions. This is attributed to the convective cooling of the reaction front by excess air. The model results on the axial profile of temperature and output gas composition are in agreement with the experimental results. Klose and Wolki (2005) investigated gasification of beech wood char and oil palm shell char at CO_2 and steam environment and observed that the reaction rate is proportional to the reactive surface area of the char particle.

Melgar *et al.* (2007) developed a mathematical model based on chemical and thermodynamic equilibrium and studied the effect of air/fuel ratio and moisture content on the gasification performance. This study observed that at low moisture, CO fraction increases with higher fuel/air ratio, as air is limited in the reaction zone, which leads to incomplete combustion. However, at higher moisture content of the fuel, more water available in the reaction zone leads to water gas shift reaction and production of H_2 and CO_2. This study concludes that the reaction temperature is the driving parameter of the gasification process and influences the thermal states of the

process and thereby the gas composition. Di Blasi (2009) reviewed the kinetic rates and constants for gasification process with carbon dioxide and steam; yields and composition of the pyrolysis process. This study also explores the effect of heating rate, temperature, feedstock composition on char reactivity. Park *et al.* (2010) studied pyrolysis of wood sphere both experimentally and numerically. It is found that model and experiments results show good agreement with both temperature and mass loss measurements. It is observed that at high temperature, thick wood particle split due to high internal pressure and weakened structure. However, at low temperature pyrolysis, the wood particle does not split.

Puig-Arnavat *et al.* (2010) analyzed various gasification models and concluded that thermodynamic equilibrium models are good for initial understanding of the process parameters and kinetic models are more intensive and provide better results. Ahmed and Gupta (2011) studied the effect of particle size, porosity and reactor temperature on char particle conversion. It is observed that after a certain time of char conversion process, which is diffusion controlled, particle starts to shrink and its porosity increases, which allows high diffusivity of the gasifying medium. It is found that as the particle radius decreases, resistance to diffusion of gasifying medium decreases, consequently conversion time of the char particle decreases. It is also found that as the rate constant increases, the complete conversion time decreases. Higher reaction rate constants shift the process to diffusion controlled. Enrico and Baldi (2011) determine the kinetic parameters of weight loss, gas and tar production of beech and pine wood samples at two different heating rates. The experiments clearly identified two different phases in the pyrolysis process. In the first phase, rapid decomposition of wood with large and rapid tar generation is observed. In the second phase, slow tar and gas production occurs and ended at 950-1000 K temperature. It is also observed that the surface and inner core of the wood pellets have considerable temperature difference.

Barman *et al.* (2012) developed a modified equilibrium model and considered tar as a product from biomass gasification systems. The model results are validated with the experimental results. It is found that modified equilibrium model predicted with considerable degree of accuracy in comparison with simple equilibrium model. This study shows that tar mass needs to be included in the model to obtain better results. Puig-Arnavat *et al.* (2012) developed thermodynamic equilibrium model which includes certain modifications. The model is used to predict producer gas composition and compare the reported experimental results in the literature. The study also evaluates the effect of operating parameters like equivalence ratio, steam and oxygen injection on the output gas. The model results are validated with different types of gasifier experimental results and found good agreement. It is also observed that steam injection into the system improves the H_2 concentration in the output gas. Antonopoulos *et al.* (2012) developed a non-stoichiometric model to simulate the gasification process and later use the results to design a wood gasification reactor. The study observed that the heating value of syngas reduces with an increase in moisture content of the fuel samples. It is also found that CO fraction reduces significantly as the moisture content increases and thus reduces the heating value of the output gas.

Janajreh and Shrah (2013) used wood based downdraft system to investigate its conversion efficiency through experiments and numerical modeling. It is found that the temperature near the air nozzle is higher in case of model compare to experimental results. This study concluded that equilibrium modeling does not capture the science inside the downdraft gasifier as compared to other type of gasifiers. Ranzi *et al.* (2014) developed a mathematical model considering pyrolysis of biomass particle, homogeneous gas phase reaction and heterogeneous reactions of the residual char at the particle level and reactor scale. This study observed that heat controlling or residence time is the important parameter for the gasification process. Ghassemi and Shahsavan-Markadeh (2014) studied the effect of operation parameters like equivalence ratio, gasifying medium, fuel type and temperature on the gasification performance. The study considered the equilibrium model based on Gibbs free energy

minimization and considered carbon conversion and tar formation in the model. It is found that air with O_2 as gasifying medium improved the cold gas efficiency and the higher heating value of the output gas. However, this study did not compare the model results with the experimental results.

Baruah and Baruah (2014) reviewed various models based on the type of gasifier, feedstock used, modeling consideration and output of the models. The review works largely focused on various equilibrium models for fluidized bed and downdraft gasifiers. It is observed that the equilibrium models have limitations due to the non-existence of equilibrium conditions inside the reactor. However, modified equilibrium models with certain empirical relations based on experimental results will improve its accuracy. This study concludes that the kinetic models are accurate and provide results close to the experimental results. Mendiburu *et al.* (2014) developed modified stoichiometric equilibrium models considering certain empirical relations to study the effect of operating parameters on the gasification process. It is observed that modified model provides results close to the experimental results.

Patra and Sheth (2015) has done a comparative analysis of different available models like thermodynamic equilibrium, kinetic, CFD, ANN and ASPEN Plus for downdraft gasifiers. The analysis found that thermodynamic equilibrium modeling is widely used as it is simple and easy to develop. However, these models are not reliable as equilibrium conditions are never reached in the reactor. It is suggested that model based on transport and kinetic models need to be developed based on individual particle and bed to obtain more realistic results. ANN and ASPEN PLUS models are used by the various researchers, but the experimental and model results correlation with actual operating conditions has a wide gap. CFD models are also used by various researchers, but still it is in nascent stage to get an insight of the gasifier reactor performance. Mahmoudi *et al.* (2015) use numerical model considering energy, mass, and momentum conservation equations to understand the pyrolysis, combustion and gasification process of a single particle, interaction of particles with each other at the

bed and the surrounding gas phase interactions in a fixed bed reactor. The temperature profile along the reactor and mass loss are also measured through experiments and validated with the model results. The model results showed good agreement with the experimental results.

Various researcher has developed mathematical models of gasification process using the sub-model i.e. pyrolysis, heterogeneous char reaction kinetics, heat and mass transfer for packed bed gasification system. These models vary from simplistic approach of thermodynamic and chemical equilibrium to the rigorous approach of simulating reaction kinetics, heat and mass transfer between the particles in a packed bed. In the initial ignition time, the fuel particle is heated through radiation and or convection process and the heat transferred inside the particle through conduction process. The pyrolysis kinetics has a critical influence on the gasification process. As the temperature increases, the volatiles are released from the particle and react with the surrounding environment. During the process, the pore size of the particle increases and char combustion is initiated. Basic conservation equations with appropriate boundary conditions are modeled for a single particle and later on extended to packed bed analysis for char gasification. It will be interesting to estimate the propagation rate, gas composition, and other parameters by using a mathematical model and compare the results with experimental results from co-current gasification system.

1.6 Approach of the present work

Studies on biomass gasification as a thermo-chemical conversion of solid biomass to gaseous fuel have been carried out by various researchers since Second World War II. Various reactor configurations have been developed towards ensuring generation of consistent gas quality with the objective of low tar content in the gas. The process parameters that decide the performance of the reactors are related to the air mass flux, fuel sample physical properties like size, shape, density, and L/D ratio of the reactor, etc. It is important to understand the influence of the operating parameters,

where the transformation of energy from solid fuel to gaseous fuel is maximized and resulting in higher system efficiency. Each of the processes involved in gasification of the solid fuel has a specific time scale depending upon the fuel properties like density, thermal conductivity, particle size, density and the reactive environment surrounded the particle. It is also important to note that the tar fraction in output gas can be minimized if the pyrolysis products are exposed to higher temperature and has higher residence time for its cracking. The propagation rate which is primarily influenced by air mass flux, combustion, and heat transfer, also depends on the fuel physical properties like, shape, size, density, thermal conductivity, moisture, ash content and calorific value. However, there is no strong evidence reported in the literature on the effect of each of these parameters on the front propagation rate with particular focus on the co-current configurations. The size of the fuel (surface area per unit volume) particle is crucial to achieve the better conversion rate with the acceptable quality of gas. However, most of the reported work in the literature deals with counter-current configurations and the results on propagation flame front/ignition mass flux and temperature mostly under the combustion regime.

With the above background, the thesis addresses the critical parameters that influence the performance of a co-current reactor configuration using extensive experiments and analysis. The fuel properties (size, surface area to volume ratio and density) influences on the gasification process has been studied using single particle analysis and packed bed reactors. The influence of fuel properties, sharing of air from the nozzle and top which indirectly influences the residence time on tar generation is explicitly explained. The flame propagation front movement, bed movement and effective movement for a co-current packed bed reactor of different reactor capacities at various air mass flux has been carried out. The co-current reactor configuration is used towards addressing for the first time bed movement influence on the propagation rate with other fuel properties as variables; by introducing a variable '*effective propagation rate*'. With fuel shape and size having a major impact on the thermo-chemical process, the surface area per unit volume of the reactor is used to

evaluate the '*tar*' generation in the output raw gas. The work also tries to correlate the experimental results with the model results and available literature data. The modeling for packed bed reactor developed in-house provides a comprehensive understanding on the dependence on mass flux on gas composition and propagation rate in a packed bed under gasification conditions and is also used to compare with the experimental results.

Work	Purpose of the work
o **Experimental investigations**	
❖ Single particle analysis	o Towards addressing the influence of fuel properties like density, surface area/volume ratio, size etc. on the combustion characteristics towards evolving flaming and glowing time. o Compare with results available in the literature.
❖ Air gasification using two different sized co-current reactors	o Influence of fuel particle size on the tar generation and importance of residence time to reduce tar in the product gas. o Parametric study of various operating parameters towards increasing residence time like varying air mass flux, addressing temperature profiles, output gas composition, propagation rate, bed movement and related aspects towards arriving at operational regime of the gasification.
o **Analysis**	
❖ Model validation with experimental results and literature reported data	o Use an existing model for a co-current packed bed reactor and comparison with the experimental results like temperature profile, flame front propagation movement, bed movement, effective propagation movement, gas composition. o Comparing the experimental results with literature data on effective propagation movement, peak temperature. o Effect of air mass flux on volatiles fraction, surface area/volume ratio and conversion time on gasification process.

1.7 Summary

In this chapter, a detailed background on the gasifier and gasification technology has been presented. Further the review of available literature on single particle

combustion, propagation front in a packed bed, the influence of particle properties on tar generation, modeling and simulations of biomass gasification systems has been reported. The combustion characteristics of biomass samples have two distinct phase (i) flaming combustion and (ii) glowing or char combustion. The effect of different operational parameters on the flame front speed in the gasification regime is established. The combination of flame front and bed movement bears significant importance in designing reactor and also the operation range of the gasification systems. It has been established that equilibrium models are easy to interpret the gasification process, but do not represent the actual operation inside the reactor. There are very limited studies on the propagation rate or gas composition in a co-current/open top downdraft biomass gasification system.

1.8 Organization of the thesis

The thesis consists of seven chapters. The first chapter provides the background, literature reviews for this work and approach of the present study. In this chapter, a detailed review of available work reported in the area of propagation front in a packed bed, the effect of physical properties of biomass sample on gasification process and tar generation and modeling and simulations studies on gasification are explored. Chapter II provides the details of experimental setup and methods used in this study, measurement instruments details and calculation procedures. Chapter III presents the effect of fuel particle size and air input share through top and air nozzle on tar generation. The flaming and char combustion time are estimated for different fuel particles. Experiments are conducted to estimate tar generation in the raw gases by using different fuel samples and the effect of increased residence time with a twin-air entry on tar generation. Chapter IV presents the results related to propagation rate in a fuel bed under gasification regimes in an open top downdraft gasifier. The influence of air mass flux on the propagation rate, peak temperature, and gas composition is measured. The effect of particle size and density on propagation rate is also measured and analyzed. This chapter also addresses the effect of reactor size on effective propagation. Chapter V presents the mathematical model used in the study to

compare the model results with the experimental results and literature data. Chapter VI presents the model results with respect to the influence of the input variables, such as air mass flux rate, particle physical properties, and its effect on propagation rate and output gas composition in a packed bed. Chapter VII presents the overview of the contribution of the present study and scope for further research in this context.

Apart from the scientific investigations into the co-current reactor performance analysis, the current thesis also presents the biomass gasification systems as distributed power generation with the focus on modeling off-grid renewable energy systems like biomass gasifier based systems or photovoltaic systems and comparing them with grid extension towards access to electricity in the remote villages in Appendix A.

Experiments - Materials and methods

2.0 Introduction

This chapter presents the details of the experiments conducted and instruments used to study the gasification process in an open top downdraft gasifier. The experimental setup for measuring tar and particulate, propagation rate in the packed bed and the instrumentation used for measuring the temperature inside the packed bed, exit gas composition, fuel and gas flow rates are described.

2.1 Single particle experiment

Fuels have different physical properties like size, shape, density, etc. affect the pyrolysis and heterogeneous char reactions process. The pyrolysis product distribution depends on reactor temperature, heating rate, residence time and influence of the heat and mass transfer processes. The process of combustion of the fuel consists of two distinct phases. The first phase involves '*flaming combustion*' wherein a flame envelopes the sample, and the second phase involves '*glowing combustion*' wherein char burns. In the first phase, an inward movement of pyrolysis front with pyrolysis gases coming out from the surface and combustion of volatiles with the available oxidiser occurs in the gas phase. With the thermal front reaching the core, the pyrolysis process is nearly completed, and the gaseous flame surrounding the particle quenches. The next phase constitutes of glowing combustion involving diffusion of oxygen to the surface of the porous char and heterogeneous oxidation. The chemical structure of biomass char is similar to coal char, but large physical differences exist between them, such as density, thermal conductivity, porosity, surface area, and particle shape and size (Sharma *et al.* 2015).

In the present study, experiments have been conducted to measure the flaming and glowing time of certain fuel species, to have a better understanding of the above two

processes which influence the packed bed operating parameters. Flaming time is defined as the time taken for all the pyrolysis products to be released, i.e. the time after ignition of the sample and quenching of the flame surrounding the sample. On release of volatiles, biomass sample has residual char, i.e., after the flaming period, where char undergoes heterogeneous combustion with air consuming the carbon to from CO_2 and CO in oxidizer starved conditions. The time taking for complete conversion of left over char (after flaming process) to ash is known as glowing time.
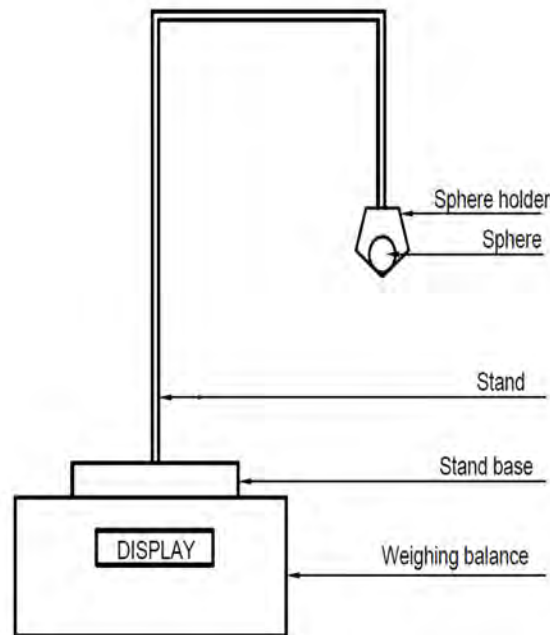
Fig 2.1 Experimental setup for flaming and glowing time measurement

Single particle studies are carried out using an experimental setup as shown in Fig 2.1. The experimental set up is simple, consisting of a stand with pin holder to hold the sample. The stand along with sample has been placed on a weighing electronic balance with the least count is 0.01 g for determining the mass loss with time. The fuel is ignited by using a lamp with a wick. The ignition source is removed immediately after the fuel has ignited, and the yellow flame is observed enveloping the fuel sample. The duration (flaming time) is noted from the moment the ignition has started till the flame ends for flaming and further (glowing time) till the char is reduced to ash after the glowing combustion. Simultaneously, the weight of the fuel sample is noted after

the flame is off. This has been done for estimation of the weight lost during the flaming time. Experiments are conducted on wood spheres (casuarina), wood flakes (eucalyptuses) and coconut shells for obtaining the flaming time; a reflection of the pyrolysis process. Table 2.1 depicts the properties of the fuel samples with different densities and sizes used in the experiments. It is evident from Table 2.1 that fuels with varying properties are used in the experiments with density varying from about 357 ± 17 kg/m^3 to about 1352 ± 12 kg/m^3. It is noticed during experiments that the char particle breaks up into small pieces on the smallest mechanical disturbance. Hence, necessary care has been taken during the experiment to make sure to minimize these problems.

Table 2.1 Properties of fuel sample used in the study

Fuel sample details	Wood flakes	Coconut shells	Wood spheres
Photograph			
Dimension of fuel sample (mm)	25×22×4	25×22×4	Diameter: 10-25
Equivalent diameter (mm)	16.2±0.57	16.2±0.57	10-25
Particle density (kg/m^3)	357 ±17	1352±12	610
Bulk density (kg/m^3)	200±20	650±20	462±20
Moisture content (%)	8-9	8-9	8-9
Ash content (%)	1.0-1.5	<1	<1

2.2 Reactor configurations used in the study

Biomass gasification technology systems consist of a reactor, gas cooling and cleaning system. Fig 1.6 (in Chapter I) represents a typical gasifier systems schematic diagram developed at Indian Institute of Science. Three different reactor configurations are used in the study to address the objectives cited in Chapter I. Table 2.2 presents the specifications of various reactor configurations.

Table 2.2 Different reactor configurations

Size/capacity (kg/hr)	Reactor diameter (mm)	Purpose
3	103	Propagation front movement, bed movement, bed temperature, gas composition
35	350	Field gasifier to validate the propagation front movement, bed movement, bed temperature
60	500	Tar and particulate measurements

Fig 2.2 Gasifier (3kg/hr) with 103 mm diameter reactor

The experiments are conducted in packed bed gasifiers as presented in Table 2.2. Fig 2.2 presents the 3kg/hr capacity or size gasifier of 103 mm reactor diameter. An air nozzle as shown in Fig 2.2 acts as an ignition port. The reactor under consideration is an open top downdraft gasification system with a possibility of sharing the air from the top as well as at the air nozzle. The reactor configurations that are considered in the study are rated at about 3 kg per hour, 35 kg per hour and 60 kg per hour with 103 mm, 350 mm, and 500 mm reactor diameter respectively, developed at the Indian Institute of Science. The other elements of the gasification system under test are the cooling and cleaning system along with the blower. The reactor (3kg/hr) is insulated

with a ceramic blanket throughout its length while the 35 kg/hr and 60 kg/hr are insulated with high alumina bricks to reduce the heat losses.
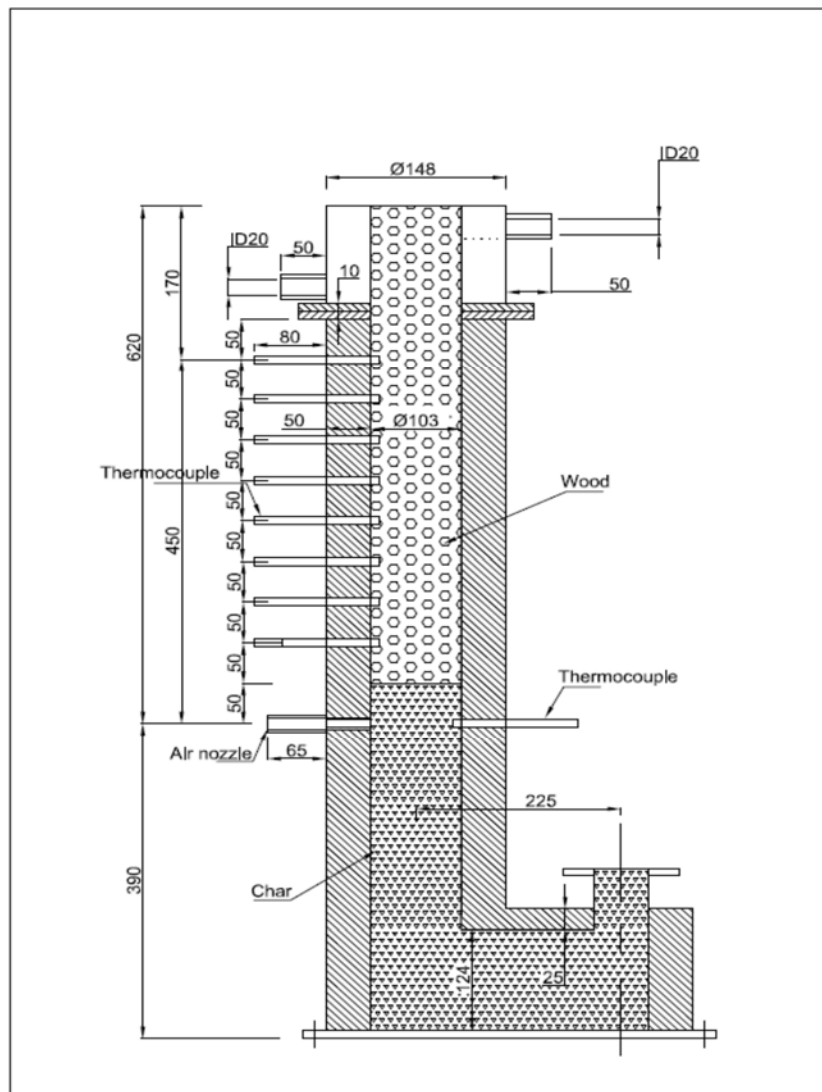
Fig 2.3 Thermocouple arrangement in 3kg/hr gasifier reactor

The thermocouple arrangement along the reactor length for 103 mm diameter reactor is shown in Fig 2.3. The measured parameters during the experiments are gas flow rate, biomass consumption rate, gas composition, bed temperature at reference locations along the length of the reactor, pressure drop at the reactor outlet, reactor exit gas temperature, gas flow rate and gas composition measurement. The gas flow rate is measured by using a calibrated venturi meter, biomass consumption is based

on the topping up method, K type thermocouples are used to measure the bed temperatures at various locations in the reactor and an online gas analyzer (SICK Maihak: S715 Extractive gas analyzers) is used for measuring the different gases like CO, CO_2, CH_4, O_2, and H_2. A high-speed data acquisition system (IOtech, PDAQ 56) is used to record the bed temperature. Table 2.3 represents the ultimate and proximate analysis of *Casuarina equisetifolia* fuel sample used in the experiments.

Table 2.3 Ultimate and proximate analysis of biomass sample
(Casuarina equisetifolia)

Parameter	Ultimate analysis (% dry basis)	Parameter	Proximate analysis (% dry basis)
C	42.83	Fixed carbon	18.38
H	6.236	Volatile matter	81.28
N	0.124	Ash content	0.34
S	0.419	Calorific value (MJ/kg)	18.2
O$^\$$	50.391		
$^\$$ *Measured by difference of weight*			

2.3 Tar and particulate measurement

Different fuels like wood flakes, coconut shells and wood chips with different physical properties are used in the gasifier system towards the measurement of tar and particulates in the exit gas. In this study, the sampling method has been used as reported by Hasler and Nussbaumer, 2000, Mukunda *et al.* 1994, Dasappa *et al.* 2004. Tar and particulates are measured by passing 0.5 m³/hr of gas from the main gas output line and bubbled through distilled water and a solvent to extract dust and tar separately as shown in Fig 2.4. The gasification system is operated at 60 kg/hr for all the fuels, and the gas-sampling rate was 0.5 m³/hr. Iso-kinetic samples are drawn and analyzed to obtain the tar and particulate content in the hot gas. Tar and particulate sampling is carried out using the wet method (Ueki *et al.* 2011). Particulate matter is the amount of solid matter which is filtered from liquids and deposited on the micro-fiber filters. Tars absorbed on the particles are extracted using anisole solvent. Heavy tars are considered as combination of all higher molecular organic compounds with high boiling points, typically above 200 ^{0}C. The heavy tars are determined

gravimetrically as the evaporation (vacuum distillation) residue at 155 ^{0}C that corresponds to the boiling of the solvent used (anisole). The solvent is evaporated after particle removal and extraction with water. The gas sampling consists of a nozzle, gas bubblers, thimble filter, vacuum pump followed by a gas flow meter and a burner in the iso-kinetic setup.
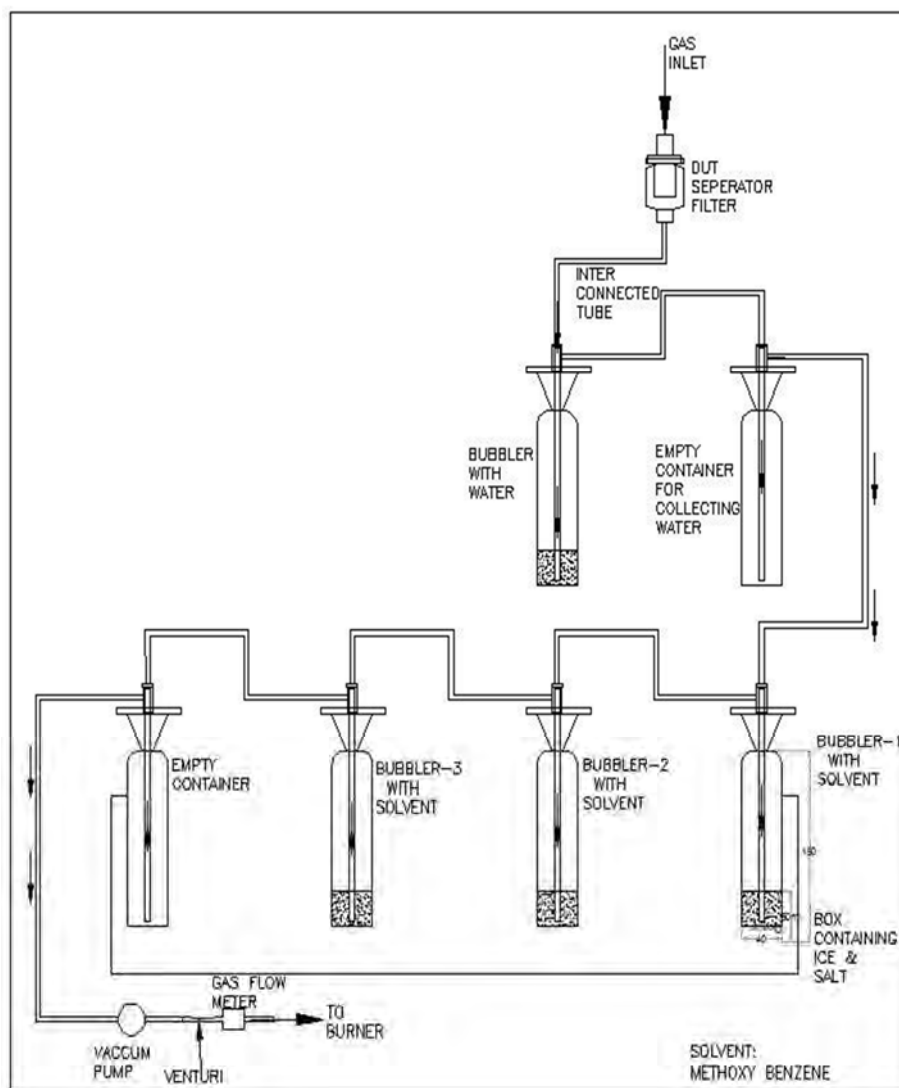
Fig 2.4 Tar and particulate measurement setup

The gas bubbles pass through a bottle containing distilled water and moves to an empty bottle to remove/trap the moisture or water droplet if any carried over from the previous system. The next three bottles contain a solvent, namely anisole (*methoxy*

benzene) followed by an empty bottle as a trap. All the bottles are placed in an ice and salt bath. The gas finally passes through a thimble filter. The thimble filter must be large enough to ensure that the fine dust collection does not pose any serious pressure drop on the suction pump. The gas after being pumped out of the system passes to a swirl burner.

The burner introduced in the circuit has two important features; one is to ensure that the gas is burnt, and secondly to ensure that gas burns in a diffusion mode. If there is any air leakage in the sampling train, it will be evident in the burner apart from measuring the oxygen fraction in the gas. After the sampling, the equipment is cleaned by washing with water and appropriate solvents. Soxhlet extraction process is used to ensure all the tar is extracted from the filter paper used in the capturing of tar and particulate. It is important to state that the sampling has to begin when the system is close to steady state, even if this is not so, the temperature must be reasonably high. In order to achieve this, the flow rates are raised slowly so that this approach would permit the bed temperatures to be built up gradually and also the gas temperature. The reactor exit temperature is in the range of 400 to 450^0C towards ensuring the system has reached steady state before the tar sampling is conducted. The entire ducting carrying the gas to the sampling train is washed using anisole and the sample is mixed with the one collected in the bottle. This procedure is carried out for all the samples.

2.4 Measurement and instrumentation

The instrumentation used for measuring temperature, gas flow rate, and gas composition while conducting the experiments is highlighted in the following section.

2.4.1 Temperature measurement

K type thermocouples are used to measure the bed temperature inside the reactor, and a personal data acquisition system is used to convert the analog voltage signal and connected to the computer. The thermocouples used in the experiments have a bead size including insulation of 1.5 mm. These thermocouples are insulated using a

mineral insulation throughout the length. The thermocouples are connected to the personal data acquisition board using a Teflon cable.

2.4.2 Personal Data Acquisition (PAQ) system

The IOtech make personal data acquisition system is used to acquire the data from thermocouples. Fig 2.5 represents the personal data acquisition system (PDAQ 56) that is used to acquire the temperature data. The analog signal (voltage output) from the thermocouple is acquired into a personal computer through this data acquisition hardware. The data acquisition board has a maximum scanning speed of 80 Hz. In case if more than ten channels are to be connected then an expansion module (PDQ1) is used, and this PDQ1 is connected in series with PDAQ 56. The sampling duration has a direct bearing on the sampling rate. The thermocouple output is connected to the analog input of the data acquisition board. The temperature data are stored in the computer in *.txt format. In this study, the temperature acquisition frequency is 5 s.

Fig 2.5 Personal Data Acquisition System

2.4.3 Flow measurement

The instrumentation used for gas flow measurement is a combination of venturi meter and a manometer. The range of the manometer is 0–100 mm of the water column with the least count of 1 mm of the water column. The discharge of the blower is connected to the venturi meter. The relation for calculating the gas flow rate is given below.

$$Q = k \sqrt{\Delta H}$$

Where Q is the gas flow rate (g/s), k is the venturi constant and ΔH is the pressure head across the venturi in mm of the water column.

2.4.4 Gas composition measurement

The producer gas composition is measured continuously using online gas analyzer SICK Maihak: S715 Extractive gas analyzers. This gas analyzer can measure the composition of carbon monoxide (CO), carbon dioxide (CO_2), methane (CH_4), oxygen (O_2) and hydrogen (H_2). The percentage composition of each of these gases is directly displayed on the screen of the instrument. Fig 2.6 shows the online gas analyzer used for the measurements.
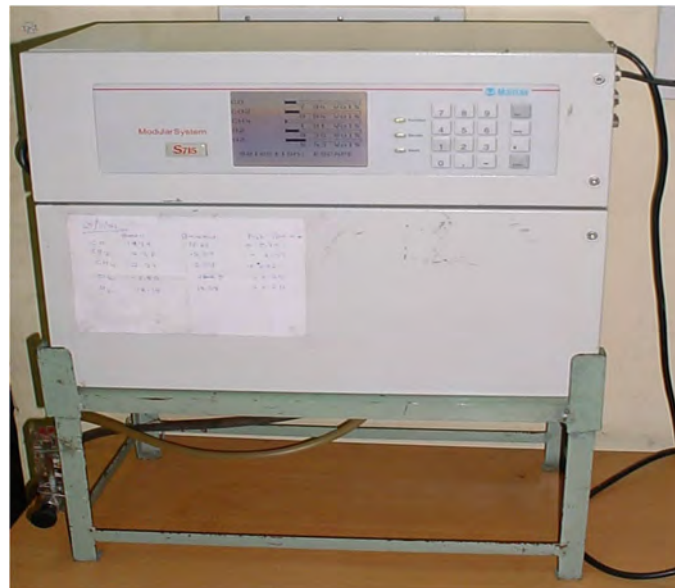
Fig 2.6 Online gas analyzer

The gas analyzer consists of different sensors working on different principle for measuring the percentage composition of the producer gas. The gas sensor used for measuring different gases in the analyzer are Paramagnetic sensor (OXOR-P) to determine the oxygen concentration, Infrared sensor (FINOR) operates with the interference filter-correlation (IFC) principle for measurement of $CH_4/CO_2/CO$ and thermal conductivity sensor (THERMOR) for measurement of H_2 concentration in the gases respectively. The gas composition measurement range for $CO/CO_2/H_2$ is 0-100% and for O_2/CH_4 is 0-25% by volume respectively. The gas analyzer is pre-calibrated

using calibrated gas cylinder, in a range of producer gas composition. The sampling flow rate is maintained at 1-2 liter per minute as per the specification of the analyzer. The gas is cooled by using a copper coil dipped into water and later on cleaned by passing through a cotton filter with a layer of calcium chloride for moisture removal. The gas composition data is acquired every 30 s interval. A special arrangement has been made to remove the contaminants entering the gas analyzer as shown in Fig. 2.7. Fused calcium chloride is used to remove the moisture content in the gas, and the tar particles are removed by cotton. For drawing the gas from the gas line, a vacuum pump is used whose suction side is connected to the gas line and the delivery side is connected to the inlet of the gas analyzer. The gas analyzer is calibrated periodically for accurate measurement of the gas composition.
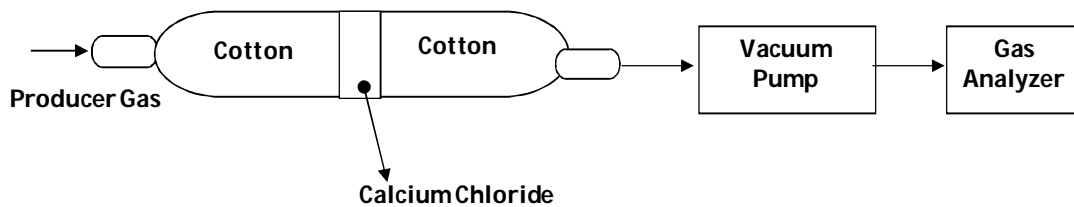
Fig 2.7 Arrangement used for producer gas measurement in gas analyzer

2.4.4.1 Calorific value of producer gas

The calorific value (CV) of producer gas is calculated by considering the lower heating value of the combustible gas. The calorific value formulae used during calculation is given below.

$$CV \left(\frac{MJ}{kg}\right) = \frac{Lower\ heating\ value\ of\ producer\ gas\ (LHV)}{Equivalent\ molecular\ weight\ of\ producer\ gas\ (M)}$$

The lower heating value of producer gas with reference to a sample producer gas composition of CO = 20%, CO_2 = 12%, CH_4=2%, H_2 =20% and rest N_2=46% can be calculated by using the following relations.

$$LHV\ (MJ) = (\%\ CO \times heating\ value\ of\ CO\ ) + (\%\ CH_4 \times heating\ value\ of\ CH_4)$$
$$+ (\%\ H_2 \times heating\ value\ of\ H_2)$$

$$LHV\,(MJ) = (0.2 \times 283\ MJ/kmole\,) + (0.02 \times 795\ MJ/kmole)$$
$$+ (0.2 \times 242\ MJ/kmole) = 120.9\ MJ/kmole$$

The equivalent molecular weight of producer gas is calculated with reference to the same producer gas composition used in the earlier calculation.

$$M\,(kg) = (\%\ CO \times 28) + (\%\ CO_2 \times 44) + (\%\ CH_4 \times 16) + (\%\ H_2 \times 2) + (\%\ N_2 \times 28)$$

$$M = (0.2 \times 28) + (0.12 \times 44) + (0.02 \times 16) + (0.2 \times 2) + (0.46 \times 28)$$
$$= 24.48\ kg/kmole$$

Therefore, the calorific value (LHV) of producer gas is,

$$CV = \frac{120.9\ MJ/kmole}{24.48\ kg/kmole} = 4.93\ MJ/kg$$

2.4.5 Front propagation measurement

The reaction front propagation movement is measured in two different rated capacity reactors (3kg/hr and 35 kg/hr) at various superficial air mass fluxes. In order to measure the progress of the flame front moving up in the reactor, temperatures are measured inside the reactor bed. The flame propagation speed (v_{pm}) is determined by using the following equation;

$$v_{pm} = \frac{\Delta x}{\Delta t} \qquad (2.1)$$

where Δx is the distance between two thermocouples and Δt is the time the flame front needs to move between the respective thermocouples. The flame propagation rate is calculated by knowing the distance between two thermocouples and the time required to reach a particular temperature between those thermocouples. The temperature measurement at reference locations along the length of the reactor suggests that the temperature profile is well established around 773 K (500 ^{0}C) for a range of mass fluxes chosen in the present study. Further, it is also evident from the temperature profile that the time scale for flame propagation between 500 ^{0}C and 900 ^{0}C is not different. Also, the slope of all the profiles (at the different section) in this temperature is approximately same. Hence, the reference temperature for calculation

of flame propagation is chosen at 773 K (500 ^{0}C) in all the sets of experiment. The distance between two consecutive thermocouples is 50 mm in the case of 103 mm diameter reactor and 100 mm in the case of 350 mm diameter reactor. The time required to reach the reference temperature between two consecutive thermocouples is calculated by using the temperature profile of the reactor.

The mass flow rate of output gas is the sum of biomass flow rate and air flow rate. The superficial air mass flux (kg/m^2-s) is calculated by using equation 2.2.

$$Superficial\ air\ mass\ flux = \left(\frac{AtF}{AtF + 1}\right) \times \left(\frac{k\sqrt{\Delta H}}{1000 \times A_c}\right) \qquad (2.2)$$

where AtF is the Air to fuel ratio, which is ranging from 1.5 to 1.8 for biomass gasification, k is the venturi constant, ΔH is the difference in water column height (mm), and A_c is the cross sectional area of the reactor (m^2). Experiments are conducted to calculate the propagation rates in packed bed at varying superficial air mass flux. However, each experiment is conducted under the same initial starting condition. The moisture level in the wood particle is tested before every experiment. The biomass feeding rate is measured by measuring the average biomass feed per hour into the reactor during its operation by topping up method. The bed movement is arrived at by measuring the average bed movement (downward) per unit time interval. In the case of downdraft configuration, the effective propagation rate has two components, the front velocity (flame propagation rate) moving into the fresh fuel bed against both the air flow and the fuel bed, and the bed movement moving downwards. All the experiments are performed at sub-stoichiometric or gasification regimes only.

2.4.6 Experimental procedure

Initially, the reactor is loaded with charcoal slightly beyond the ignition port and for rest of its height is filled with wood particles of a particular size. A blower is used to provide the required suction to draw the air through the top and the nozzle. After the ignition, and ensuring the bed is red hot, the air nozzle is closed, allowing all the air to

be drawn from the top of the reactor. Experiments are conducted with different gas flow rate (air mass flux), and different moisture level and particle sizes of biomass. During this period, the temperature at various locations and the gas composition are recorded. The bed movement and biomass consumption are measured at specific intervals during the experiments. As the bed moves down due to biomass consumption, the reactor is topped up with biomass at regular interval. The topping is done manually depending upon the consumption rate. The output gas is cooled and cleaned before flaring. Specific experiments are conducted for the raw gas tar measurements where hot gas is analyzed using the protocol described in section 2.3. Provision has been made to operate the system with varying air flow from the top as well as through air nozzle in the case of tar measurement. Sharing of air between the nozzle and open top has been carried out by adjusting the top valve seal. After each experiment, the gasifier (reactor) is unloaded and prepared by loading the fresh biomass for further experiments. The moisture level in the wood particle is tested for each experiment. The parameters measured or collected during each experiment are (i) moisture content in biomass samples, (ii) gas flow rate (air mass flux), (iii) gas composition, (iv) biomass consumption (v) bed movement and (vi) temperature profile inside the reactor.

2.5 Summary

The measurement rationality, tools, properties of the fuels used and experimental techniques related to flaming and glowing time for a single biomass particle, tar and particulate measurements for different fuel samples, propagation rate measurement and gas composition experiments are presented in this chapter. The various instruments used for the measurement are also described in this chapter.

Influence of particle size and residence time on gasification process

3.0 Introduction

Biomass gasification yields essentially three different products: gases, condensable tars, and solids (char and ash). Tars are loosely defined as organic condensable (at room temperature) compounds formed during thermo-chemical reactions (Kinoshita *et al.* 1994). Tar in the final gas output is one of the major issues related to the performance of a biomass gasification system. Tar condenses at reduced temperature, blocking the process equipments such as engines, turbines and burners. The gasification temperature and equivalence ratio have significant impact on tar yield and tar composition. Tar yield decreases with the increase in temperature or equivalence ratio (Kinoshita *et al.* 1994). However, actual concentrations of tar in the gas depend upon the reactor design, properties of the feedstock and operating conditions. In order to generate better gas quality, the gasifier performance needs to be optimized by its design and operation practices. In case of a packed bed gasifier two crucial processes take place (i) the heterogeneous reactions between the particle and the reacting ambient resulting in the gaseous species and (ii) gas-phase interaction in the bed resulting in the final products of gasification. Fuels having different physical properties, like size and density, have an effect on pyrolysis and heterogeneous char reaction. This chapter [6] presents the results from experiments on the influence of fuel properties like particle size, shape and density on tar generation in a fixed bed downdraft gasification system. Further, in the case of an open top downdraft gasifier, due to the flame propagation front moving towards the reactor top, the combustion zone is extended, effectively increasing the residence time for the

---

[6] *This work published in*
Mahapatra, Sadhan, Dasappa, S. Influence of surface area to volume ratio of fuel particles on gasification process in a packed bed. Energy for Sustainable Development 2014; 19:122-129.

gas. This has an important influence on the reduction of higher molecular weight compounds in the output gas.

3.1 Studies on fuel particle combustion

The influence of varying biomass properties on the thermo-chemical conversion processes are addressed with simple experiments using individual particles. Wood spheres, wood flakes and coconut shells are used as fuel to establish some of the combustion characteristics of the fuel relevant for gasification. Fig 3.1 represents a typical thermo-gravimetric analysis of biomass (wood) sample where about 75 % to 80 % of the weight loss is recorded below 500 ^{0}C. The initial weight loss is related to the release of moisture, recorded up to 150 ^{0}C. The maximum weight loss occurs between 375 and 500 ^{0}C, during which all the volatiles are driven away from the biomass leaving behind char. The primary products of pyrolysis may repolymerize and undergo further fragmentation (cracking and reforming) and/or react with free radicals. For those pyrolysis processes which are intended for the production of chemical intermediates, the physical parameters such as particle size, heating rates and the nature of the heat transfer medium are all controllable process variables.
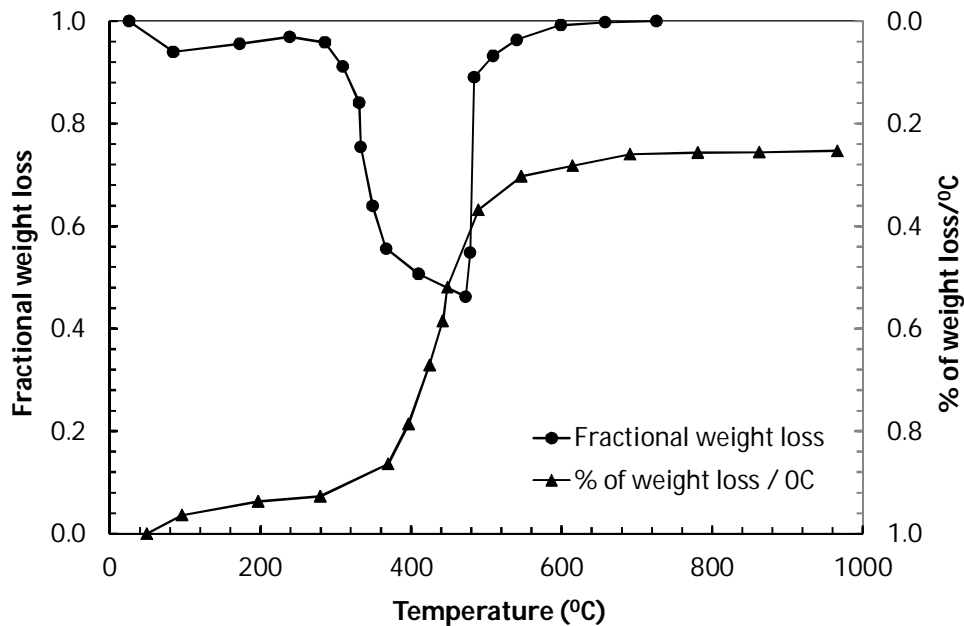
Fig 3.1 Thermo-gravimetric analysis of wood sample

Heat transfer is one of the major experimental variables exercising control over fast pyrolysis. An understanding of the nature of heat transfer is therefore implicit in the definition of fast and slow pyrolysis. The complex chemical mechanisms involved in pyrolysis are a function of heating rate, temperature, gaseous environment, pretreatment, extent of inorganic impurities and catalysis. During slow pyrolysis, biomass particles are subjected to low heating rates while higher heating rate dominates in fast pyrolysis. The typical products of pyrolysis are liquid, solid and gaseous fraction of the C-H-O complex. The ratio of each of these yields depends on the process parameters. The products of slow and fast pyrolysis are significantly different. Fast pyrolysis process is adapted to achieve higher liquid fractions from biomass. Pyrolysis involves the thermal degradation of the solid fuel to lower molecular weight compounds with fractions as $C_nH_mO_p$ involving large number of compounds to products like water, carbon monoxide and carbon dioxide along with char. Fragmentation predominates at higher temperatures, greater than 350 ^{0}C and involves the depolymerization of biomass to tar whose nature depends on the type and composition of the biomass feed and the temperature it is subjected to.

During the char combustion, it is observed that particle size decreases in size with a coating of ash on the outer surface. This phase constitutes of glowing combustion involving diffusion of oxygen to the surface of the porous char and heterogeneous oxidation. These processes are similar to the wood combustion process cited in the literature (Murthy, 1972; Mukunda *et al.* 1984). Gas phase reactions are faster in comparison to solid phase reactions. Murty (1972) attempted to describe the physics of pyrolysis and chemical transformations on the processes of heat and mass transfer. This study included external heat flux to the particle which leads to accumulation of heat within the particle. This accumulation of heat resulted in an inward heat conduction and an outward diffusion of gaseous products. This increase in thermal energy starts the devolatization process and production of smaller molecular weight compounds which diffuse both inwards ahead of the thermal wave and outwards through the hot char layer. The energy conservation inside the particle defines the

internal heat transfer, chemical decomposition and external heat transfer at the surface, modeled by a global heat transfer coefficient that describes the symmetry at the particle centre (Murthy, 1972). A characteristic time τ may be associated with each process:

$$\text{Internal heat transfer } (\tau_{\text{internal}}) = \rho C_P L^2/\kappa$$

$$\text{External heat transfer } (\tau_{\text{external}}) = \rho C_P L h$$

$$\text{and, Chemical reaction } (\tau_{\text{reaction}}) = A e^{(-\frac{E}{RT})}$$

In the above expressions ρ, C_P, L, κ, and h are the particle density, specific heat, characteristic dimension, thermal conductivity and heat transfer coefficient respectively. The chemical reactions are typical of rate expression with A, E, R and T as Arrhenius constant, activation energy, gas constant and temperature respectively. The pyrolysis process is controlled by the devolatilisation rate. The primary condition for this process demands smaller particle size to increase the surface-to-volume ratio and the external heat transfer, while decreasing the internal thermal gradient. Thermal equilibrium between the particle and its surrounding is reached much faster than pyrolysis completion. The relative importance of the internal heat transfer to the external heat transfer is defined by the ratio of their respective characteristic and denoted as Biot Number (B_i).

$$\frac{\tau_{\text{internal}}}{\tau_{\text{external}}} = \frac{hL}{\kappa} = B_i$$

Estimation of the Biot number for various conditions provides an insight into the concept of thermally thin and thick fuel particles. In case of packed bed, the biomass particles are comparatively large in diameter (few millimeters to a few centimeter sizes). In the present case, Biot number varies between 0.4 - 8 for a particle diameter of 2 mm to 40 mm respectively. Therefore, the pyrolysis of biomass particle in packed bed system falls in thermally thick regime. Heat transfer from the surface to core or the conduction of heat plays an important role on the overall rate of pyrolysis and particle conversion time. In the gasification process, apart from pyrolysis, char-gas reaction is equally important phenomenon. Char oxidation and reduction is a complex

phenomenon governed by diffusion, adsorption and desorption of reactants and products coupled with reaction.

3.1.1 Results from single particle experiment

The entire process of wood combustion consists of distinct flaming and glowing combustion processes. The flaming and glowing times for wood and briquette spheres for various diameters are presented in Table 3.1. The briquette sphere data is taken from literature (Gnandendra *et al.* 2012).

Table 3.1 Flaming and char glowing time for fuel samples

Diameter	Flaming time (s)		Char glowing time (s)	
(mm)	Wood	Briquette	Wood	Briquette
10±2	60 ± 5	55 ±8	220 ±8	450 ±10
15±1	120 ±6	134 ±10	500 ±10	757 ±15
20±1	200 ±6	160 ±15	750 ±13	970 ±20
25±1	270 ±8	265 ±18	950 ±15	2154 ±22

It can be observed from the Table 3.1 that the glowing time is about 3.5 to 4.2 times higher than flaming time in the case of wood sphere. It also can be observed from Table 3.1 that the flaming time for a 10 mm wooden sphere with a density of 610 kg/m^3 is about 60 s and the glowing time is about 250 s; briquettes of the same diameter with a density of 910 kg/m^3, the flaming time is almost same, and the char glowing time is 450 s. In case of wood sphere the volatile fraction is 81% (Table 2.3) against 70 % in case of briquettes, whereas the ash fraction in the wood sample is 0.34 % (Table 2.3) and for briquettes it is 11 %. The flaming time for the briquettes is similar to the wood sphere, except that the volatile fraction is lower and ash content is higher compared to wood. The results clearly indicate that the char glowing process has a distinct effect of density. However, the effect of density on flaming time may not be suitable to comment as the volatile fraction and ash fraction of both the samples are different. The char glowing time is found to be about 4 to 5 times higher in comparison to the flaming time, which suggests that the heterogeneous char reaction is much slower than the flaming process. Earlier work in this laboratory has shown that the typical particle size shrinkage is about 10-12 % during flaming combustion,

which affects some of the bed parameters in a packed bed configuration (Mukunda *et al.* 1984; Dasappa *et al.* 1998). Reed *et al.* (1988) has also evaluated the dependence of flaming pyrolysis time of a wood particle on density and is given by

$$t_{fp} = 0.207\rho F_s(1 + 1.76F_m)D(1 + 0.61D)\ exp\left(\frac{4369}{RT}\right)/(1 + 3.46F_{O2})$$

Where, D=typical dimension (cm), ρ=fuel density (g/cm^3), F_m=moisture content (%), F_{O2}= fraction of oxygen (%), F_s=sphericity. Hence, the time for flaming pyrolysis is dependent on particle size, shape, density etc.

Wood flakes and coconut shells with different physical properties are studied for the combustion characteristics under flaming combustion. Table 2.1 (Chapter II) presents the thermo-physical property details of these fuel samples used in this study. The duration (flaming time) is noted from the moment the ignition has started till the flame ends for flaming using the procedure discussed in Chapter II.

Table 3.2 Equivalent diameter and flaming time of wood flakes and coconut shells

Length (mm)	Width (mm)	Depth (mm)	Volume (mm³)	Equivalent diameter (mm)	Particle density (kg/m³)	Flaming time (s)	Surface area / volume (mm⁻¹)	Flaming time/density (s/kg-m⁻³)
Wood flakes								
24	21	4	2016	15.7	358	36	0.68	0.10
23	22	4	2024	15.7	341	33	0.68	0.10
27	24	4	2592	17.0	347	40	0.66	0.12
24	22	4	2112	15.9	368	37	0.67	0.10
26	22	4	2288	16.4	372	39	0.67	0.10
25	20	4	2000	15.6	355	35	0.68	0.10
26	24	4	2496	16.8	356	43	0.66	0.12
Average				16.2	357	37.5	0.67	0.11
Coconut shells								
24	21	4	2016	15.7	1347	158	0.68	0.12
23	22	4	2024	15.7	1353	160	0.68	0.12
27	24	4	2592	17.0	1346	179	0.66	0.13
24	22	4	2112	15.9	1372	166	0.67	0.12
26	22	4	2288	16.4	1356	169	0.67	0.12
25	20	4	2000	15.6	1367	155	0.68	0.11
26	24	4	2496	16.8	1320	173	0.66	0.13
Average				16.2	1352	165.7	0.67	0.12

Table 3.2 summarizes the results from several experiments using wood flakes and coconut shells as fuel samples. Equivalent diameter for a non-spherical sample has been arrived at based on the volume relationship. It is important to identify that the surface area/volume is about same for both wood flakes and coconut shells. However, it can be observed that there is a distinct difference in the density of these two fuel samples. It is clear that the overall conversion time normalised with respect to density is about the same 0.11 ±0.01 s/kg-m^{-3}. Hence, it can be concluded that the increase in time for conversion for coconut shell is due to the higher density. This aspect of increased time for flaming pyrolysis will be revisited during the discussion on the evaluation of tar during the producer gas generation.

Table 3.3 Analysis of flaming time for different fuels

Fuel	Particle density (kg/m^3)	Flaming time (s)	Flaming time/ particle density (s/kg/m^3)	Ratio of surface area to equivalent diameter in compare to wood sphere
Wood sphere	610	120	0.200	1
Wood flake	357	38	0.106	1.88
Coconut shell	1352	166	0.123	1.97

It is observed from Table 3.3 that the flaming time for wood flakes is almost one fourth that of coconut shells for same equivalent diameter fuel samples and one-third that of standard wood sphere. The comparison of time for flaming normalized with respect to the density is also presented in Table 3.3, where the effect of particle density is addressed. For a fuel sample with 15 mm equivalent diameter of wood sphere with density 610 kg/m^3, the flaming time is 120 s. Comparing with wood sphere, the normalized value is nearly one half for wood flakes and coconut shells. It must be observed that the density of the coconut shells is more than two times that of wood spheres. It is clear from the above findings that the flaming rate which is an indication of pyrolysis rate is double in the case of flakes compared with the wood sphere. It is also observed from Table 3.3, that the ratio of surface area to equivalent diameter in comparison to wood sphere is nearly double in the case of flakes and also the coconut shell. This is reflected in the data on the flaming time thus increasing the pyrolysis rate in a given packed bed reaction volume. The normalized flaming time in both the cases

has reduced by half while the surface area to equivalent diameter ratio is increased twice compared with wood sphere. Increased rate of pyrolysis enhances volatiles release, which further increases the gas volume fraction thus reducing the residence time in a given packed bed reactor geometry. With increase in temperature, rate of pyrolysis increases and at heating rates of the order of 100 K/s fast pyrolysis process is predominated based on the energy flux received on the small size particles resulting in higher fractions of long chain hydrocarbon in the pyrolysis gases. With the reduction in residence time, cracking of the higher molecular weight compounds is significantly affected. These factors increase the tar fraction in the producer gas. The studies on single particle analysis can be summarized as (i) increased surface area increases the pyrolysis rate, (ii) increased density of the particle increases flaming time and (iii) ratio of surface area to equivalent diameter plays an important role on the flaming time. Having identified the surface area/volume, as an important fuel property along with the density, experiments are focused on the influences of this parameter on gas quality. These aspects are important while changing fuels for a given reactor geometry where various dimensions are fixed.

3.2 Tar and particulates measurements

Experiments are conducted in a downdraft gasifier (500 mm diameter reactor) (Table 2.2) using wood chips, flakes and coconut shells to measure the tar and particulates in the exit gas. The reference fuel (Standard wood chips of sizes 30×30×30 mm), with an equivalent diameter of 37 mm is used in the experiments. Tar and particulate sampling is carried out as per the procedure presented in Chapter II. The gasification system was operated at 60 kg/hr for all the fuels with top closed and only air nozzles open. This ensured the overall gas throughput and hence major thermal energy balance of the reactor nearly same. The reactor exit temperature is found between 450 to 500 ^{0}C in all the cases. The gas sampling rate is 0.5m^3/hr. The sampling duration varied between 1 and 2 hours. Iso-kinetic samples are drawn at the hot end of the gasifier and analyzed to obtain the tar and particulate content in the raw gas after steady state of operation. Table 3.4 present the tar and particulate

measurements in the gas for wood flakes, coconut shells and standard wood chips. It is clear from Table 3.4 that the amount of tar is in the range of 336 to 416 mg /m^3 in the case of wood flakes, about 1650 to 2000 mg/m^3 for coconut shells and for standard wood chips, the measurements indicate a range of 48 to 77 mg/m^3. The particulate matter in the gas is slightly higher in the case of flake owing to smaller fuel size probably resulting in higher dust loading in the gas.

Table 3.4 Tar and particulate tests data for wood flakes, coconut shells and standard wood chips

Total gas flow (m^3)	Time duration (hr)	Total particulates (mg/m^3)	Total tar (mg/m^3)
Wood flakes			
0.469	1	1103	351
0.417	1	929	376
0.821	2	1054	336
0.883	2	1516	416
Coconut shells			
0.44	1	656	1768
0.42	1	832	1970
0.90	2	689	1651
0.85	2	666	1960
Standard wood chips			
0.450	1	875	77
0.470	1	773	56
0.965	2	830	68
0.904	2	678	48

3.2.1 Analysis of the results

In typical downdraft gasifiers with air as gasifying medium, the tar content in the raw gas is in the range of 500-3000 mg/m^3 which strongly depends on the reactor design, feedstock, moisture content in the feedstock and also the operating load conditions (Knoef, 2012). The strong dependence of type of biomass is evident from the data on field evaluated values of tar. The tar fraction with rice husk as the fuel is about 40 times that of wood (Knoef, 2012). It is shown in the study by Phuphuakrat *et al.* (2010) that as the equivalence ratio increased from 0.30 to 0.32 and the temperature increased marginally from 995 to 1014 ^{0}C, the tar content in the syngas decreases from 11800 to 6560 mg/m^3 at the exit of reactor (before cleaning), in a downdraft fixed bed gasification systems. Dogru *et al.* (2002) study reported that the tar and dust

content is in the range of 6370–8380 mg/m^3 in a throat type downdraft gasifier, whereas the throat less type downdraft gasifier produced the highest tar yield of 13000 mg/m^3. Comparing the current measured data on tar in raw gas and those available in the literature clearly suggests that there is a strong dependence on particle size/shape and tar generation on reactor geometry. In order to address the solution of such concern, further analysis towards improving the residence time and its influence on tar present in the gas is described in the following section.

Towards arriving at typical processes occurring inside the gasifier, where heat transfer to particle from gas phase occurs; hence heat transfer analysis is carried out. A simple numerical evaluation suggests that for a heat flux of 20 kW/m^2, the heating rate is about 3 K/s for a 30 mm wood particle. However with the same heat flux for a 4 mm thick wood flake, the heating rate is about 12 K/s. Heat flux has a significant influence on the pyrolysis rate and hence on the product of pyrolysis. Thus it is evident that the flake behavior is different compared with the sphere.

The major consideration for the design of downdraft configuration is to reduce the tar level in the raw gas, improve the carbon conversion in the reactor and eliminate any channeling. The central part of the argument towards tar cracking is promoted by two means (i) uniform distribution of high temperature across the char bed and (ii) presence of reactive char. High temperature in the reaction zone being favorable for cracking of complex chemical structures to smaller ones is a well known phenomenon. It is reported that tar fraction is reduced substantially if a tar filled gas passes through a hot bed of charcoal (Kaupp and Goss, 1984). The other consideration is the residence time in the reactive zone. The effective bed thickness in which char and high temperature exists depends on the flow of air in the reactor. At low flow rates implying improved contact time in the bed, nominal bed temperatures attained which is sufficient to crack the tar. This is due to the total travel distance being same in the case of a closed top gasifier. Higher bed temperature provides compensatory effect for the lower residence, so that the effective tar cracking is maintained throughout the

load range. Thus, bed temperature, surface area and the residence time are critical for the thermal cracking of tar.

For a given reactor geometry, the residence time is designed to meet throughput of fuel gas generation of a desired quality. Hence, with the change in pyrolysis rate, both the quantity of pyrolysis and the quality of products variation has a significant influence on the quality of the gas generated. It is in this connection that particle size is empirically fixed or arrived as a multiple of throat diameter to have a certain designed pyrolysis rate process, in the case of downdraft fixed bed gasification system (SERI, 1979).

Based on the particle aspect ratio, the pyrolysis process has a significant influence on the volatile fractions. The experiments are designed using wood as fuel to address the influence of the gas residence time in the reduction zone on tar fractions. This is carried out using an extended reducing zone by providing air at varying location and also by varying air flow at nozzle (Fig 3.2).
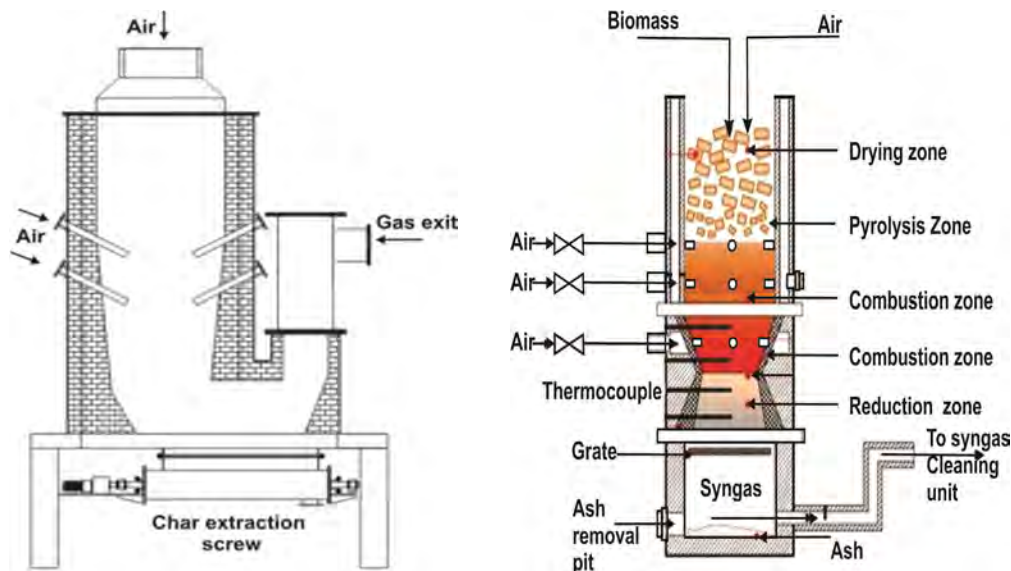
Fig 3.2 Reactor with multiple air entry

Table 3.5 presents the average data from several experiments on tar and particulates in a downdraft gasification system operated with different ratio of air between the

nozzles at the bottom and from the reactor top. It can be observed from Table 3.5 that with the decreasing fraction of air flow from the nozzle, the tar level at hot gas reduces. This is due to the consequence of increasing the residence time of the gas in the high temperature zone. Introduction of air above the air nozzles helps in increasing the combustion zone length, allowing pyrolysis to occur above the air nozzle with reference to case 1 as in Table 3.5. In the case 3 and 4, with increase in the air fraction at 600 mm above the air nozzle, the combustion and the reduction zone has extended, resulting in an increased residence time. With the superficial velocity at 0.42 m/s in the reactor calculated at 1000 K temperature, the additional increase in residence time of the gas is about 1000 ms from case 1 to case 4. The actual velocity through the bed depends on the porosity which is a strong function of particle sizes and fragmentation occurring during pyrolysis process.

Table 3.5 Effect of increase in residence time on tar and particulate

Case	Nozzle air flow to total air flow ratio	Particulates (mg/m^3)	Tar (mg/m^3)
1	0.986	1850±32	1058±29
2	0.690	1260±29	217±16
3	0.506	895±22	49±8
4	0.353	743±18	47±8

As an extension of improving the residence time, preliminary investigations are carried out using wood flakes and coconut shells towards addressing the importance of residence time on the gas quality. With multi nozzle downdraft reactor configuration used in the present study, the analysis is based on the air flow rates from top and through nozzle and the pressure drop across the bed reveal that the air flow through the nozzle has been high compared with the standard wood configuration. Table 3.6 summaries the results on the effect of air flow share between nozzle and top for two different fuel samples.

Table 3.6 Effect of air flow behavior (nozzle and top) on tar and particulate with wood flakes and coconut shells

Case	Nozzle air flow to total air flow ratio	Particulates (mg/m^3)	Tar (mg/m^3)
Wood flakes	0.5	1850±32	5638±59
Coconut shells	0.35	776±18	108±12

In the case of wood flakes, the bed resistance is about five times higher than that of coconut shells and three times higher than wood spheres resulting in an increased air flow from the nozzle in comparison with the wood sphere or coconut shells. In order to address the bed resistance, Ergun equation is used towards estimating the pressure drop along the length of the packed bed (Green and Perry, 2007). Equation 3.1 depicts the dependence of the pressure drop across the bed, with properties related to bed porosity, particle size, cross sectional area of the reactor and fluid (air) properties like density and viscosity.

$$\frac{dP}{dL} = -\frac{(1-\varepsilon_b)V_a}{D_p\varepsilon_b^3 A_C}\left[150\frac{(1-\varepsilon_b)\mu}{D_p} + 1.75\frac{V_a\rho_a}{A_c}\right] \qquad (3.1)$$

In the above expression, P is the pressure, L is the length of the reactor, ε_b is the bed porosity, V_a is the air flow rate, μ is the air viscosity, D_p is the particle diameter, ρ_a is the air density and A_c is the reactor cross sectional area. It is evident from equation 3.1 that for a given particle size and air flow rate; porosity is one of the critical parameters influencing the bed resistance.
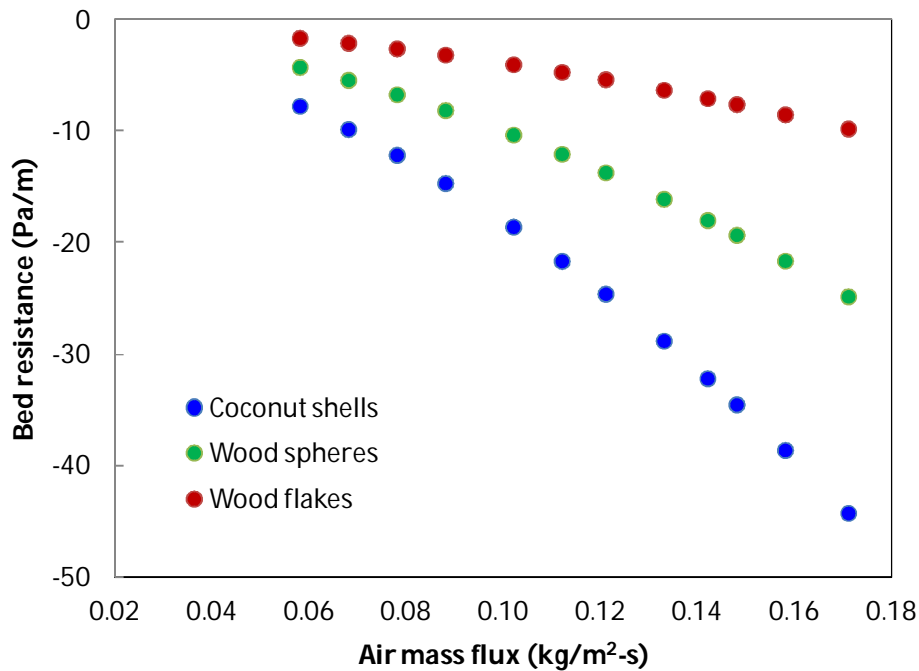
Fig 3.3 Bed resistance for wood flakes, wood spheres and coconut shells in a 500 mm diameter reactor

Fig 3.3 compares the bed resistance for coconut shells, wood spheres and wood flakes as a function of the air mass flux estimated based on equation 3.1 for similar equivalent particle diameter. For a given air mass flux, the bed resistance for the air to flow from the top of the reactor with wood flakes as the fuel is higher than wood spheres and coconut shells. This is attributed to the lower bed porosity for wood flakes (0.37) as compared to wood spheres (0.43) or coconut shells (0.55). This allows preferential air flow rate from the nozzle and hence the thermal front as well as the residence time is affected. The experimental result also indicates the same. With increase in bed resistance the air flow from the top of the reactor reduces and hence the operation moves towards closed top configuration. This affects the propagation rate and reduces the effective reactive bed height. This has an influence on the residence time of the gas in the hot bed which influences the cracking process and the tar level seems to have significantly reduced. The results using coconut shells is found favorable due to the overall bed porosity which allowed more air to be drawn from the top compared to wood flakes. Further work is required both in regulated/controlled, which is partly development studies and beyond the scope of the present study.

3.3 Summary

This chapter has depicted the importance of air flow rate, particle size and density on the overall thermo-chemical process and in particular on the tar generation. The experiments have clearly indicated the need for improvement in residence time inside the reactor for reducing the tar content in the raw gas. The flaming time has been estimated for different biomass samples. The flaming rate an indication of the pyrolysis rate is higher for higher surface area per unit volume particles. Particles with higher surface area per volume are subjected to higher pyrolysis rate resulting in fast pyrolysis products. It is also important to note that at increase in surface area per unit volume, fast pyrolysis can also predominate based on the energy flux received on the small size particles resulting in higher fractions of long chain hydrocarbon in the pyrolysis gases. It is observed that the tar level in the raw gas is about 80 % higher in the case of wood flakes compared with standard wood pieces. The analysis suggests

that the time for pyrolysis is lower with a higher surface area particle and is subjected to fast pyrolysis process resulting higher tar fraction with low char yield. Increased residence time with staged air flow has a better control on residence time and lower tar in the raw gas. The quantity of tar generated depends on the heat flux that the particle is exposed to. The experiments and analysis provide a scientific basis for the generation of high tar in fixed bed gasification system for small size wood pieces.

Propagation front under gasification regimes in packed bed

This chapter presents the results from experiments on the packed bed towards analysing the influence of air mass flux on flame propagation rate, bed movement, bed temperature, gas composition and associated parameters. The primary objective is to evaluate the process parameters to increase the residence time of gas at a higher temperature.

4.0 Introduction

The propagation front [7] in a packed bed can be classified as counter-current and co-current propagation, relative to the direction of the air and solid fuel movement. In the case of counter-current propagation, flame front propagates in a direction opposite to that of air flow (Fig 1.9). In the case of a co-current (downdraft) configuration, apart from the flame front moving upwards into the fresh fuel bed, the bed moves (contributed by size reduction during pyrolysis and fuel consumption) downward direction. Further, the bed movement due to conversion process also influences the propagation front. These aspects has been introduced in Chapter one. The rate of propagation front movement is primarily controlled by air mass flux, volatile fraction of the fuel and the surrounding reactive environment of the particle. In the case of a packed bed, depending upon the air flow rate, propagation flame front moves into the virgin fuel. The propagation rate, which is influenced by air flow, combustion and heat transfer process also depends on the fuel properties like size, density, thermal conductivity, moisture content, ash content and calorific value. However, not all these parameters are independent variables. Most of the identified parameters are interrelated and drawing conclusions on the dependence of each

---

[7] *This work published in*

Mahapatra, S., Dasappa, S. Experiments and analysis of propagation front under gasification regimes in a packed bed. Fuel Processing Technology 2014; 121: 83-90.

parameter separately on the propagation front movement seems impractical. The other factors that have an influence are related to the bed parameters, like, bed porosity, peak temperature and heat loss from the reactor.

In an open top downdraft gasifier or co-current configuration, air enters from the top and the output gas is drawn from the bottom in the form of a combustible gas. In a gasifier, variation in the air flow rate leads to change in the ambient condition in the vicinity of the particle leading to changes in the combustion zone profile and the rate of combustion. This essentially leads to variation in the rate of movement of the biomass particles. The air mass flux is an important parameter associated with the gasifier/reactor design. Most of the performance characteristics of gasifier depend upon the air mass flux, which controls the gas production rate, gas energy content, fuel consumption rate, power output, etc. In an open top downdraft gasifier, as air is drawn from the gasifier top, after ignition there is an upward movement of the combustion (reaction or propagation) front into the moving bed of wood char particles. The propagation front movement with respect to air mass flux acts as a design tool for fixing the gasifier/reactor dimensions. It is also possible to establish the turndown ratio for the gasifier system based on the understanding of the propagation front propagation.

The results discussed here are from the experiments conducted in the present study towards establishing the effect of air mass flux on the propagation rate, bed temperature, gas composition and related aspects under sub-stoichiometric operating conditions in an open top downdraft packed bed configuration. Depending upon the air flow rate for a given reactor volume and surface area of the particles in the packed bed, the overall process varies between gasification (rich) and combustion (lean) regimes. Further, in the case of downdraft configuration, it is important to consider the propagation flame front along with bed movement to address the overall influence on the temperature profile in the reacting bed. In the co-current (downdraft) configuration, the bed movement (contributed by size reduction during pyrolysis and

fuel consumption) is in the downward direction and the flame front movement into the fuel bed in the upward direction against the air flow. Effective propagation rate is calculated as a sum of flame propagation rate and bed movement. Hence, in the case of downdraft configuration, the effective propagation rate has two components, the front velocity (flame propagation rate) moving into the fresh fuel bed against both the air flow and the fuel bed, and the bed movement in the downward direction. The flame propagation, bed movement and effective propagation rates are measured for different air mass flux. Table 4.1 summarizes the results from the literature on various reactor configurations and the present study. It can be observed from Table 4.1 that except in the present study, in all other cases, reverse downdraft or counter-current configurations are used for the experiments and analysis. The surface area per unit volume has been calculated for all the cases, and it has been found that the surface area per unit volume for wood chips and pine shavings is relatively high compared to that in all other cases. Similarly, the void fraction in the packed bed is also high in these two cases. In all the experiments, except in the present study and Horttanainen *et al.* (2000) study, the fuel samples are spherical. The sphericity for all the cases is calculated, and it has been found that the sphericity is close to one except in this present study and for wood chips (Horttanainen *et al.* 2000).

Table 4.1 Fuel properties and reactor configurations summary from literature and present study

Fuel sample	Dimension (mm)	Equivalent radius (mm)	Surface area / volume (mm^{-1})	Sphericity	Density (kg/m^3) Bulk	Particle	Void fraction	Moisture (%)	Heating value (MJ/kg)	Reactor configuration	Reference
Casuarina	14×10×10	7	0.49	0.889	370	610	0.39	0	18.2	Downdraft/ co-current	Present Study
	14×10×10	7	0.49	0.889	370	610	0.39	10	18.2		
	17×13×10	8	0.47	0.787	345	610	0.43	5	18.2		
	20×12×10	8.5	0.47	0.773	350	610	0.43	5	18.2		
	h=30, d=30	17	0.20	0.874	410	610	0.33	10	18.2		
Not available	6.4	3.2	0.94	0.998	300	663	0.60	Not available	14.0	Reverse downdraft/ counter-current	Fatehi and Kaviany, 1994 [8]
	10	5	0.60	0.999	200	500	0.55	10	18		Gort, 1995 [9]
Wood chips	5-20	3	1.89	0.561	157	500	0.69	10.8			Horttanainen et al. 2000 [10]
Pine	8	4	0.75	0.999	307	579	0.47	9.1	19.3		Rönnbäck et al. 2001 [11]
Wood pellets	3.8	3.8	0.79	0.999	690	1180	0.42	6.2	16.3		Porteiro et al. 2010 [12]
RDF pellets	7.4	7.4	0.41	0.999	340	560	0.39	17.9	14.6		
Pine shavings	1.3	1.3	2.31	0.998	150	530	0.72	8.5	17.5		

---

[8] *Wood particle diameter is 6.4 mm, bulk density is calculated by considering the void fraction to be 0.6.*

[9] *In this study, 10 mm diameter wood particles are used and the density of the particle is considered to be 500 kg/m^3.*

[10] *Wood chips are 5-20 mm, the average size 12.5x5x1.5 mm is considered for surface area per unit volume calculation.*

[11] *Diameter of the wood particle is 8 mm.*

[12] *In this study, the fuel particle size is given in equivalent radius.*

4.1 Experimental results and discussion

4.1.1 Temperature profile in the packed bed

Fig 4.1 represents the typical temperature profile inside the reactor over a two-hour period operation at an air mass flux of 0.12 kg/m^2-s. The propagation front is seen moving from the ignition port towards the top of the reactor into the fuel bed. The downstream of the flame front, i.e., below the ignition nozzle, has a slightly lower bed temperature due to the reduction reactions occurring in the char bed.
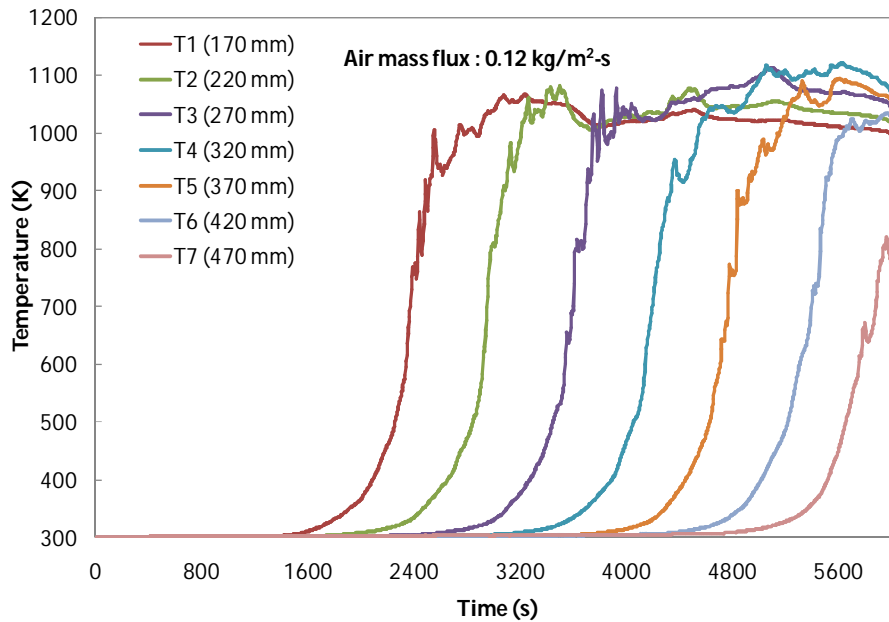
Fig 4.1 Temperature profiles at an air mass flux 0.12 kg/m^2 s

Fig 4.2 presents the temperature profile more than the two-hour period at an air mass flux of 0.20 kg/m^2-s. It can be observed from Fig 4.2 that temperature profile is not moving upward from the air nozzle point (T_0 thermocouple) to the bed. At an air mass flux of 0.20 kg/m^2-s, the flame front is not moving into the virgin fuel bed, as heat balance has established between the heat generation and heat loss due to convective cooling that leads to higher heat loss from the reaction zone. This indicates that front is moving either downward towards the char bed or no upward movement. This phenomenon suggests that beyond this air mass flux (0.20 kg/m^2-s), the reactor ceases to function as gasification configuration providing high residence time, due to

the reverse propagation of the front. The propagation front movement is calculated from the temperature profiles at various air mass fluxes.
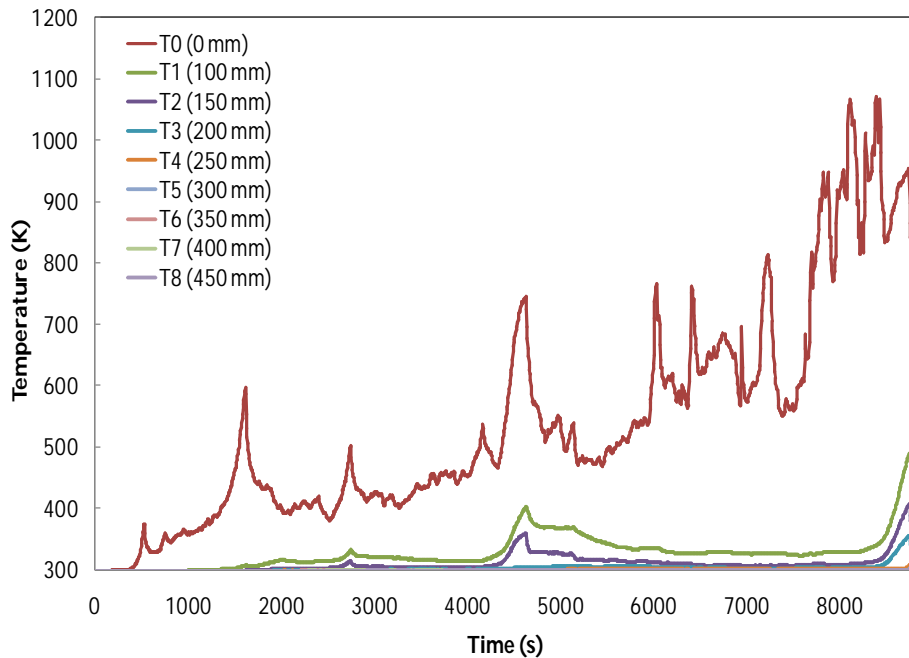
Fig 4.2 Temperature profile at an air mass flux 0.20 kg/m²-s

4.1.2 Flame front propagation at various air mass flux

Fig 4.3 presents the flame front propagation, bed movement and effective front movement variation for the bone-dry wood sample in the co-current configuration over a range of air mass flux. The flame propagation front is derived from the axial temperature profile along the length of the reactor. The bed movement is an indication of the biomass consumption due to bed shrinkage factor resulting from pyrolysis and char consumption and shows a nearly linear variation with the air mass flux. The flame propagation rate initially increases, reaches a maximum and then decreases with increasing air mass flux. The peak flame propagation rate is 0.089 mm/s at 0.132 kg/m²-s air mass flux for bone-dry wood. It is observed that in the range of air mass flux used in the system, the effective propagation rate reaches a maximum of 0.21 mm/s at 0.147 kg/m²-s air mass flux and beyond that no significant increase is observed.
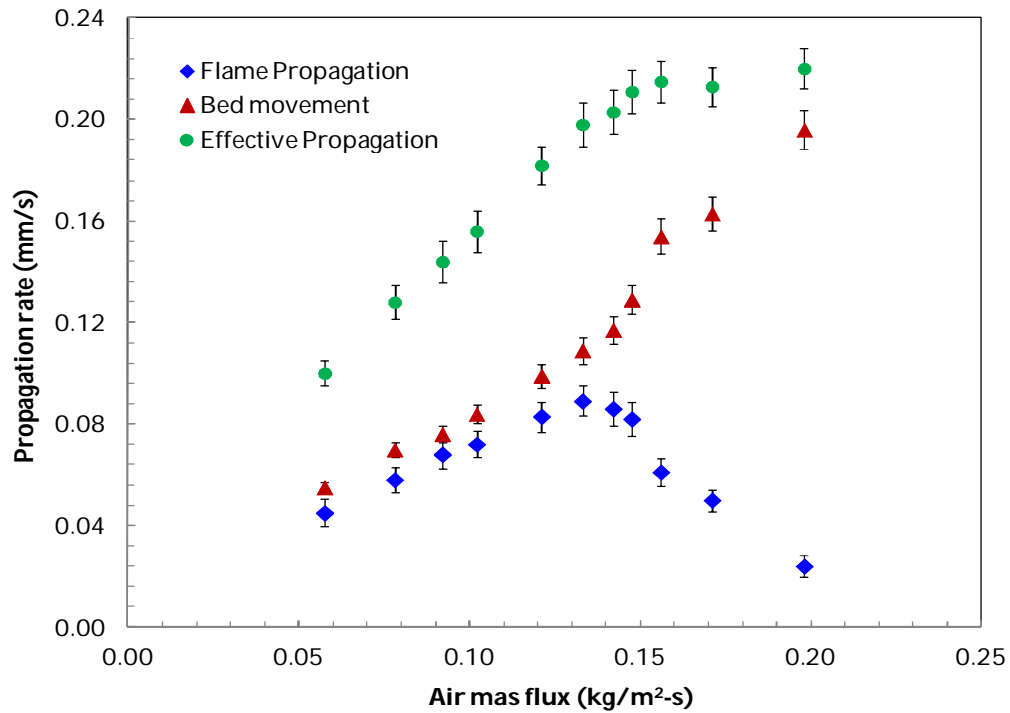
Fig 4.3 Propagation rate for bone-dry wood at different air mass flux

In the flame front propagation profile (Fig 4.3), a balance is established between heat generation by chemical reactions, radiant heat transfer to the unburnt fuels, convective cooling by primary air, and heat loss rate from the reactor surface. As the gasification process in a packed bed is sub-stoichiometric combustion process, associated with fuel rich conditions, the amount of fuel consumed depends on the oxidizer available in the bed. At lower air mass flux, suggesting low fuel consumption rate leads to overall lower heat generation. With the increase in air mass flux, oxidizer fraction in the given reaction zone improves heat generation resulting in an increase in the bed temperature. The flame front propagation rate also increases. When the flame front propagation rate reaches its maximum (peak), the heat generation from the fuel is higher. In the peak flame front situation, a balance is established between the heat generation by chemical reactions and the heat transfer to the unburnt fuels, convective cooling and the heat loss from the reaction zone. With further increase in the air mass flux, convective cooling dominates resulting in flame propagation rate reduction, while the peak bed temperature increases, though marginally.

4.1.3 Effect of moisture on propagation rate and peak temperature

The variation of flame front propagation rate and peak bed temperature with air mass flux for different moisture content is presented in Fig 4.4. There is a distinct variation in the propagation rate with moisture variation. The peak flame front rate for bone-dry wood shifts at higher air mass flux compared to that for moist wood as seen in Fig 4.4. This aspect is related to the fraction of combustibles generated in the bed. With the increase in moisture content both temperature and volatile fraction in the gas phase change and influence the combustion process that occurs within the packed bed. It may be noted that this aspect is similar to an increased heat loss from the reaction zone reducing the peak propagation rate.
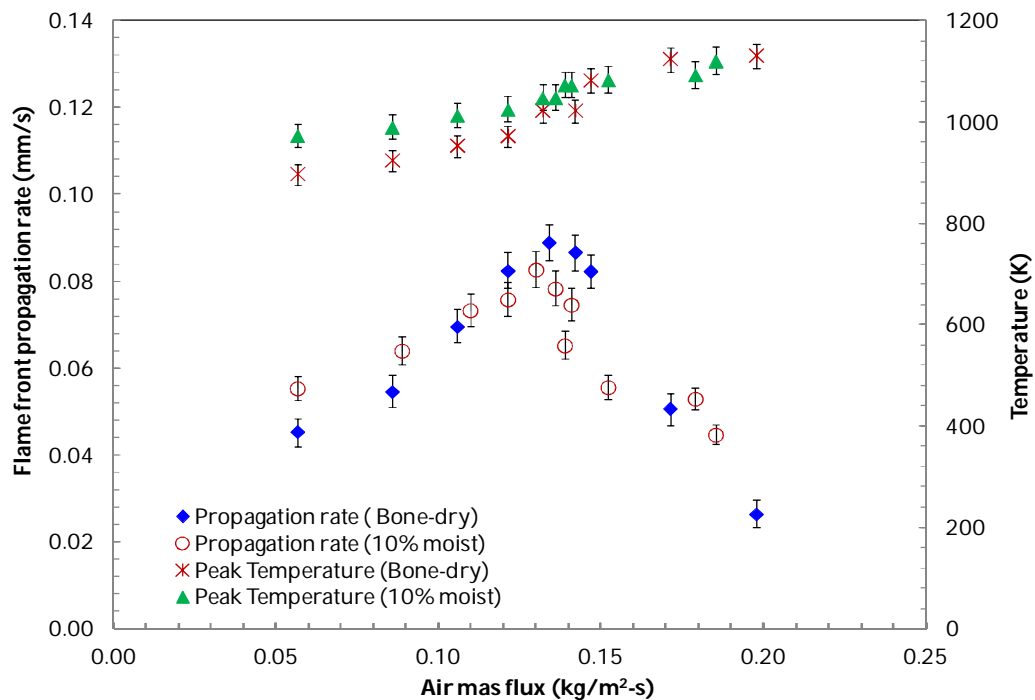
Fig 4.4 Flame front propagation rate and peak temperature for different air mass flux

It is evident from Fig 4.4 that the flame propagation rate initially increases as the air mass flux increases, reaches a peak propagation rate at a certain air mass flux, and further increase in the air mass flux results in a decrease in the flame propagation rate, both for bone-dry wood and 10 % moist wood. However, the peak bed temperature increases with the increase in air mass flux. Increasing the air mass flux

is accompanied by a higher flame front propagation rate, with increased heat generation in the reaction zone. The peak flame front propagation rates are 0.089 mm/s for 10 % moist wood and 0.095 mm/s for bone-dry wood respectively. These peak propagation rates occur with the air mass flux in the range of 0.130 to 0.134 kg/m^2-s. The experiments also revealed that the flame front propagation rate decreases with the increase in moisture content of the fuel. This is due to endothermicity involved in the drying of the moist wood. In the present case, the propagation rate for bone-dry wood is about 6 % higher than that for the wood with 10% moisture content. The trend of flame front propagation in the present case is very similar to that observed by Dasappa and Paul for charcoal in the downdraft configuration (Dasappa and Paul, 2001). An increase in air mass flux increases the heat release in the bed, which corresponds to higher bed peak temperature. However, there is not much variation of peak temperature for bone-dry wood and 10% moist wood, and the peak bed temperature is about 1100 K.

It is also observed from Fig 4.4 that the peak flame temperature rises with the increase of primary air flow rate. At lower air mass flux, the moist fuel has slightly higher peak flame temperature than bone-dry wood. However, for higher air mass flux ranges moisture did not have any noticeable effect on the maximum bed temperature. Yang *et al.* (2006) state that the peak flame front propagation rate is inversely proportional to the moisture content of the fuel. While this is not evident from the data, it is true that the endothermicity associated with the drying of the biomass affects the propagation rate. Further, it is not evident from the analysis that higher moisture content in the fuel results in higher moisture evaporation rate and intensifies the char burning but reduces the devolatilization rate (Dosanjh, 1987). The possible explanation for this phenomenon is that if the bed temperature is to be maintained; with increase in H_2O content in the reactive environment, char conversion is higher compared with the case of CO_2 based on the reactivity of char with steam and CO_2. Comparing the conversion time for the different reactive environment, it has been shown that the conversion time depends on the reactive

ambient and the particle size (Dasappa and Paul, 2001). Thunman and Leckner (2001) study observed that propagation movement depends on the airflow rate and moisture content of the fuel samples, as the moisture content of the fuel increases, the reaction front propagation slows down. Horttanainen *et al.* (2000) and Porterio *et al.* (2010) also conclude that higher moisture content in the fuel lowers the maximum ignition flux achieved, regardless of any other parameters. These aspects are related to the amount of moisture and volatiles released in the reaction zone and need further investigations.

4.1.4 Gas composition at different air mass flux

Fig 4.5 presents the average cold gas composition (dry) at the exit of the cooling and cleaning system of the gasifier, along with estimated calorific value at different air mass flux values for both bone-dry and 10% moist wood. The variation of calorific value for bone-dry wood is between 3.4 and 3.8 MJ/kg and for 10% moist wood, it is 3.4 to 4.1 MJ/kg over the entire air mass flux range. The calorific value is lower than the measured value for a field system of larger capacity, which is in the range of 4.5 ± 0.1 MJ/kg (Dasappa *et al.* 2004). The reason for lower calorific value is probably the scaled-down nature of this small capacity reactor, which has higher heat loss per unit surface area of the reactor. However, these considerations are not part of the present investigations. The CO concentration is almost constant throughout the air mass flux range for both bone-dry wood and 10 % moist fuel. The hydrogen fraction is slightly different in these cases, and the balance is established by CH_4 variations in both the cases. Table 4.2 provides the average gas composition and calorific value over the entire range of air mass flux for bone dry and 10 % moist wood. It can be concluded from Table 4.2, that over the entire range of air mass flux, the gas composition is nearly constant, and it suggests that the overall reaction occurs in the sub-stoichiometric regimes within the bed.

(a)

(b)
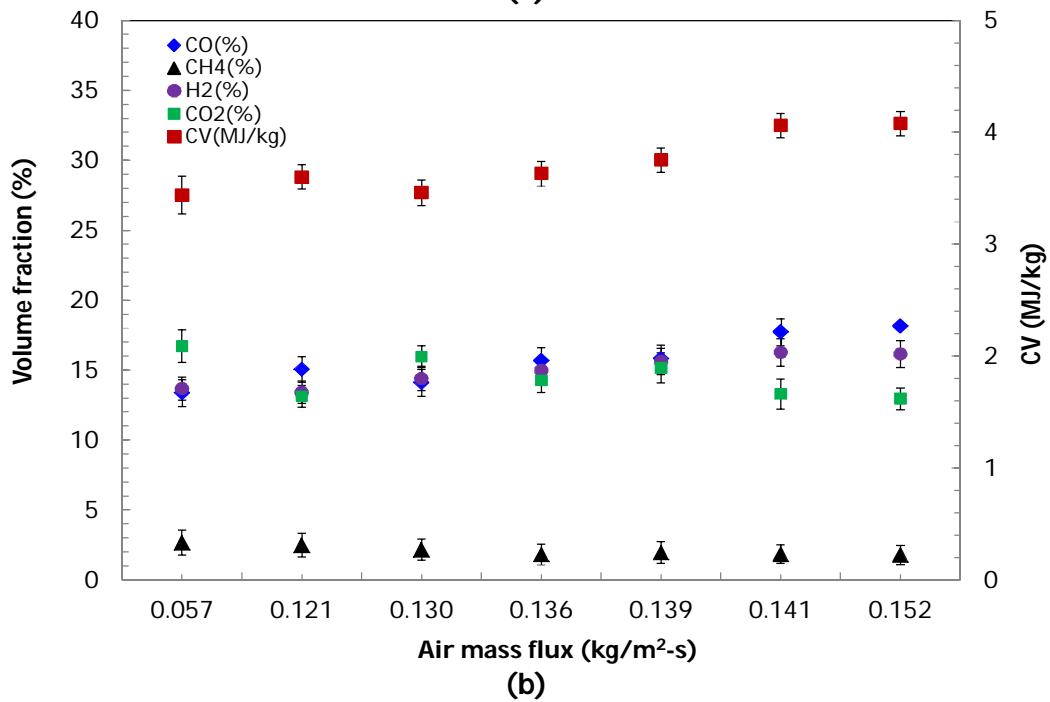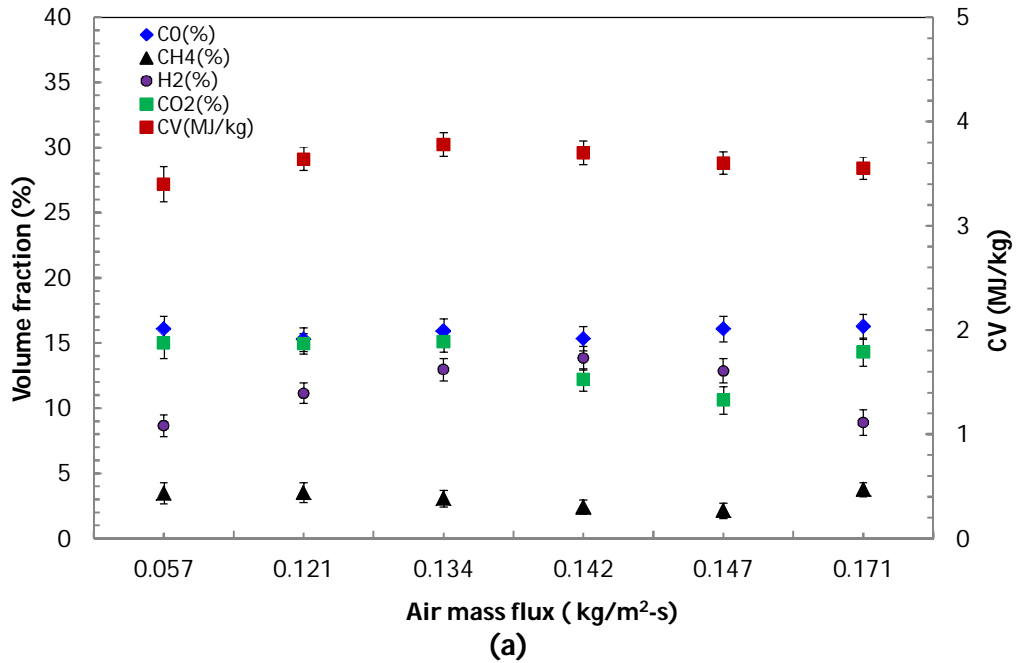
Fig 4.5 Gas composition and calorific values at different air mass flux for (a) bone-dry (b) 10% moist wood

Table 4.2 Average gas composition and calorific value for bone-dry and 10% moist wood

Wood	CO (%)	CO_2 (%)	CH_4 (%)	H_2 (%)	CV (MJ/kg)
Bone-dry	15.83±0.42	13.70±1.86	3.08±0.65	11.40 ±2.21	3.62±0.13
10% moist	15.70±1.75	14.49±1.49	2.10±0.35	14.92 ±1.15	3.71±0.26

4.1.5 Flame front movement, effective movement and peak temperature for different fuel size and different capacity gasifier

Fig 4.6 presents the flame front propagation for different fuel sizes at two different size reactors (3kg/hr and 35kg/hr). It can be observed that the peak flame front occurs for the bone-dry biomass sample. In all the experiments, the flame front profiles are nearly same, and the peak occurs in a narrow band of the air mass flux for the 3kg/hr gasifier capacity. However, in the case of 35 kg/hr gasifier capacity, the peak flame front shifted slightly towards lower air mass flux compared to the 3 kg/hr gasifier capacity.
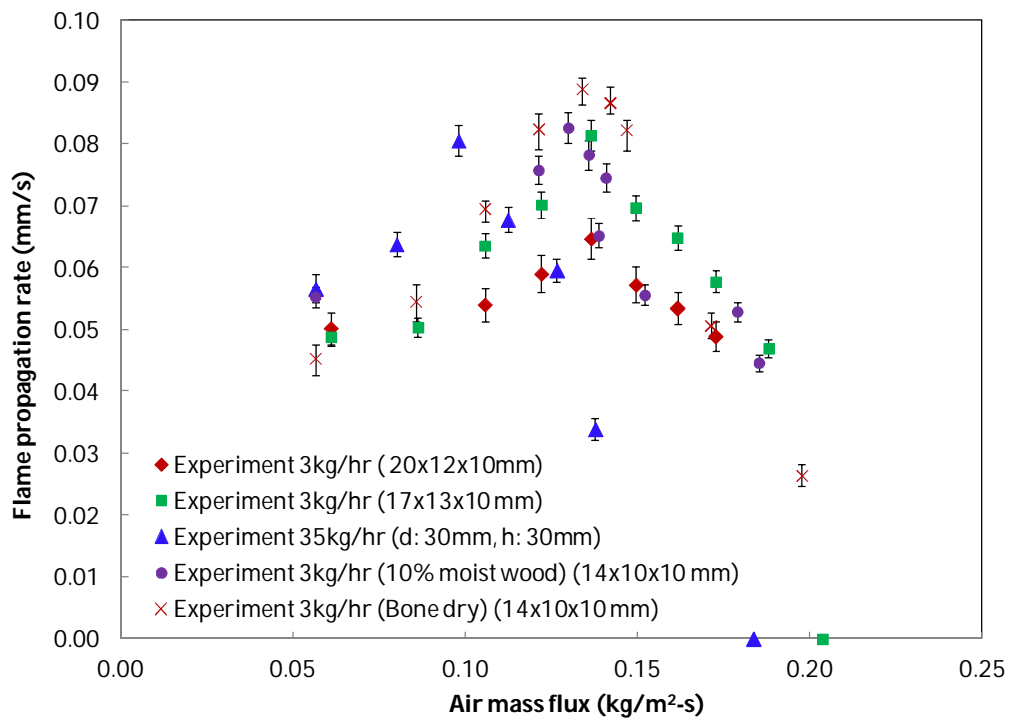
Fig 4.6 Flame front propagation rate for different fuel size

The extinction limit is also established for both the gasifiers, at which flame front propagation become zero. However, the general trend as observed in Fig 4.6, the flame front propagation rate increases as the air mass flux increases, attains a peak and then decreases with further increase in air mass flux and leads to extinction at higher air mass flux. In the case of 3 kg/hr gasifier, the surface area/volume ratios of the fuel samples are very close to each other (0.47 to 0.49). However, in the case of 35 kg/hr gasifier, the fuel sample used in the experiment has the surface area/volume ratio of

0.20. Horttanainen *et al.* (2000) observed that as the surface area/volume increase, the front propagation is faster. It is also found that the ignition mass flux increases with the increase of the porosity of the bed and sphericity of the particles (Horttanainen *et al.* 2002). In this study, the bed porosity of the fuel samples in case of 35 kg/hr is 0.33 and in the case of 3 kg/hr gasifier, it is in the range of 0.43-0.49. Pérez *et al.* (2012) study found that the reactor diameter does not have a significant effect on the propagation rate. Shin and Choi (2000) also observed that as the particle size increase, means smaller surface area per unit mass decreases leads to decrease in flame propagation speed. Ryu *et al.* (2006) found that the ignition front speed is inversely proportional to the bulk density of the fuel samples. It is also observed that small particles have higher ignition front speed in comparison with large size particles. This is due to the slow devolatilization of the large size particle due to thermally thick. Based on the current experiments as well those observation available in the literature suggests that the difference in peak propagation in these two different capacity gasifier (3 kg/hr and 35 kg/hr), primarily depends on the different in fuel sample surface area/volume ratio and the bed porosity.

Fig 4.7 presents the effective propagation movement for different fuel sample sizes and gasifier capacities. The effective propagation movement in a co-current configuration is the summation of flame front movement and bed movement. It can be observed from Fig 4.7 that the effective propagation movement linearly increases with the increase in air mass flux. It lies in a narrow band in case of all the fuel sample sizes and gasifier capacities. It also can be observed that the bulk density of the fuel bed in all these cases is close in nature (345-410 kg/m^3). Hence, the variations in effective propagation movement are not significant. In a later section, the effect of bulk density on the effective propagation movement is discussed in details.
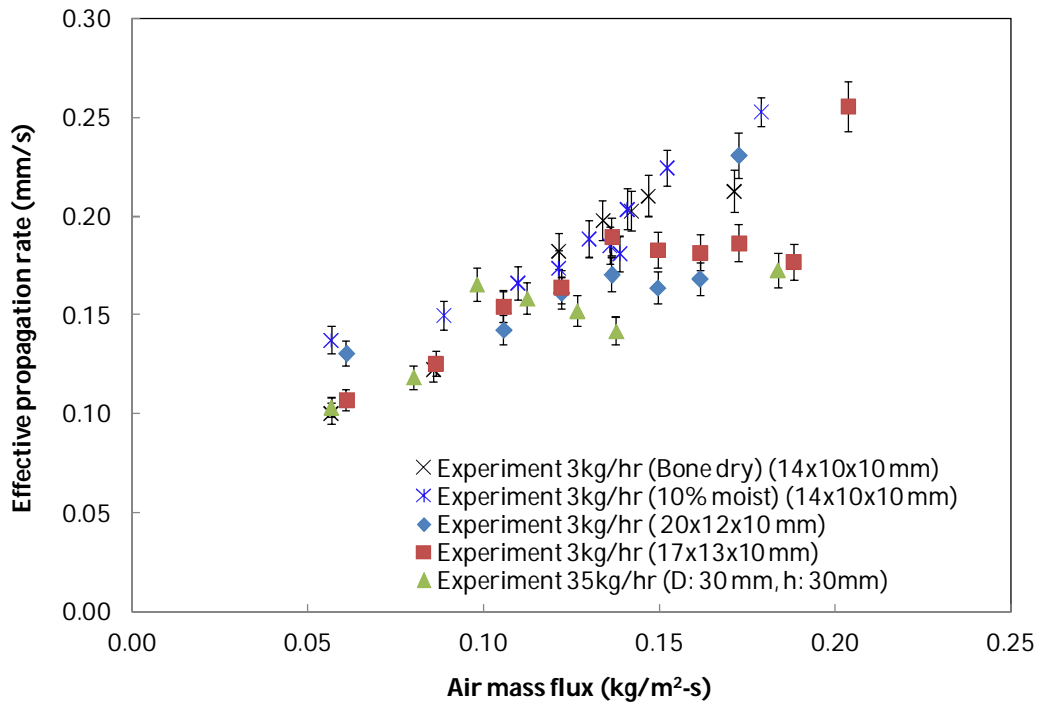
Fig 4.7 Effective propagation for different fuel size
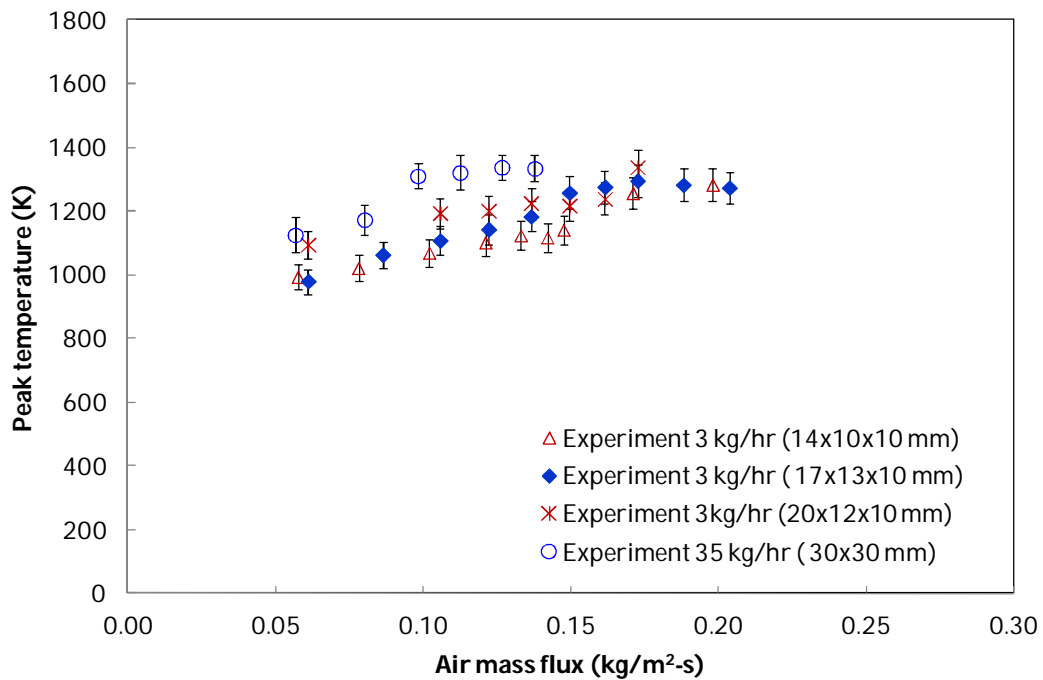
Fig 4.8 Peak temperatures at different air mass flux

Fig 4.8 presents the peak bed temperature for different fuel size samples in both the gasifiers. It can be observed that the peak bed temperature lies very closely in all these

cases. The bed temperature increases with the increase in air mass flux. At higher air mass flux, the bed temperature is almost flat. The heat loss term dominates as the air mass flux increases, due to higher convective cooling from the system. The bed temperature in the case of 35 kg/hr is slightly higher than the 3 kg/hr gasifier is due to the better insulation in the first case.

4.2 Comparison with the literature data

4.2.1 Effect of air mass flux on propagation rate

Fig 4.9 represents the effective propagation rates at various air mass flux values. Presenting the results using effective propagation rates is appropriate to compare the propagation rate from the literature with different experimental configurations (downdraft / co-current or reverse downdraft / counter-current). The effective front movement increases with the air mass flux until a certain air mass flux beyond which the rate has a declining trend.
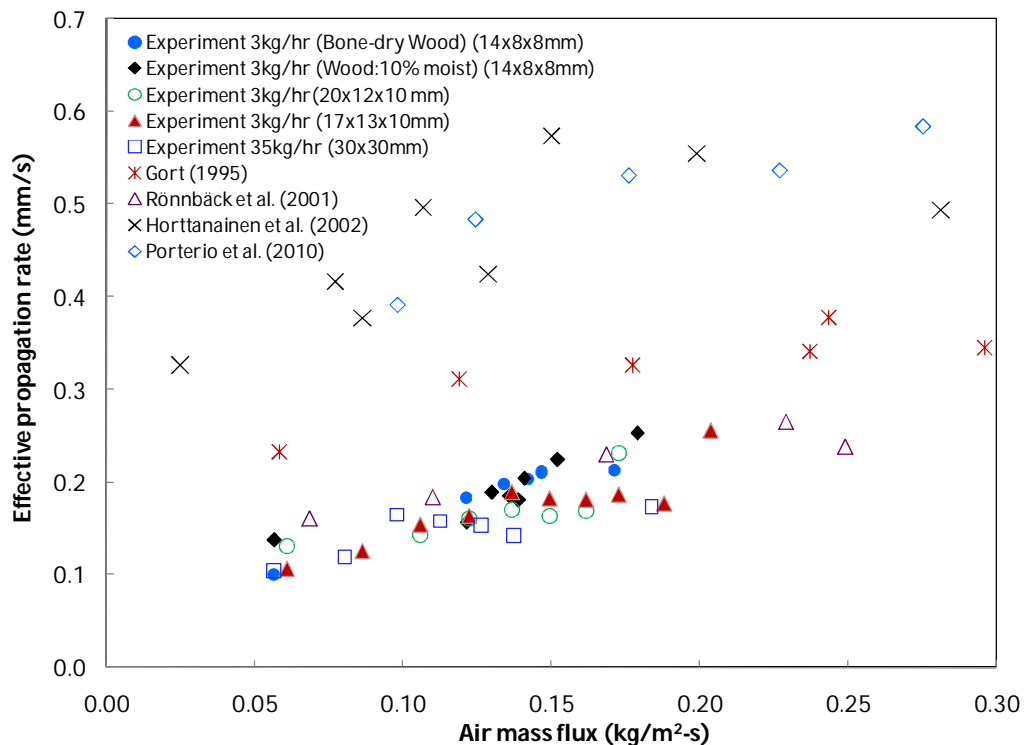
Fig 4.9 Effective propagation rate at different air mass flux

The effective propagation rate for the present experiments is compared with those in the experiments of Gort (1995), Horttanainen *et al.* (2000), Rönnbäck *et al.* (2001) and Porterio *et al.* (2010). It can be observed from Fig 4.9 that, except for wood chips (Horttanainen *et al.* 2000) and pine shavings (Porterio *et al.* 2010) all the other results fall in a narrow band, within experimental error limits considering varying configurations and test conditions. The surface area per unit volume for wood chips and pine shavings are relatively high compared with the other cases. However, the bulk density of these two fuels is very low compared to the other fuels (Table 4.1). The effect of bulk density on effective propagation is discussed in later section.

It is important to highlight that for the range of air mass flux (gasification regime) the effective propagation front reaches a peak of about 0.2 mm/s. Beyond a certain air mass flux, propagation rate decreases with an increase of the air mass flux, but the bed movement increases with the air mass flux in the co-current configuration. The attributes to these two factors are different. However, beyond a certain air mass flux, the heat loss term dominates and reduces the propagation rate. While in the case of bed movement, the rate of increase in bed movement (fuel size shrinkage and consumption) is much higher than the rate of decrease in the propagation flame front. This also can be observed from Fig 4.9; at lower air mass flux the rate of effective propagation is much higher and at higher mass flux ranges the rate is almost constant.

4.2.2 Effect of particle surface area on propagation rate

It can be observed from Table 4.1 that the surface area per unit volume for wood chips and pine shavings is 1.89 and 2.31 mm^{-1} respectively and for all the other cases, this value ranges from 0.4 to 0.9 mm^{-1}. Horttanainen *et al.* (2000) concluded that the increase in bed porosity makes the flame propagation quicker since the thermal energy required to heat the bed volume to the ignition temperature is reduced when bed density decreases and the particle surface area to volume ratio increases. It is observed from Fig 4.9 and the discussion on the packed bed analysis in the previous section, that higher front movement is observed in the case of wood chips and pine

shavings. This is due to the higher surface area per unit volume as a result of smaller particle size and shape. Similarly, the bulk densities of wood chips and pine shavings are much lower than the bulk densities of all other fuels and hence the void fraction is higher compared to other fuels. Lower surface area/volume ratio reduces the inter-particle heat transfer and leads to lower propagation rate. It is also to be noted that the time for pyrolysis is inversely proportional to the surface area, thus increasing the surface area increases the pyrolysis rate for the same temperature. Further, it is clear that the propagation rate depends on the surface area and bed porosity. The higher the surface area, the higher will be the heat transfer rate process; while the increase in the void fraction tends to reduce the convective heat transfer coefficient but again radiative heat transfer becomes prominent (Dasappa and Paul, 2001), which compensates for the convective mode of heat transfer. The combination of higher surface area per unit volume and void fraction together enhances the heat transfer from the hot zone to the colder particle layer. Thus, the higher surface area per unit volume and the lower bulk density are the reasons for higher propagation rate for wood chips and pine shavings. Hence, the propagation flame front with thin particles is high compared to that for particle beds that consist of spherical or cubical particles. Further, it is also important to mention that the surface area per unit volume is more important parameter than the size of the particle. Gort (1995) and Horttanainen *et al.* (2000) showed that the particle size does not have a significant effect on the effective propagation rate. The scatter in Fig 4.9 can be attributed to the differences in the physical properties of the fuel used in experiments by various authors.

Fig 4.10 represents the propagation flame front flux (kg/m^2-s) at different air mass flux values. The flame front flux is defined as the flame front movement normalized with the bulk density. It represents the amount of fuel ignited per unit area per unit time. It can be observed from Fig 4.10 that the results for wood chips and pine shavings are nearly the same in comparison with the other data from the literature. Thus, it may be appropriate to normalize the flame propagation rate with the bulk density to account for any variation in the bed properties. Hence, it can be concluded

that the front velocity has a direct correlation with the density of the fuel bed. Horttanainen *et al.* (2000) also found similar kinds of results. It is evident that the physical properties of the fuel like particle shape and size, bed density, particle density, and moisture content influence the effective front movement. However, it is very difficult to specify a single parametric dependence on the front propagation rate.
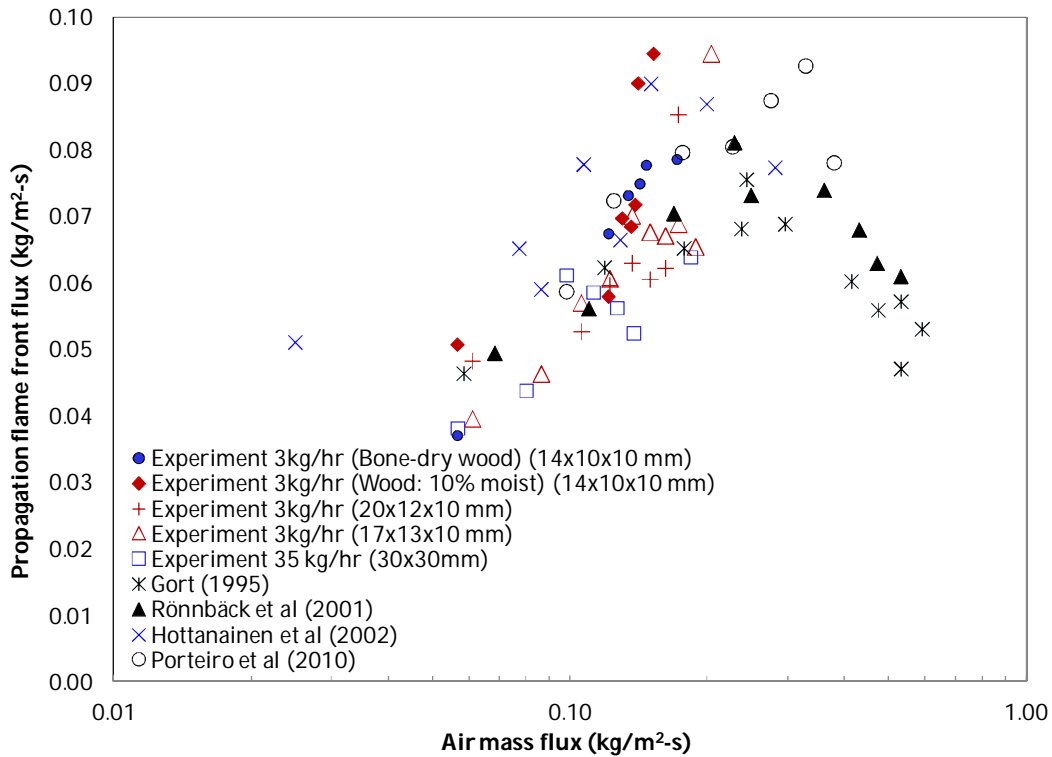
Fig 4.10 Propagation flame front flux at different air mass flux

4.3 Summary

This chapter analyses the results of experiments on the propagation rate in a packed bed under gasification conditions in a co-current reactor configuration. Experiments using wood chips with different size and moisture content are carried out under gasification conditions. The influence of air mass flux on the propagation rate, peak temperature, effective propagation and the gas quality are investigated. It has been shown that the effective propagation rate in a co-current reactor is a combination of flame front movement and bed movement unlike in a counter-current reactor. It is observed from the experiments that the flame front propagation rate initially

increases as the air mass flux increases, reaches a peak propagation rate and further increase in the air mass flux results in a decrease in the propagation rate. However, the bed movement increases with the increase in air mass flux. The experimental results provide an understanding on the influence of the fuel properties on propagation front. The surface area per unit volume of the particles in the packed bed plays an important role in the propagation rate. It has been found that the effective propagation rate compares well, and the results are found to lie in a narrow band except for the cases of wood chips and pine shavings. These differences are shown to be due to the high surface area per unit volume and the low bulk density of wood chips and pine shavings. Further, it has been shown that normalized propagation rate or the propagation flame front flux or ignition mass flux is a better way to present the result to account for the bed density variation. It can be concluded that the physical properties of the fuel like particle shape and size (surface area per unit volume), bed density, particle density, the energy content of fuel and moisture content together have an impact on propagation front movement.

CHAPTER V

Mathematical model for packed bed analysis

5.0 Introduction

In order to analyze the results from experiments and also compare with the packed bed reactor results from the literature, the in-house developed code for packed bed reactor is used in the present study. The overall process and the governing relations are highlighted in this chapter. The model has been validated for various single and packed bed operating conditions (Sandeep and Dasappa, 2015). The in-house available model for char gasification has been modified for biomass gasification system considering pyrolysis process, gas phase volatile combustion, and heterogeneous char reactions along with gas phase reactions in the packed bed (Dasappa 1999; Sandeep and Dasappa, 2015). The propagation front movement is primarily controlled by air mass flux, volatile fraction of the fuel and the surrounding reaction environment of the particle. The following paragraphs briefly present the model as per the above-cited references towards rendering details of the in-house model.

5.1 Modeling of particles in packed bed

Gasification is a complex process during which solid biomass reacts with the gasifying medium and form gaseous fuel under certain environment. The reactor consists of a packed bed of biomass particles where heterogeneous reactions take place between the reactant and the solid fuel. In the present case, biomass moves from the top of the reactor along with the air and the output gases comes out from the bottom of the reactor. Biomass consumption depends on the air mass flux, as the air mass flux increases, biomass consumption increases. Hence, any changes in the gas flow rate resulted in the changes in the downward movement of the bed (due to biomass consumption and shrinkage) unlike the counter current configuration. Similarly, with the increase in air mass flux in the reactor bed, gas flow rate increases, leading to change in the conditions in the vicinity of the particle. Hence, during biomass

movement inside the reactor, particles are exposed to varying ambient/surrounding conditions. To reinstate the gasification process, after the ignition in the packed bed reactors, the particles react with the incoming air/gaseous species surrounding the particle to form the gasification products. The process involves diffusion and convection of the species and energy in the porous medium of the particle and heterogeneous reactions between the gaseous species and the solid char. Heterogeneous reaction, takes place within the particle resulting in release of gases from the particle. The gaseous species surrounding the particle act as a reactant for the heterogeneous reaction. Hence, the heterogeneous reactions between the particles and surrounding ambient results in the gaseous products and the gas phase interaction between the gaseous products and bed results in the gasification products.

Studies related to bed parameters and influence of the input variables, such as air mass flux, fuel samples physical properties (size, density, moisture), etc. on gasification performance or producer gas composition is limited. In the present study, the model is set out for a single particle and later on extended to packed bed towards addressing the performance of a co-current packed bed reactor. Validation of the model for pyrolysis has been extensively carried out by Sandeep and Dasappa (2015) for both inert and reactive environment and the analysis is further extended to packed bed. The model comprises of sub-process like pyrolysis, gas phase volatile combustion, and heterogeneous char reactions along with gas phase reactions in the packed bed. The following approaches are used for the analysis of thermal degradation of biomass fuel in the packed bed reactor.

(a) detailed solid and gas phase reaction mechanisms to address the variability in the thermodynamic properties in the packed bed,

(b) multi-component problem, with an approach towards variability in the biomass properties,

(c) single particle detailed analysis addressing the intra and inter-phase transport phenomena at the particle and the packed bed reactor and,

(d) estimation of flame front movement, bed movement, gas composition, and effects of particle size, bed temperature within the bed.

The propagation rate, gas composition and other parameters are estimated by using this model and compared with the experimental results from two different capacities/sizes gasifier using wood as the fuel and available results from the literature.

The physical processes occurring for single particle are modelled by using unsteady spherically symmetric one-dimensional conservation equations. The assumptions made in this model are (i) conversion process is one-dimensional (ii) pressure gradient within the particle is neglected since the porosity of the particle is high (iii) uniformity in temperature between gas and solid (char) (iv) uniformity in the emissivity of entire biomass/char particle and (v) volatile constitutes 80% of the particle weight and rest 20% is char or fixed carbon (typical for wood). The gasification process is like a transition from solid biomass to gaseous phase due to the reaction inside the particles. As the solid biomass is converted (due to reaction) to gases, the porosity of the solid (char) particles also changes (increasing). The assumption for packed bed analysis are (i) gasifier reactor is considered as control volume with individual particles as a point source in the bed with a given bed porosity, (ii) quasi-steady conditions in the continuity equation neglecting the time derivative term and (iii) model analysis is carried out by setting out the conservation equations for mass, species, and energy. Properties of bulk fluid vary continuously as the reaction proceeds. These are determined by solving the set of conservation equations assuming variations only across the bed height.

Fig 5.1 presents a schematic diagram showing the process occurring in the packed bed. The bed is divided into a number of layers or computational cells, and conservation equations for a typical particle representing each cell are solved. Heat transfer between the particle and the surrounding particles, and properties of the bulk

fluid surrounding the particles is added in the packed bed analysis apart from single particle considerations.
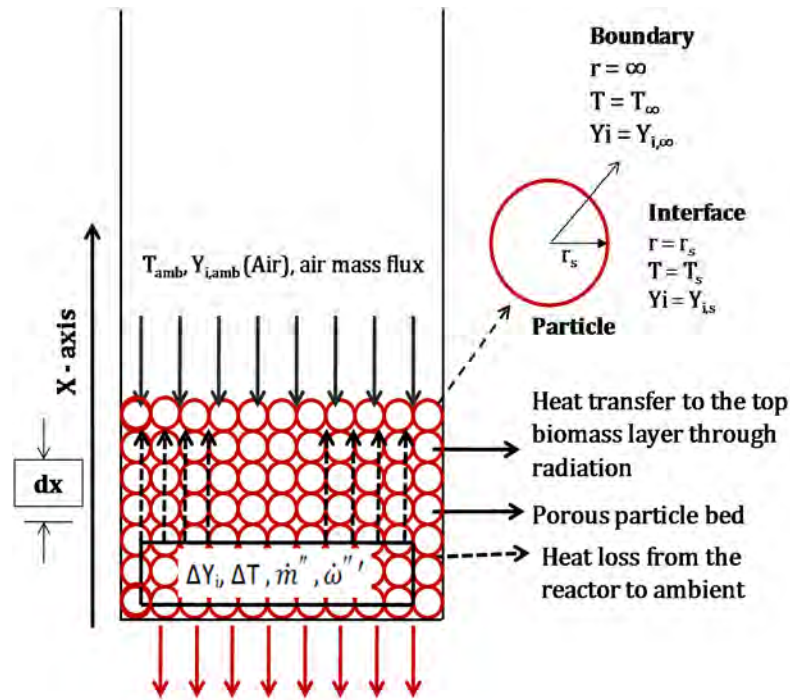
Fig 5.1 Packed bed representation for analysis

The model used here is the one developed by Dasappa and Paul (2001) for char and further extended by Sandeep and Dasappa (2015) for packed bed of wood particles where the packed bed is divided into a number of layers, or computational cells, and conservation equations for a typical particle representing each cell are solved. The mass conservation equation in rectangular coordinate is;

$$\frac{\partial(\rho\varepsilon)}{\partial t} = -\nabla.(\rho V) + \dot{\omega}_c''' \qquad (5.1)$$

Neglecting the time derivative term in equation 5.1 (assuming quasi-steady conditions in the continuity equation) the above equation in x-direction (along the bed height) translates to;

$$\frac{\partial(\rho u)}{\partial x} = \dot{\omega}_c''' \qquad (5.2)$$

The superficial mass flux passing through the bed is $\dot{m}'' = \rho u$, and the volumetric char reaction rate term ($\dot{\omega}_c'''$) can be substitute with $n\dot{m}_p$. Here, u is the superficial

velocity of gas, n is the number of particles per unit volume, $\dot{m}_p$ is the gasification rate which signifies the conversion rate and derived from the solution of single particle analysis. Hence, equation 5.2 can be written as;

$$\frac{\partial(\dot{m}'')}{\partial x} = n\dot{m}_p \qquad (5.3)$$

Heat transfer between the particle and the surrounding particles, and properties of the bulk fluid surrounding the particles is used in the packed bed analysis apart from single particle considerations. These are determined by solving a set of conservation equations for the bulk gases assuming variations only with the height of the bed (x-direction). The species conservation equation is following.

$$\frac{\partial(\rho\epsilon_b Y_i)}{\partial t} + \frac{\partial(\dot{m}''Y_i)}{\partial x} = \frac{\partial}{\partial x}D\rho\frac{\partial Y_i}{\partial x} + n[\dot{m}_p Y_{i,s} + K_D(Y_{i,s} - Y_i)] + \dot{\omega}_i''' \qquad (5.4)$$

Here, K_D (kg/s) is the mass transfer coefficient through the gas film surrounding the particle. The second term on the right-hand side of the equation 5.4 represents the mass production of species Y_i in the packed bed. The third term on the right hand side represents the product of number of particles per unit volume (n), mass transfer from the concentration $Y_{i,s}$ to Y_i. The bed porosity (ϵ_b) is considered in place of char porosity (ϵ). The gas phase energy conservation equation is represented by equation 5.5.

$$\frac{\partial(\rho\epsilon_b C_P T)}{\partial t} + \frac{\partial(\dot{m}''C_P T)}{\partial x}$$
$$= \frac{\partial}{\partial x}\kappa\frac{\partial T}{\partial x} + H_R + n[\dot{m}_p C_P T_{gas} + hA_s(T_{gas} - T)] + h_l A_{sr}\Delta T \qquad (5.5)$$

The first term of the right-hand side of equation 5.5 represents the effective conductive heat transfer to a single particle in the control volume, the second term represents the heat generation due to reaction per unit volume due to gas phase reaction, the third term represents the heat carried away by the hot gases, the fourth term represents the convective heat that transfer from the gas films to surroundings and the last term is the heat loss from the reactor wall. Radiation is the major mode of heat exchange, and conduction has very little effect, as the contact between the

particles in a packed bed is very small and emissivity of the char particle is high (Dasappa, 1999). A particle views the surrounding particles at various heights with different temperatures. It has been considered that all particles have a uniform surface temperature representing the average height at which these particles reside within the bed, and the emissivity of all the particles are also same. The total radiative flux falling on the sphere and the net radiation absorbed is estimated by using the following equations (Dasappa, 1999).

$$Q = \sum_j f_j \sigma T_j^4 \qquad (5.6)$$

$$H_R^{''} = A_s \alpha (Q - \sigma T_s^4) \qquad (5.7)$$

Where, Q is the total radiative flux incident on the surface, A_s is the surface area of the sphere and α is the absorptivity (or emissivity) of the surface.

5.2 The governing equations for single particle

The physical processes occur for single particle are modelled by using unsteady spherically symmetric one-dimensional conservation equations. With the conversion of solid biomass to gaseous phases and char, the porosity of the solid (char) particles changes (increasing) and this is used to estimate the end of conversion (porosity becomes one). The governing mass, energy and species conservation equations are.

$$\frac{\partial}{\partial t}(\rho \epsilon) = \frac{1}{r^2}\frac{\partial}{\partial r}(-\rho v r^2) + \dot{\omega}_c^{'''} \qquad (5.8)$$

$$\frac{\partial}{\partial t}(\rho \epsilon Y_i) = \frac{1}{r^2}\frac{\partial}{\partial r}\left(-\rho v r^2 Y_i + \rho D \frac{\partial Y_i}{\partial r}\right) + \dot{\omega}_i^{'''} \qquad (5.9)$$

$$\frac{\partial}{\partial t}(\bar{\rho} C_P T) = \frac{1}{r^2}\frac{\partial}{\partial r}\left(-\rho v r^2 C_P T + r^2 \kappa \frac{\partial T}{\partial r}\right) - H_c \dot{\omega}_c^{'''} \qquad (5.10)$$

Apart from these, average density ($\bar{\rho}$) of the porous char particle is related with the following relation.

$$\bar{\rho} = \rho_C (1 - \epsilon) + \rho \epsilon$$

The mass of the porous char particle is related to the porosity of the particle. As the porosity increases, the mass will reduce. So the relation can be written in the following way.

$$\frac{\partial \epsilon}{\partial t} = -\frac{\dot{\omega}_c'''}{\rho_c} \qquad (5.11)$$

5.3 Initial, interface and boundary conditions and solution methods

The conservation equation (5.8 - 5.11) presented in the earlier section is solved by using initial, interface and boundary conditions. The initial conditions at $t=0$ (time) are the temperature and concentration profile within the particle. The temperature is set to the ambient condition or the condition dependant on the experimental requirement. The precise nature is not very important as the transient condition dies down in a small fraction of the conversion time. This is due to diffusion dependant heterogeneous reactions. The boundary conditions are at large distance from the particle $(r \rightarrow \infty)$, the temperature is set to be $T \rightarrow T_\infty$ and at the particle surface $(r = r_S)$, temperature is considered to be $T = T_S$. The unsteady spherically symmetric one-dimensional energy and species conservation equations in case of quasi-steady gas phase (steady state in nature means no time dependent and reaction term is zero, since no reaction occurs for pure evaporation) are following.

$$\frac{\dot{m} C_P}{4\pi r^2} \frac{\partial T}{\partial r} = \frac{1}{r^2} \frac{\partial}{\partial r}\left(r^2 \kappa \frac{\partial T}{\partial r}\right) \qquad (5.12)$$

$$\frac{\dot{m}}{4\pi r^2} \frac{\partial Y_i}{\partial r} = \frac{1}{r^2} \frac{\partial}{\partial r}\left(r^2 D_e \rho \frac{\partial Y_i}{\partial r}\right) \qquad (5.13)$$

The solution of the equations 5.12 and 5.13 can be evaluated assuming Lewis number to be unity. The energy and species equations are integrated and taken into consideration of the boundary conditions (at $r \rightarrow \infty, T \rightarrow T_\infty$ and $r = r_S, T = T_S$, and $r \rightarrow \infty$; $Y_i \rightarrow Y_{i\infty}$ and $r = r_S$; $Y_i = Y_{iS}$). The solution of energy and species energy conservation equations can be written in the following form.

$$\frac{(T - T_\infty)}{(T_S - T_\infty)} = \frac{(Y_i - Y_{i\infty})}{(Y_{is} - Y_{i\infty})} = \frac{(1 - \eta)}{(1 - \eta_S)} \qquad (5.14)$$

where, $\eta_S = exp\left(-\frac{\dot{m}C_P}{4\pi\kappa r_S}\right)$ and $\eta = exp\left(-\frac{\dot{m}C_P}{4\pi\kappa r}\right)$

The subscript 's' refers to the value at the surface of the sphere. Differentiating equation 5.14, at the surface $r = r_S$ provides the interface conditions both for energy and species conservation equations and final form of the equations are following.

$$\kappa\frac{\partial T}{\partial r} = C_P Q(T_\infty - T_S) - \dot{R}'' \tag{5.15}$$

$$D\rho\frac{\partial Y_i}{\partial r} = Q(Y_{i\infty} - Y_{iS}) \tag{5.16}$$

where, $Q = \left[\frac{\dot{m}}{4\pi r_S^2}\frac{exp(-B_0)}{\{1-exp(-B_0)\}}\right]$, $B_0 = \frac{\dot{m}C_P}{4\pi\kappa r_S}$ and $\dot{R}''$ is the radiative heat flux from the surface of the sphere.

The energy and species conservation equations are integrated through parabolic partial differential equation system and considered the initial and boundary conditions reported earlier for its solution. The independent variable r is transformed into the volume *(V)* to make the equations fully conservative and remove the singularity at $r = 0$. The transformed energy and species conservation equations are following.

$$\frac{\partial}{\partial t}(\bar{\rho}C_P T) = \frac{\partial}{\partial V}\left(-\dot{m}C_P T + (4\pi)^{2/3}(3V)^{4/3}\frac{\partial T}{\partial V}\right) - H_C\dot{\omega}_C''' \tag{5.17}$$

$$\frac{\partial}{\partial t}(\rho Y_i \epsilon) = \frac{\partial}{\partial V}\left(-\dot{m}Y_i + D_e\rho(4\pi)^{2/3}(3V)^{4/3}\frac{\partial Y_i}{\partial V}\right) + \dot{\omega}_i''' \tag{5.18}$$

where, $\dot{m} = \rho A v_S = 4\pi r^2 \rho v_S$. The mass flow rate of the gases, coming out from the porous char and to be consistent with respect to the unsteady formulation, the equation of state is used to get the following relation.

$$\frac{\rho\epsilon}{\bar{\rho}}\frac{\partial(\rho\epsilon)}{\partial t} + \rho\left(1 - \frac{\rho_C\epsilon}{\bar{\rho}}\right)\frac{\partial\epsilon}{\partial t} - M_g\sum\frac{1}{M_i}\frac{\partial}{\partial t}(\rho\epsilon Y_i) - \left(\frac{\rho\epsilon}{\bar{\rho}TC_P}\right)\frac{\partial}{\partial t}(\bar{\rho}C_P T) = 0 \tag{5.19}$$
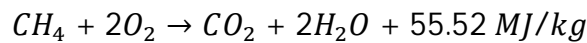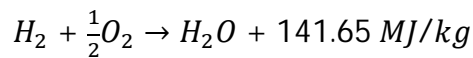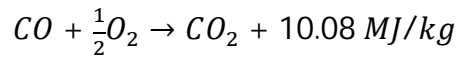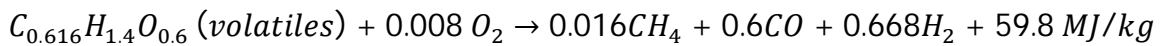
5.4 Kinetics of the governing reactions

The process during the combustion or gasification of a single particle (wood sphere) is diffusion and convection of the species and energy and heterogeneous reaction

between the gaseous species and char. In packed bed analysis, pyrolysis process of the biomass samples and volatile combustion along with heterogeneous porous char combustion/gasification are added with the single particle analysis. The important reactions are pyrolysis of biomass particles, char and gas reactions and water gas shift reactions in the gas phase. Pyrolysis, water gas shift reaction and char reactions are considered in single particle analysis, whereas volatile combustion and water gas reaction constitutes the reaction set in packed bed analysis. Pyrolysis as a process or thermal decomposition of wood releases volatiles leaving behind the carbon in the form of porous char. The lower temperature regime of decomposition of wood showed that mainly H_2O, CO_2 and CO are evolved and at the higher temperature regime, the primary decomposition products are oil, H_2O, H_2, hydrocarbon gases and lower concentrations of CO and CO_2. The particles are subjected to varying temperature profiles as they travel through the packed bed, also allowing for the possibility of combustion of some of the volatiles. Based on the particle size and the heat flux, predominantly slow pyrolysis takes place in case of the gasification process. Typically for the reactor configuration considered in the study, slow pyrolysis prevails with very low heating rates, and char is the primary output along with gases. While addressing the overall packed bed model, conservation of enthalpy and the elemental balance of C, H and O are more relevant for pyrolysis than characterisation of the species in the volatiles and kinetics of volatile cracking or combustion. The output products of volatiles in the gasification process are primarily CO and H_2, with a little amount of CH_4 (Sandeep and Dasappa, 2015). The pyrolysis reaction is assumed to be slightly endothermic with the heat of reaction being -0.42 MJ/kg (Di Blasi, 2004). Further, these gases undergo stoichiometric combustion and release the heat of reaction.

The pyrolysis process releases volatiles leaving behind the carbon in the form of porous char. In this process, biomass breaks down to char, various gases and liquids. The fraction of biomass converted to volatiles or char residual is dependent on the temperature or heating rate, residence time and heat losses, etc. In the pyrolysis process, particle diameter decreases by about 10% and weight loss by 75-80%

(Mukunda *et al.* 1984). This reduction in weight is due to loss of the volatiles of the wood particle. In case of low temperature with slow heating rate, char is the major output and at higher temperature, gases are the major output. In case of gasification process, slow pyrolysis takes place, and char is the primary output along with gases. The output products of volatiles in the gasification process are primarily CO and H_2, with a little amount of CH_4. Further, these gases undergo stoichiometric combustion and release the heat of reaction. The following reaction takes places in this process.

$$CH_{1.4}O_{0.6} \ (wood) \rightarrow C_{0.616}H_{1.4}O_{0.6}(volatiles) + 0.384 \ C \ (char) - 0.42 \ MJ/kg$$

$$C_{0.616}H_{1.4}O_{0.6} \ (volatiles) + 0.008 \ O_2 \rightarrow 0.016CH_4 + 0.6CO + 0.668H_2 + 59.8 \ MJ/kg$$

$$CO + \frac{1}{2}O_2 \rightarrow CO_2 + 10.08 \ MJ/kg$$

$$H_2 + \frac{1}{2}O_2 \rightarrow H_2O + 141.65 \ MJ/kg$$

$$CH_4 + 2O_2 \rightarrow CO_2 + 2H_2O + 55.52 \ MJ/kg$$

The following three important overall reactions are considered in the analysis with respect to char combustion.

$$C + O_2 \rightarrow CO_2$$
$$C + CO_2 \rightarrow 2CO$$
$$C + H_2O \rightarrow CO + H_2$$
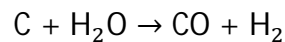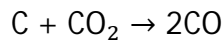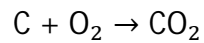
The reaction rate and various constants are presented in Table 5.1, which are used in the model.

Table 5.1 Rate expressions used in the model

Reaction	Rate expression	Constant	Reference
$C + O_2$	$\varpi''_{C+O_2} = -\dfrac{M_c S_1 S_2 X_{os}}{(S_1 X_{os} + S_2)}$ $S_1 = A_c P \exp(-\dfrac{E_1}{RT})/(\sqrt{2\pi M_{O_2} RT})$ $S_2 = A_f \exp(-\dfrac{E_2}{RT})$ $\varpi'''_{C+O_2} = \dfrac{2\varpi''_{C+O_2}\varepsilon}{r_p}$	A_c : 1/150 E_1/R : 1700K E_2/R : 20,000K A_f : 0.0875 mol/m2-s	Howard (1967), Dasappa (1999)
$C + H_2O$	$\varpi'''_{C+H_2O} = -\dfrac{k_1 p_{H_2O} + K_4 p_{H_2} p_{H_2O} + K_5 p_{H_2O}^2}{1 + K_2 p_{H_2} + K_3 p_{H_2O}}$	$k_1 = 3.6 \times 10^7$ mol/cm3-s-atm $K_2 = 35$ atm-1, $K_3 = 0.025 \times 10^{-6}$ atm-1 $K_4 = 2.1 \times 10^{-3} \exp(E_4/RT)$ atm-1 $K_5 = 91.8 \exp(E_5/RT)$ atm-1	Blackwood and McGrory (1958), Dasappa and Paul (2001)
$C + CO_2$	$\varpi'''_{C+CO_2} = -\dfrac{k_1 p_{CO_2} - K_2 p_{CO}^2}{1 + K_3 p_{CO} + K_4 p_{CO_2}}$	$k_1 = 2.2 \times 10^9 \exp(E/RT)$ mol/cm3-s-atm $K_3 = 15.0$ atm-1, $K_4 = 0.25$ atm-1 K_2 is obtained from equilibrium	Dasappa (1999)
$CO + H_2O$	$K_p = \dfrac{p_{CO2} \, p_{H2}}{p_{CO} p_{H2O}}$ $K_p = \exp^{(\frac{a_1}{T} + a_2 + T(a_3 + T(a_4 + T(a_5 + T \times a_6))))}$	$a_1 = 4.89 \times 10^3$, $a_2 = 4.75$, $a_3 = 1.28 \times 10^{-3}$, $a_4 = 2.89 \times 10^{-6}$, $a_5 = 1.76 \times 10^{-9}$ and $a_6 = 3.77 \times 10^{-13}$	SERI (1979)
Pyrolysis	$\omega'''_{pyr} = A_{pyr} X_{bio} \exp(-\dfrac{E_{pyr}}{RT})$	$A_{pyr} = 1.44 \times 10^4$ s-1 $E_{pyr} = 88.6$ KJ/mol X_{bio} is the biomass fraction available at a given time	Sandeep and Dasappa (2015), Di Blasi (2004)

5.5 Choice of parameters

The physical, thermodynamic and transport properties are used in the model is based on various literature. The density of the biomass (ρ_b) sample (*Casuarina equisetifolia*) is measured and used for the present work. The density of non-porous char particle (ρ_c) and the calorific value (H_c) of carbon are taken from Dasappa (1999). The pore radius (r_p), tortuosity factor (τ) are chosen from Groeneveld (1980). The non-porous char (k_c) and gas (k_g) thermal conductivity are chosen from Dasappa (1999) and the porous char conductivity is 0.4-0.5 (Goldman *et al.* 1985). The thermal conductivity of gas phase (k_g) is calculated taking into account the presence of H_2. The un-reacted char porosity is chosen from Dasappa (1999). The various parameters used in the model for char particle are presented below.

$$\rho_c = 1900 \; kg/m^3, \; r_p(t = 0) = 50 \; \mu m, C_p = 1.25 \; KJ/kg$$

$$H_c = 32.6 \; MJ/kg, k_c = 1.85 \; W/mK, k_g = 0.071 \; W/mK$$

$$\tau = 1.5, \varepsilon = 0.88 \; (unreacted \; char)$$

The diameter and density of the biomass particle are considered as 12.5 mm and 610 kg/m^3 respectively.

5.6 Solution procedure adapted in the in-house developed packed bed model

The packed bed is divided into a number of computational cells with height *dx*. The conservation equation of a typical single particle representing each cell is solved. Biomass particles are represented as the source term in the bed. The equations for the single particles are solved and its output, in terms of gas species and energy released or diffused translates to be a source term for the packed bed. Solutions of the equations of the particle provide the conditions at the surface of the sphere and the net mass flux from the sphere that are used in the next fractional time step. Knowing the temperature profile, at a particular location in a given cell, the temperature at other location is obtained through interpolation. Thus, the temperature distribution within the bed is obtained. In this study, the modified model is used to obtain the temperature profile, gas composition at different time interval. The input parameters are particle diameter, and air mass flux. The model provides output temperature

profile for a particular air mass flux, and this is used to calculate the propagation rate in that air mass fluxes. Detailed results and its analysis, comparison with experimental results focussing on the propagation rate with varying mass flux, temperature profiles, estimating the effective propagation rate and the gas composition are presented in the chapter VI.
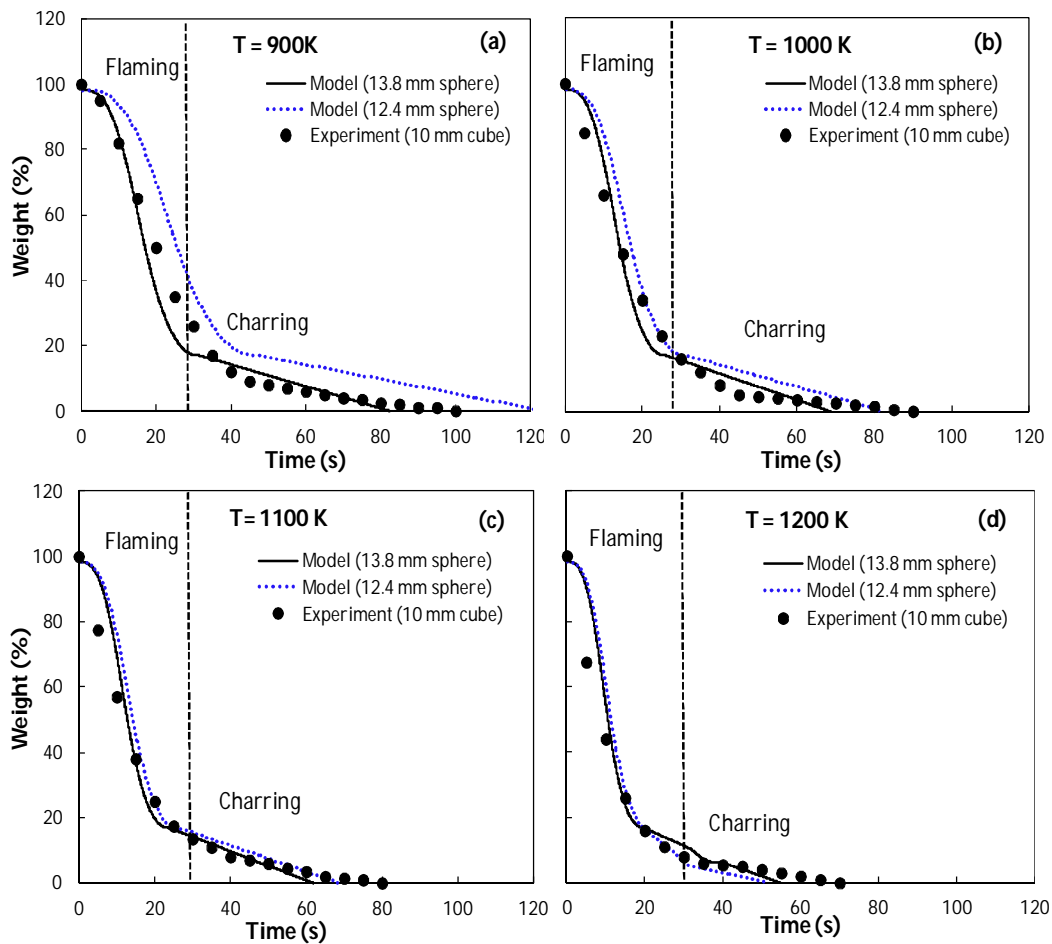
Fig 5.2 Comparison of experimental weight loss profile of 10 mm pine cube (Simmons and Ragland, 1986) with model results of 12.4 mm and 13.8 mm pine wood spheres *(adapted from Sandeep and Dasappa, 2015)*

Sandeep and Dasappa (2015) in Figure 5.2 (a-d) compare the weight loss with time for the model and the experimental data from Simmons and Ragland (1986). This result adapted from Sandeep and Dasappa (2015) is towards depicting the capability of the model towards predicting the pyrolysis and the char conversion profiles under various conditions. The conversion profile of the 10 mm pine cube lies in between the

conversion profile of two different diameter spheres. With the increase in temperature, the weight loss profile of both the spheres approaches with the one under consideration (10 mm cube). It is evident from the Figure 5.2 (d) that at 1200 K temperature, the small difference that exists at lower temperatures with respect to the weight loss profile of both the cube and spherical particle almost diminishes. Such behaviour is justified based on the internal resistance to be nearly same irrespective of the external flux; flaming time is nearly same, suggesting the process is limited by conduction.

5.7 Summary

This chapter has presented the principal methodology used for the modeling of the packed bed in co-current configuration based on the in-house developed code and validated for various sub-process in the thermo-chemical conversion. The model captures all the physical processes and the input parameters are chosen from the earlier literature and current experiments. The modified packed bed model is used to estimate the propagation rate, effective propagation rate, bed temperature, gas composition, unreacted volatile fractions in the bed. The model predictions are also compared with the present experimental results as well as with literature in Chapter VI.

Results and discussion on Packed bed analysis

This chapter compares the results from the model, experimental study and also from the literature. Aspects related to the bed temperature, gas composition, propagation rate, which depict the overall performance of the packed bed reactor, are used for comparison. In this study, the model is used to obtain the temperature profile and gas composition at different time intervals. The input parameters are particle diameter and air mass flux. The model provides temperature profile in the packed bed for a particular air mass flux, and this is used to calculate the propagation rate in that air mass flux. The detailed results and its analysis, comparison with experimental results and available literature data are presented in the following sections[13].

6.0 Temperature profile in the packed bed

Biomass sample used in the model has the properties identical to *Casuarina equisetifolia*, with a spherical particle diameter of 12.5 mm with no moisture, and particle density of 610 kg/m^3. Fig 6.1 represents the typical temperature profile obtained from the model at an air mass flux of 0.12 kg/m^2-s. Flame propagation rate in model (Fig 6.1) is calculated as difference between effective propagation rate and bed movement. The bed movement is evaluated considering the shrinkage of particles (during pyrolysis) and carbon conversion (during char reduction). Shrinkage of the particle diameter is typically about 10 % as detailed measurements carried out in the laboratory and the reduction in the char diameter is estimated based on the layers of carbon conversion occurring due to the chemical reactions at the surface depending upon the reacting species in the vicinity of the particle undergoing the conversion. The temperature profile in Fig 6.1 is the flame propagation rate obtained from model (diference between effective propagation rate and bed movement) to arrive at the

---

[13] *This work published in*

Mahapatra, S., Kumar, S., Dasappa, S. Gasification of wood particles in a co-current packed bed: experiment and model analysis. Fuel Processing Technology 2016; 145: 76-89.

corresponding bed height. A typical temperature profile obtained during the experiment is also presented (Fig 6.2). After the ignition, the air nozzle is closed in both the experiment and model and the air is drawn only from the top of the reactor for the gasification process. The distance between the two temperatures measurements is presented in the respective figures.
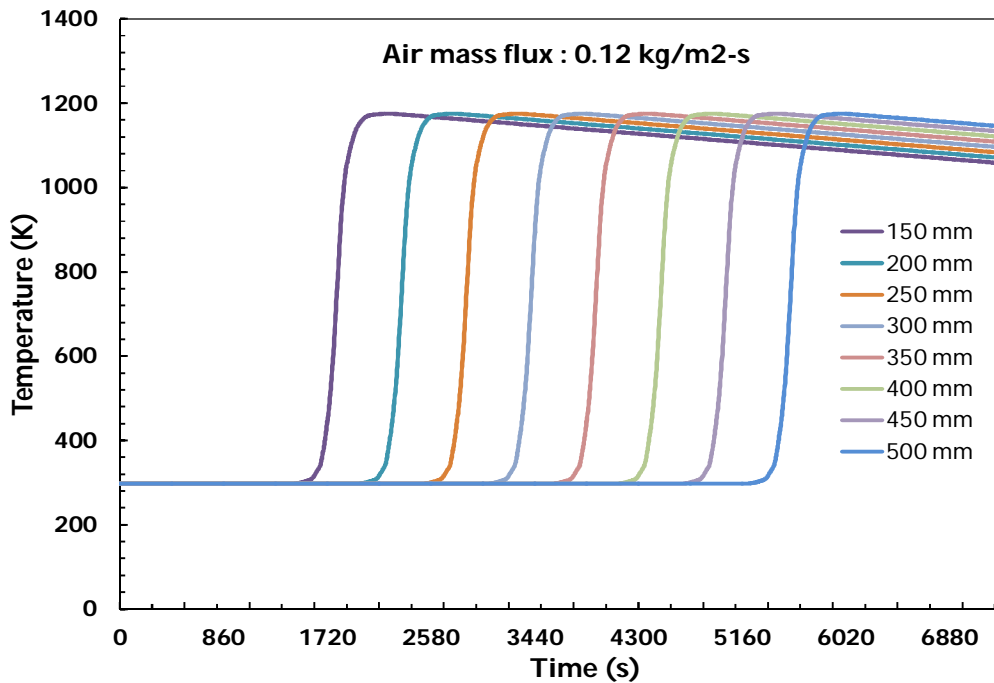
Fig 6.1 Temperature profile from model inside the reactor

It is observed from both the figures that the propagation front is moving from the ignition point towards the top of the reactor. The propagation rate as predicted from the model at an air mass flux of 0.12 kg/m^2-s is 0.089 mm/s (Fig 6.1) and from experiment, it is 0.083 mm/s at the same air mass flux (Fig 6.2). The peak bed temperatures estimated in both the cases are 1175 K (Fig 6.1) and 1115 K (Fig 6.2) respectively. The results suggest a reasonable match between the model and experimental results. The difference in the temperature is being justified based on the estimation of heat loss using the heat transfer correlations. Groeneveld (1980) and Mukunda *et al.* (1984) has estimated that 8-10% of the input energy is lost in a typical gasifier as heat, even the reactor is insulated. Dasappa (1999) estimated that the difference in peak temperature in the case of heat loss and without heat loss

consideration, from the reactor, is about 170 K for a charcoal gasifier experiment. In this model, heat transfer coefficient of 10 W/m^2-K (Dasappa, 1999) is considered in the calculation. It is also observed that further increase of the air mass flux results in negative propagation rate leading to extinction. In next section, propagation rate is calculated for different air mass flux for both the model and experiment.
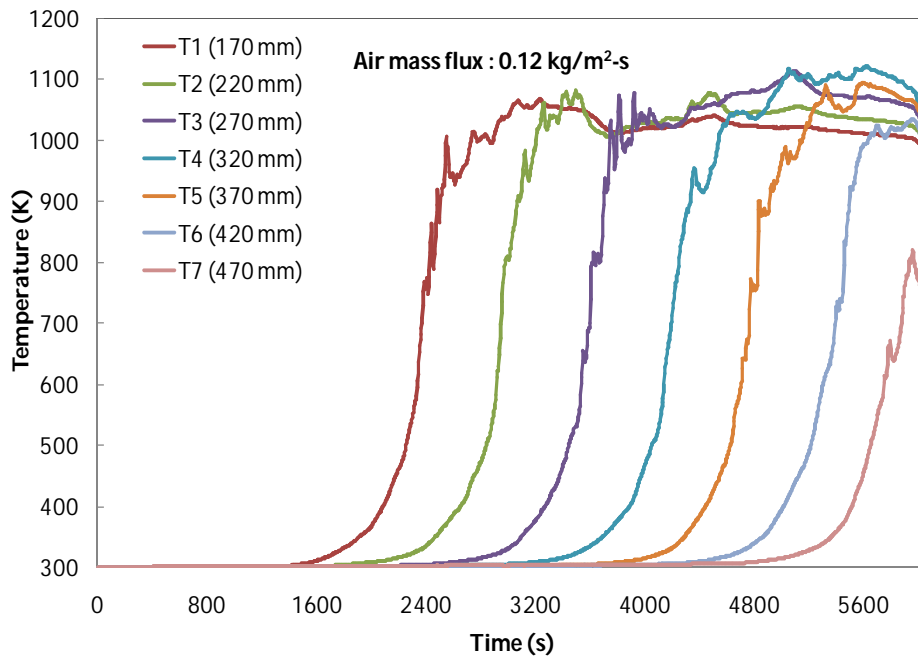
Fig 6.2 Temperature profile from experiment inside the reactor

6.1 Propagation rate and peak temperature

It is observed from Fig 6.3 that flame front movement or propagation rate increases as the air mass flux increase, attains a peak and any further increase in air mass flux, the propagation rate decreases. Fig 6.3 presents the model predictions and experimental results for the peak temperature in the bed at different air mass flux and is found to follow similar trend. It is found that the model estimated temperature, is on average 85 K higher than the experimental measurement. This is attributed to choice of heat transfer coefficient for the model based on the earlier works (Dasappa, 1999). It is evident from the analysis that the experimental reactor effective insulation is different and hence the heat loss is comparatively higher. However, by increasing the heat

transfer coefficient in the model to 14 W/m^2-K, predictions are found to be closer to the present experiments.
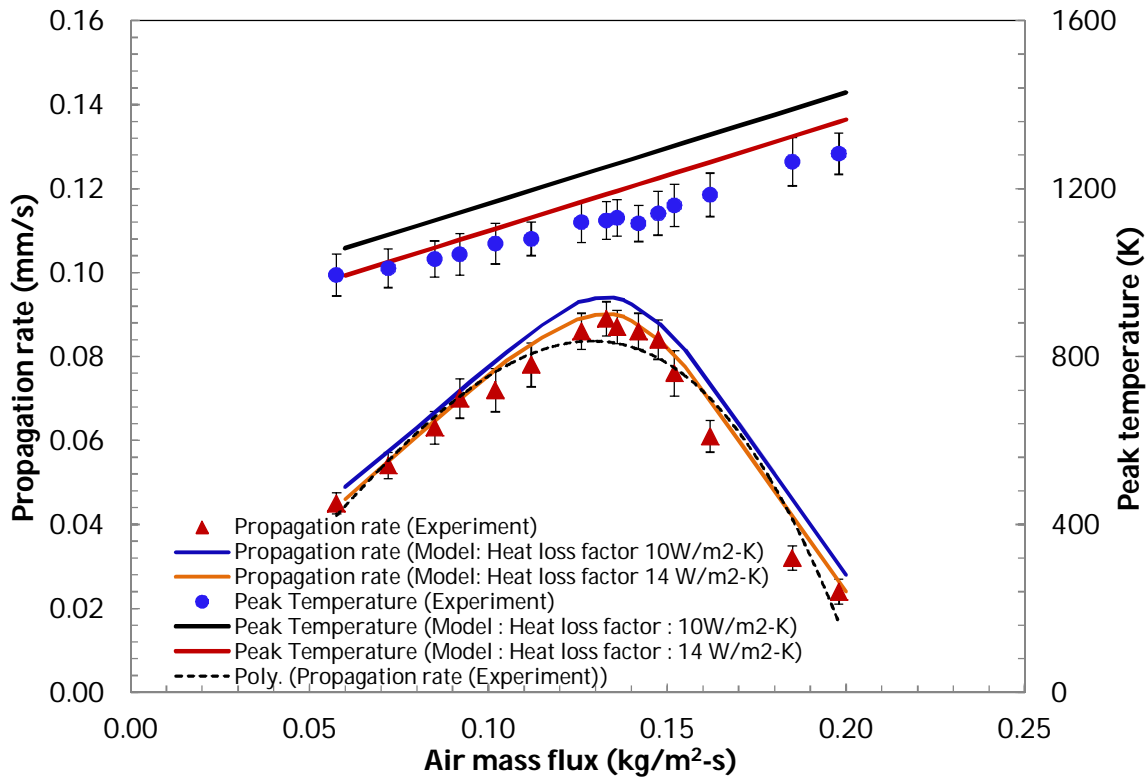
Fig 6.3 Propagation rate and bed peak temperature at various air mass flux

Having established the peak bed temperature, Figure 6.3 also presents flame propagation rate at various air mass fluxes. Comparison is made between the experiments and the model. The model predicts the peak propagation rate as 0.094 mm/s at an air mass flux of 0.135 kg/m^2-s; while it is 0.089 mm/s at an air mass flux of 0.132 kg/m^2-s from the experimental results. The results from comparison seem reasonable considering some of the differences in the shape and size of the fuel used in the experiments and the model analysis. The fuel particle size used in the experiment is 14×10×10 mm and in the model spherical particle of 12.5 mm diameter is used. Similar trend of flame front propagation is also observed by Dasappa and Paul (2001) for the co-current gasifier using charcoal as the fuel, except that the peak propagation rate for charcoal was 0.30 mm/s. The difference between these values are related with the properties of the fuel with wood having 80% volatiles while charcoal

has less than 10% volatiles. Apart from that the char consumption rate is much lower than the volatile combustion rate, implying very little energy used for preheating the fuel, where as the pyrolysis process is also endothermic.
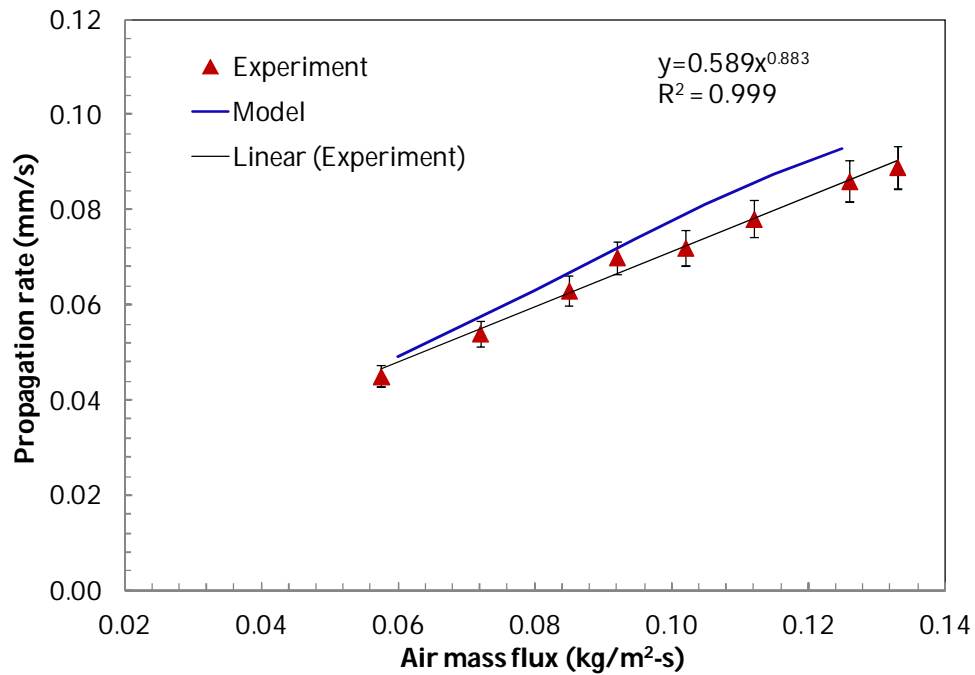
Fig 6.4 Propagation rate variation with air mass flux at the increasing regime of propagation rate

Further, it is evident from Fig 6.4 that during the increasing profile of the propagation rate regime, the propagation rate correlates with mass flux as ($\dot{m}''^{0.883}$) which is different as compared to the work on charcoal ($\dot{m}''^{0.36}$) by Dasappa (1999). In this present study, wood is used as fuel and major part of the fuel (volatiles released during pyrolysis) is consumed while the reaction front passes through the bed. In case of charcoal, only a small fraction of the fuel is consumed in the reaction front (due to low reaction rates with carbon). In both the cases, it is under fuel rich conditions unlike other studies (Fatehi and Kaviany, 1994; Gort, 1995; Horttanainen *et al.* 2002; Rönnbäck *et al.* 2001; Porteiro *et al.* 2010). The reaction front heats up more fuel in the case of charcoal than it consumes and this has influence on both the peak temperature and the propagation rate. It has been argued by Dasappa (1999) that rate of increase of front velocity with air mass flux is less than the rate of increase of mass

flux itself; the peak temperature at the front increases with air mass flux also aided by the increased heat and mass transfer coefficients between the particle and gas (Dasappa, 1999). Further, it is also important to highlight that the specific heat of biomass and endothermicity induced during the pyrolysis process of biomass and density difference between these two fuels leads to lower propagation rate for wood compared to charcoal in the co-current configuration. It is also observed from the experiments and model analysis, that further increase of the air mass flux resulted in reduction in the absolute value of propagation rate leading to extinction.

It is important to highlight that the flame front movement in a packed bed in general depends on factors involved in the fuel consumption rate, energy balance and heat generation by chemical reaction, heat loss through radiation, heat transfer to unburnt fuels, convective cooling due to the air flow along with the heat loss from the reactor surface. At lower air mass flux, means lower end of the turn-down ratio of the reactor, the energy release through volatile combustion is lower, resulting in lower bed temperature which is sufficient for the autothermal process to sustain. With the increase in air mass flux, ensuring higher oxidiser environment improves the heat generation process resulting in higher bed temperature. This in turn improves the rate process for devolatilization which leads to higher propagation front movement. One of the acceptable arguments with respect to the peak propagation front movement attaining the peak, along with increase in temperature is addressed by considering the balance between heat generation and heat loss. Any further increase in the air mass flux at which peak propagation occurs, heat loss component dominates and the propagation rate tends to decrease (Fatehi and Kaviany, 1994; Rönnbäck *et al.* 2001; Mahapatra and Dasappa, 2014a; Dasappa and Paul, 2001), which provides justification for such behaviour.

Most of the packed bed configurations studied are of counter current or reverse downdraft type (Table 4.1) where the top fuel layer comes in contact with the oxidiser as in the case of updraft (Fatehi and Kaviany, 1994; Gort, 1995; Horttanainen *et al.*

2002; Rönnbäck *et al.* 2001; Porteiro *et al.* 2010). The front movement in reverse downdraft configuration is directly linked to the oxidiser and fuel vapour combustion zone movement but has very little influence on the bed movement. In the case of open top downdraft configuration or co-current reactor, fuel and air both moves downwards (Fig 1.9). It can be observed from Fig 4.3 that with the increase in air mass flux, the propagation front attains a peak and then reduces. However, bed movement increases linearly with the increase in air mass flux due to biomass consumption and shrinkage of particle due to pyrolysis as well char conversion. Therefore, the effective propagation movement which is summation of flame front and bed movement also increases gradually with the increase in air mass flux till it reaches the extinction limit. In the case of reverse downdraft/counter-current configuration, the bed movement is zero and the flame front movement or ignition mass flux is identified as effective bed movement.

Fig 6.5 presents the model prediction of temperature profile representing the propagation flame front, for two different air mass fluxes and for two different time intervals. With an air mass flux of 0.105 kg/m^2-s, front movement is upwards into the fuel bed countering the air flow, while in the case of air mass flux at 0.235 kg/m^2-s, it shows that the front moves in the reverse direction, i.e., along with air flow. This behaviour suggests that the flame front is receding even though the bed temperature is higher. This phenomenon also indicates that beyond this air mass flux (0.235 kg/m^2-s), the reactor ceases to function as an open top gasification reactor; approaches towards closed top configuration and the transition from fuel rich regime towards stoichiometric regime.
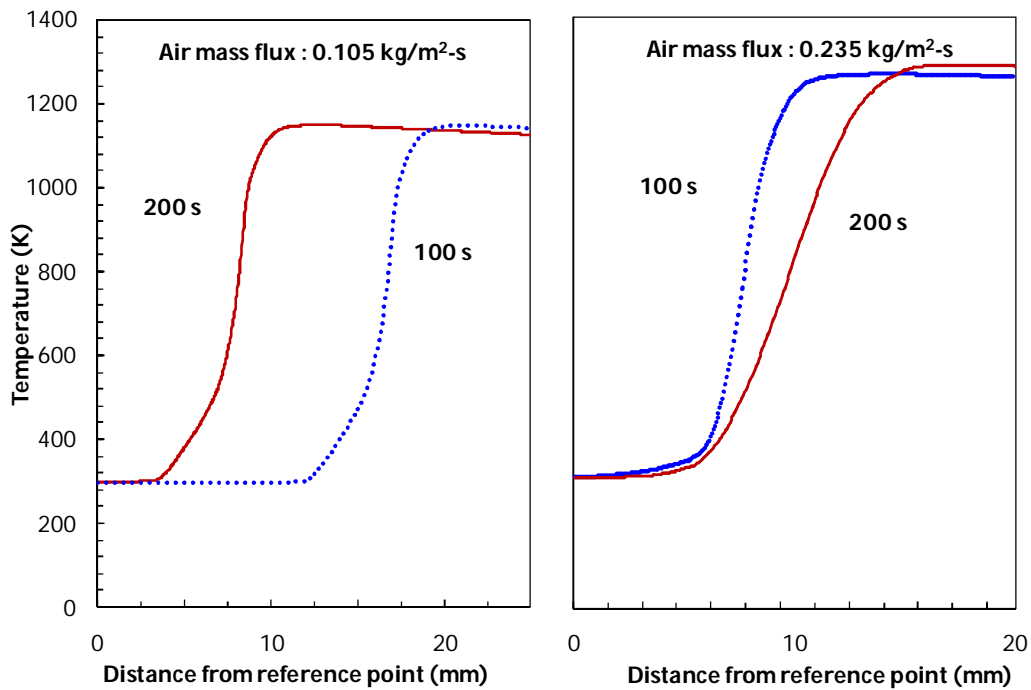
Fig 6.5 Temperature profiles at two different air mass flux

Table 6.1 presents the flame propagation rate, bed movement and effective propagation at various air mass fluxes from the experimental results. The flame propagation and bed movements are measured during experiment. The biomass consumption at various air mass fluxes is estimated based on the bulk density of the fuel samples in the reactor bed by using the following relation.

$Biomass\ consumption\ estimated\ (g/h)$

$$= Bed\ movement\ (m/h) \times reactor\ area\ (m^2) \times bulk\ density\ (g/m^3)$$

It can be observed that with the increase in air mass flux, the flame propagation increases and later reduces, but the bed movement gradually increases (Fig 4.3). Towards analysing the aspects related to the effective propagation rate, experimental data related to bed movement and propagation rate are used and compared with the estimated bed movement using bed properties. The biomass consumption at various air mass fluxes is estimated based on the bulk density of the fuel samples in the reactor bed.

Table 6.1 Flame front, bed movement, effective propagation movement and biomass consumption at different air mass flux

Air mass flux (kg/m²-s)	Flame front movement (mm/s)	Bed movement (mm/s)	Effective propagation movement (mm/s)	Biomass consumption (g/h)		Difference in biomass consumption (%)
				Experiment	Estimation	
0.057	0.0454	0.055	0.1004	551.6	610.1	9.6
0.086	0.0546	0.068	0.1226	681.2	754.3	9.7
0.106	0.0696	0.085	0.1546	873.8	942.9	7.3
0.121	0.0825	0.100	0.1825	999.0	1109.3	9.9
0.134	0.0890	0.109	0.1980	1111.8	1209.1	8.0
0.142	0.0867	0.116	0.2027	1164.1	1286.8	9.5
0.147	0.0823	0.128	0.2103	1261.9	1419.9	11.1
0.171	0.0507	0.162	0.2127	1589.3	1797.1	11.6
0.198	0.0240	0.196	0.2200	1907.0	2167.0	11.9

Fuel consumption is estimated based on the bed movement at an air mass flux and no char is removed during the experiment. The fuel sample size considered during the experiment is 14×10×10 mm with bulk density of 370 kg/m³ and the reactor diameter is 103 mm. It is also clear from the temperature profile and from the data reported in the literature that the flame front is about 1.8 to about 3 particle depths depending upon the mass flux (Fatehi and Kaviany, 1994). It is observed that in the case of flaming combustion, particle sphere diameter decreases by about 10% and weight loss is by 75-80% (Mukunda *et al.* 1984).

In the present study, the reaction zone thickness where the flame front exists is between 20–30 mm. Thus, below the propagation front in the packed bed, is mostly char, a product of pyrolysis with an estimated residence time of 35 to 70 s depending upon the mass flux. This can be comparable with a typical time scale of 60 s for a 10 mm particle to devolatize in an ambient (at 300K) with flaming pyrolysis. It can be concluded from this analysis that in the co-current reactor, the flame propagation rate movement is an important parameter compared to effective propagation which helps to decide the operating range of a gasification system. It is also observed that with the increase in air mass flux, the char consumption increases below the pyrolysis zone.

Any further increases in air mass flux, enhances the char consumption and it is depleted when it crosses the extinction limit and leads to non-performing conditions. There is a fair agreement with the data from these two independent methods considering less than 10% char is left over after the gasification process. This result also fairly agrees with the earlier assumption on extensive experiments and it also implies total carbon conversion is not achieved during the gasification process (Mukunda *et al.* 1994).

6.2 Analysis of propagation rate for co-current configuration

In order to analyse the effect of convective cooling, the enthalpy or heat balance on a wood particle bed has been studied. The energy conservation equation describes the energy balance in the packed bed. Rise or fall of temperature at a particular bed height depends on net energy balance which is the sum of the heat of gas phase reactions, reactor heat loss, and enthalpy of the gaseous species coming out of the biomass particle and convective heat transfer across the bed. One particle of 12.5 mm size in the bed is followed during air gasification process and the energy balance at the given bed height is studied. The energy conservation equation for packed bed configuration in simplified form is indicated by the following equation.

$$\Delta E = \Delta H_{convection} + \Delta H_{reaction} + \Delta H_{gas\ particle} + \Delta H_{radiative\ heat} - \Delta H_{reactor\ heat\ loss} \qquad (6.1)$$

Fig 6.6 presents the results from the model analysis for three different air mass fluxes of 0.120 kg/m^2-s, 0.134 kg/m^2-s and 0.235 kg/m^2-s, where ΔE is the energy balance at a given location in the bed. The positive ΔE, mean net addition of energy in the given control volume with time, predominantly by radiative heat transfer in the initial phase leads to the temperature rise facilitating pyrolysis. The sudden rise of the ΔE suggests the ignition point where volatiles ignite releasing enthalpy due to the reaction.
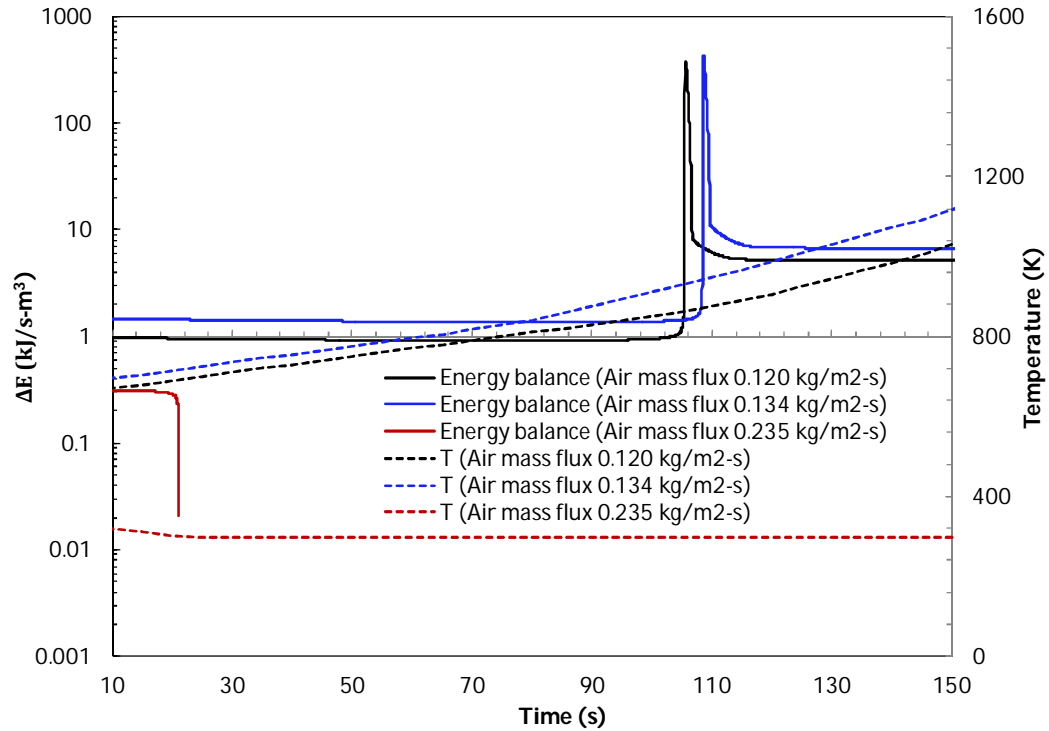
Fig 6.6 Energy balance at a particular bed height for different air mass flux

It is observed from Fig 6.3 and 6.6 that the flame front propagation rate increases with the increase in air mass flux and reached its peak (0.089 mm/s) at an air mass flux of 0.134 kg/m²-s and it is considered to be positive. The propagation rate approached negative slope and eventually quenches beyond an air mass flux of 0.235 kg/m²-s even though the balance of heat (ΔE) is positive during pyrolysis as well as volatile combustion suggesting possibility of the flame to propagate in the fresh biomass. The effective propagation movement at an air mass flux of 0.235 kg/ m²-s is 0.23 mm/s against 0.19 mm/s at an air mass flux of 0.134 kg/ m²-s. The higher effective propagation movement suggests higher char conversion rates as implied by increased air mass flux. Fig 6.6 suggests that before ignition point, ΔE at the air mass flux of 0.134 kg/ m²-s is higher as compared to air mass flux of 0.235 kg/ m²-s, suggesting increased convective cooling effect on the particle at higher mass flux. Fig 6.6 shows that the net enthalpy at air mass flux of 0.235 kg/ m²-s is lower than the net enthalpy at air mass flux of 0.134 kg/ m²-s due to the convective cooling effect of excess air, especially inert N_2, even though the peak enthalpy is higher due to the higher

devolatilisation rate and thus higher heat of reaction. The flame propagation movement is positive (0.089 mm/s) at an air mass flux of 0.134 kg/m²-s and approaches negative beyond an air mass flux of 0.235 kg/m²-s. It is important to note that at the air mass flux of 0.235 kg/m²-s, the net enthalpy or net energy balance over the particle is positive during pyrolysis as well as during volatile combustion which suggests the flame is able to propagate in the fresh biomass and propagation is in the positive direction even though the (relative) flame propagation movement is negative.

Simulation results at an air mass flux of 0.235 kg/m²-s indicate altogether a different heat balance profile. The surface temperature of the biomass particle initially increases to 410 K from ambient 298 K and then quenches. The convective cooling effect due to increased reactant flux reduces the temperature in the reaction zone affecting the overall heat transfer process in the bed leading to quenching. It is evident from the analysis that the heat transfer process is important for establishing a propagation flame front. Unlike the counter-current configuration reactors, in the case of co-current reactor geometry, higher consumption of char resulted in increased bed movement and this is an important parameter to be consider for long duration or sustained operation of the gasification system.

6.3 Comparison of the results with literature reported data

Fig 6.7 presents the peak bed temperatures measured during the experiment in two different capacity gasifier, model estimation of the peak bed temperature and the reported data from the literature. It is observed that as the air mass flux increases, peak bed temperature also increases and it is important to note that the situation in the reactor is always in fuel-rich conditions at gasification process. It can be concluded from Fig 6.7 that peak temperature estimation through the model follows similar trend of the experimental measurements. In the case of 35 kg/hr capacity reactor, as mentioned in the experimental results section, the reactor is better insulated than the 3 kg/hr reactor and hence some differences are observed. Considering the difference in density, shape and size of the particles influences the bed porosity, the differences

in the peak temperatures in case of Fatehi and Kaviany (1994), Rönnbäck *et al.* (2001) and experimental results of 35 kg/hr gasifier is justified.
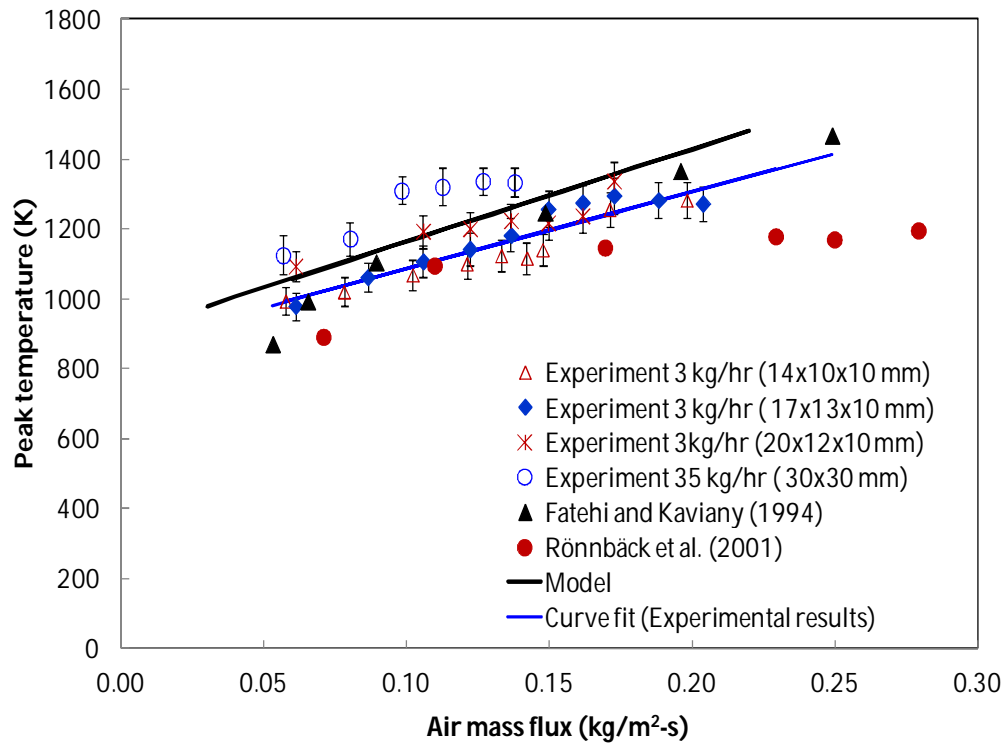
Fig 6.7 Peak bed temperatures at various air mass flux

The fuel sample used in Fathehi and Kaviany (1994) of spherical diameter of 6.4 mm and Rönnbäck *et al.* (2001) used pine wood with diameter of 8 mm in reverse downdraft configurations. Horttanainen *et al.* (2002) found that the optimal air flow rate at which the propagation rate is maximum is lower for the fuels which constitute small particles and maximum propagation rates are achieved at fuel rich conditions. Yang *et al.* (2004) reported that the reaction zone thickness in the bed increases as the combustion proceeds and becomes very hot before the combustion ends. The data from Fathehi and Kaviany (1994) is used in the fuel rich (gasification) regime, where it is observed that the burning rate increases as the air flow rate increases until a peak point is reached, beyond which further increase in the air flow rate reduces the burning rate. Porteiro *et al.* (2010) experimentally studied in the counter-current process and observed that air mass flow rate is one of the parameters that have the most influence on ignition front propagation velocity. It is also found that the

maximum front velocity is achieved at sub-stoichiometric conditions, as the cooling effect due to excess air is minimum.
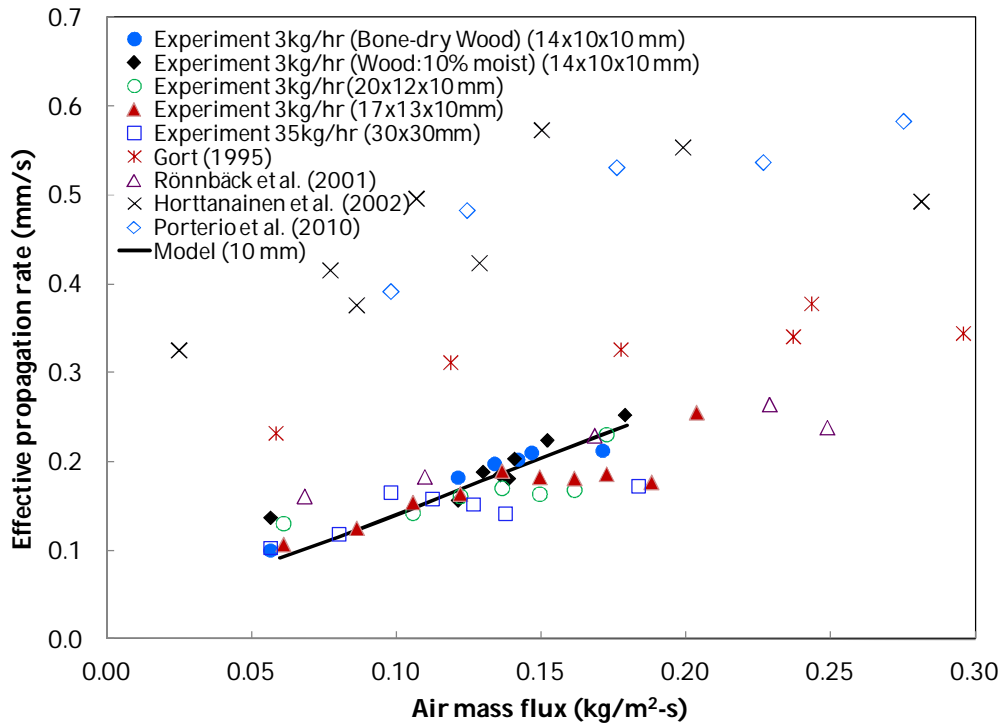
Fig 6.8 Effective movement from model and experiment at various air mass flux

Fig 6.8 represents the effective propagation front at different air mass flux and compare with the results from Gort, 1995; Rönnbäck *et al.* 2001; Horttanainen *et al.* 2002; Porteiro *et al.* 2010. It can be observed that the effective propagation rate increases with the increase in air mass flux. With increase in the air mass flux, reactant fraction implies increased oxidising environment resulting in higher fuel consumption rate. With increased fuel consumption rate leads to higher bed movement and hence net increase in effective propagation rate. However, beyond a certain mass flux, the effective propagation rate profile nearly stagnates. This must be contrasted with the flame propagation rate profile (Fig 6.3) where it reaches a maximum at a particular air mass flux and beyond that flame propagation rate start decreases. However, the rate of increase in bed movement due to fuel consumption and shrinkage is dominated the flame propagation rate decrease beyond the critical mass flux. In case of model estimation, it is observed that the effective movement linearly increases with the

increase in air mass flux. The model estimation has good agreement at lower air mass flux but differs at the higher air mass flux regimes.

Fig 6.8 presents the effective propagation rate reported by Gort (1995), Horttaninen *et al.* (2002), Rönnbäck *et al.* (2001), Porteiro *et al.* (2010). It can be observed that except Horttaninen *et al.* (2002) (wood chips), Porteiro *et al.* (2010) (pine shavings) results, all other results falls under a narrow band and follows the pattern with the model estimation. The surface area/volume ratio for wood chips and pine shavings is relatively higher than all other cases (Table 4.1). Similarly, the bulk density is also lower in these two fuel samples than the other fuels considered in Fig 6.8 and hence the void fraction is also high (Table 4.1). Horttaninen *et al.* (2002) observed that the increase in bed porosity makes the flame propagation quicker, since the thermal energy required to heat the bed reduces and also inter-particle heat transfer enhanced due to the higher surface area/volume ratio. Thus, higher surface area/volume and lower bulk density are the reasons for higher propagation rate for wood chips and pine shavings. Gort (1995) and Horttaninen *et al.* (2002) also showed that particle size does not have any significant effect on the propagation rate. The difference in the propagation rate is strongly dependent on the physical properties of fuel (surface area/volume ratio) apart from other properties like fuel conversion and possible heat loss from the reactor wall also influences the temperature profile in the packed bed.

Fig 6.9 presents the results of effective propagation rate normalised with bulk density to address the observed variations in Fig 6.8. Fig 6.9 also represents the air mass flux, at which flame propagation achieves negative value. It can be observed from the Fig 6.9 that at the extinction point, the profile changes, means the gasification regimes slowly changes towards combustion regimes. As all the experiments are carried out in the sub-stoichiometric regimes, the experimental measurements of this study limited up to the extinction point. There is no measurement beyond the extinction points. However, in the reported literature, in reverse downdraft configurations, where combustion processes are characterized, there are measurements beyond this

extinction limit (Fathehi and Kaviany, 1994; Gort, 1995; Rönnbäck *et al.* 2001). The overall trend of the model estimation closely lies in a narrow band of all the experimental measurements and the literature data.
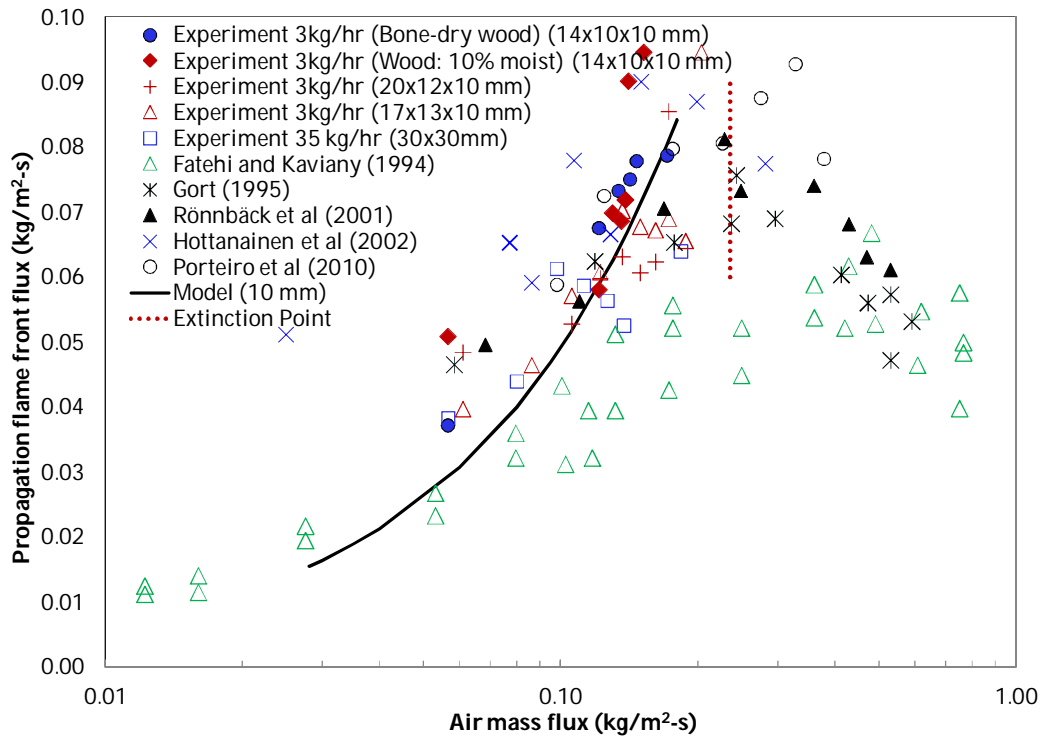
Fig 6.9 Propagation flame front flux from model and experiment at various air mass flux

Having validated the model with the experimental results with reasonable accuracy and providing insight into various processes that occur in the co-current reactor configuration for gasification, another important parameter is the gas composition, an essential requirement in a conversion process is discussed in the following section.

6.4 Gas compositions at various air mass flux

The volume fraction of various gaseous species at the reactor exits is obtained from the modelling. The volume fraction of various gaseous species evolved at the reactor exits for different reactant mass flux is presented in Table 6.2 and compared with the experimental measurements. The gaseous species comprises of CO, CO_2, H_2, CH_4, N_2 and H_2O. The hot moist output gas is used to arrive at the dry gas mole fraction used in the present analysis to compare with the experimental results.

Table 6.2 Volume fraction of different gases from model and experimental at various air mass flux
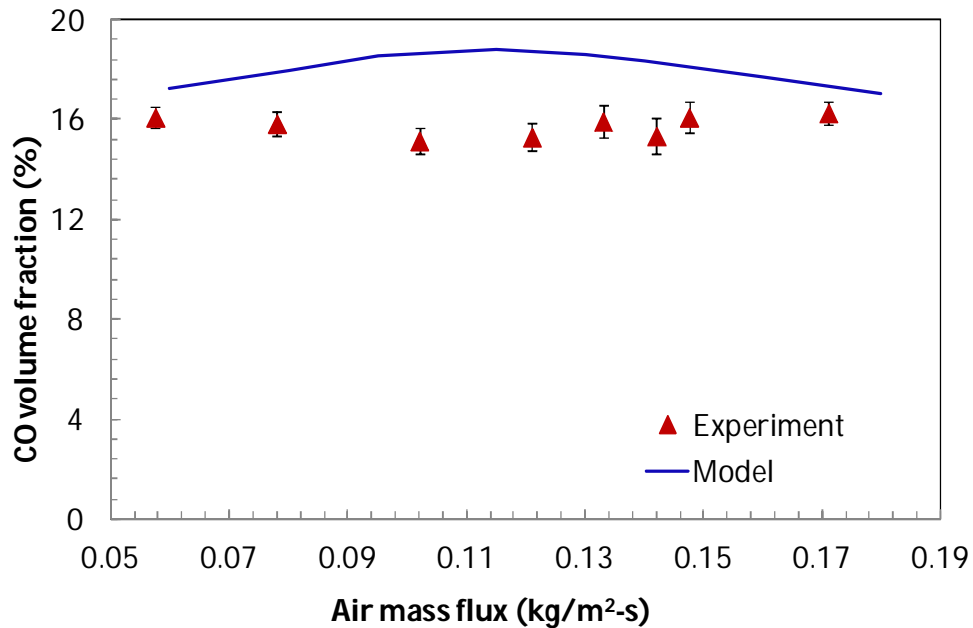
Model				Experiment			
Air mass flux (kg/m^2-s)	CO_2 (%)	CO (%)	H_2 (%)	Air mass flux (kg/m^2-s)	CO_2 (%)	CO (%)	H_2 (%)
0.060	17.98	17.25	13.02	0.058	15.00	16.09	8.65
0.080	16.85	17.98	13.76	0.078	15.05	15.84	9.52
0.095	16.46	18.56	14.54	0.102	14.90	15.15	10.85
0.105	16.23	18.69	14.98	0.121	14.95	15.29	11.15
0.115	16.26	18.78	15.54	0.133	15.11	15.92	12.97
0.130	16.42	18.62	16.14	0.142	14.89	15.34	13.85
0.140	16.77	18.32	16.18	0.148	13.10	16.09	12.86
0.160	17.25	17.72	15.92	0.171	14.33	16.27	8.89
Average	16.78 ± 0.59	18.24± 0.54	15.01± 1.16	Average	14.89± 0.28	15.75± 0.43	11.09± 1.99

Fig 6.10 to 6.12 presents the CO_2, CO and H_2 volume fraction measured during the experiments and estimated from the model for different air mass flux. It can be observed from Fig 6.10 that the experimental measurement of CO_2 is nearly constant and about 15% for all the air mass flux. However, in case of model estimation, CO_2 decreases with the increase of air mass flux, and reaches minimum 16.23% at 0.105 kg/m^2-s air mass flux, and beyond this, again it has increased. It also can be observed from Fig 6.3 that at higher mass flux, the bed temperature is high, and consequently CO_2 fraction is also high. There is a slight difference in the experiment measurements and the model estimation. This difference could be attributed to the small scale gasifier, where fuel conversion is not complete as like the model gasifier or in large gasifier in the field. It is also might be due to air nozzle off at the oxidation zone and henceforth the CO_2 fraction is relatively higher in this case than field gasifier (12%).

It can be observed from the model estimation of Fig 6.11 that the CO fraction is maximum (18.72%) at an air mass flux of 0.115 kg/m^2-s. The experimental measurement shows that the maximum CO fraction (15.11%) at an air mass fluxes 0.133 kg/m^2-s. Both the model estimation and experimental measurement shows that the variations of CO fraction over the range of air mass flux are very low.
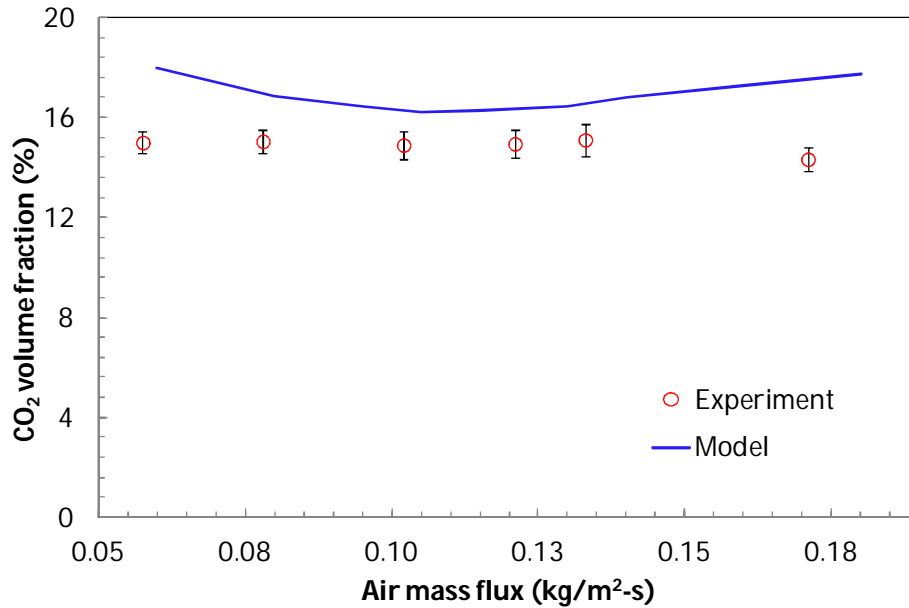
Fig 6.10 CO_2 volume fraction from model and experiment at various air mass fluxes

Fig 6.11 CO volume fraction from model and experiment at various air mass fluxes

In case of model estimation, the standard deviation over the range of air mass flux is 0.68% and for experimental measurement, it is 0.28%. Refereeing back to Fig 6.3, it can be observed that the peak propagation front rate occurs at 0.135 kg/m²-s for model estimation and 0.132 kg/m²-s for experiment measurements. Hence, it can be concluded that CO fraction is almost constant in a close band of peak propagation

front regimes (air mass flux range). This also concludes that, if the gasifier operates at an air mass flux close to the peak propagation front, CO fraction will be nearly same in this operation range. It is observed that the variations of temperature in this range in the range of 1050 K to 1350 K. It is important to note that with the increase in bed temperature, CO_2 concentration increases. However, as the operation range in the gasification regime kept in this air mass flux regimes, the increase in CO_2 concentration is very high at the higher air mass flux range only.
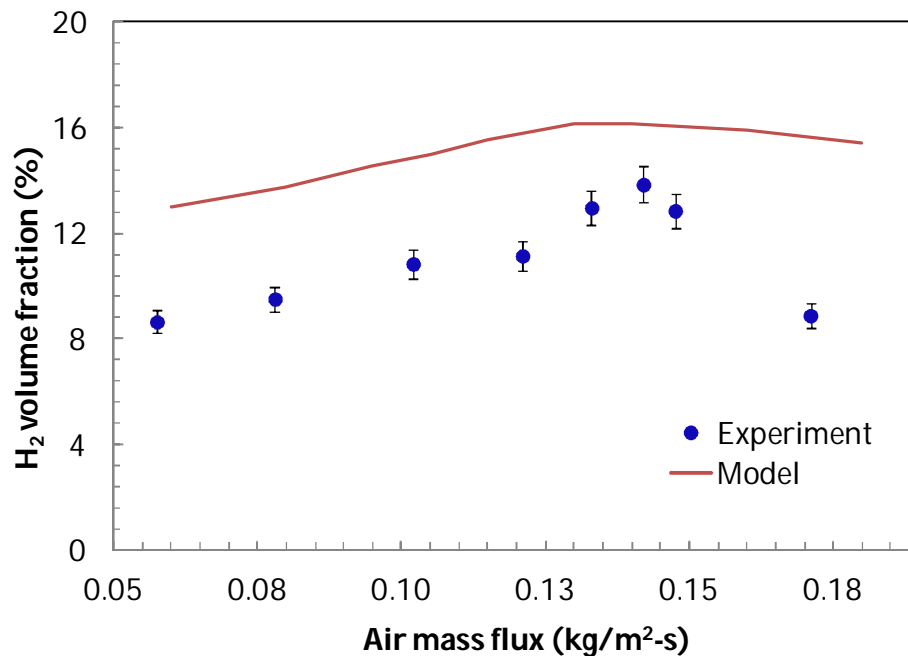
Fig 6.12 H_2 volume fraction from model and experiment at various air mass fluxes

Fig 6.12 presents H_2 fraction at different air mass flux. The biomass sample used both for the model and the experiment is moisture free. The maximum H_2 fraction in the model estimation is 16.18% at an air mass flux of 0.14 kg/m²-s and in case of experimental measurement, it is 13.85% at an air mass flux of 0.142 kg/m²-s. The H_2 fraction profile with the air mass flux is similar to the earlier two cases. As the air mass increases, H_2 fraction increases, reaches a maximum point and then decreases. The analysis related to the gas composition, model estimation and experimental measurement shows that the gas composition is nearly constant in the entire air mass flux range. This suggests that the overall reaction occurs in sub-stoichiometric regimes

in the bed. It is also found from the equilibrium analysis that this type of gas composition occurs at air to fuel ratio in the range of 1.5-1.8, which is the typical condition for the gasification process. The difference between the model estimation and the experimental measurements is expected, as the experiments are conducted in small-scale gasifier, difference in physical properties of fuel (shape of particle is spherical in case of model and, rectangular in case of experiment) etc. Further work is required to address these issues.

6.5 Air mass flux and volatile fraction in the producer gas

Fig 6.13 presents the unreacted volatile fraction at various air mass fluxes. This is the reflection of operating regime for a fixed bed reactor. The higher molecular weight fraction released as a part of pyrolysis process identified here as volatile fraction; is assumed to be a representative sample of tars that is considered in the gasification literature. The model prediction represents a typical trend as complete multi-step mechanisms for the primary and secondary pyrolysis are not captured. It can be observed that at lower air mass flux, the volatile conversion is lower due to lower average bed temperature. As the air mass flux increases, bed temperature increases (Fig 6.3) thus helping in cracking of higher molecular weight compounds present in the volatiles. At higher air mass flux (0.15 kg/m^2-s or beyond), the unreacted volatile fraction almost diminishes, with the bed temperature reaching in excess of 1300 K. Further, it is evident from the pyrolysis literature (Riaza *et al.* 2014; Fatehi and Bai, 2014; Momeni *et al.* 2013b) that the product distribution varies with temperature. In order to benefit from this situation, the open top gasification system developed at IISc uses a set of air nozzles at about two third heights below the reactor top to address this situation. This is used as re-burn of the gaseous products to improve the bed temperature at a lower air mass flux and thus reduce the volatile fraction in the gas (Dasappa *et al.* 2004). Fig 1.6 presents the schematic of such system used commercially for thermal and power generation, where measurements on tar and particulates have indicated 501-774 mg/m^3 in the raw gas and 10-146 mg/m^3 in the cold gas (Mukunda *et al.* 1994).
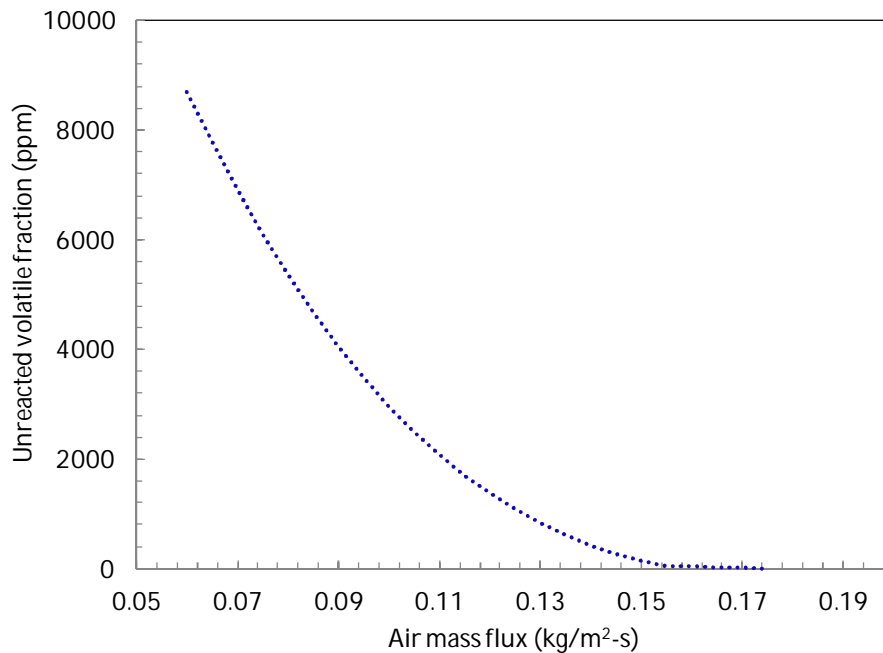
Fig 6.13 Unreacted volatile fractions at various air mass flux

Pérez *et al.* (2012) have reported that higher temperature in the reactor leads to volatile reforming reactions, which reduces tar generation. Similar to the present study, Pérez *et al.* (2012) have also observed that with an increase in the superficial air velocity in a packed bed, tar generation reduces. Kinoshita *et al.* (1994) reported that temperature and equivalence ratio have significant effects on tar generation. Tar yield decreases with the increase in temperature or equivalence ratio. Hernández *et al.* (2013) observed that with the increase of fuel/air ratio, decrease the available oxygen in the fuel bed to oxidize the volatile matter released from the fuel and as the bed temperature increases, tar generation decreases. Phuphuakrat *et al.* (2010) also found that with the increases in equivalence ratio, oxidation zone temperature increases because air promoted in the combustion reaction and amount of tar in the exit gas decreases.

6.6 Influence of surface area of particle on gasification process

Numerical analysis and experiments are carried out to address the influence of particle surface area on the overall process, for varying surface area per unit volume (SA/V) ratio in the packed bed reactor. Towards increasing the surface area per unit

volume of the reactor, as a part of the model, the higher molecular weight fraction products of pyrolysis, identified as volatile fraction is considered as a species from the reactor output. Influence of particle size on the gasification clearly identified that at higher SA/V ratio, tar levels is high from experimental measurements as in Chapter III. An attempt is made here to address this aspect using the model results. Fig 6.14 presents the conversion time variation and the unreacted volatile fraction with surface area/volume ratio of the particle within the packed bed.
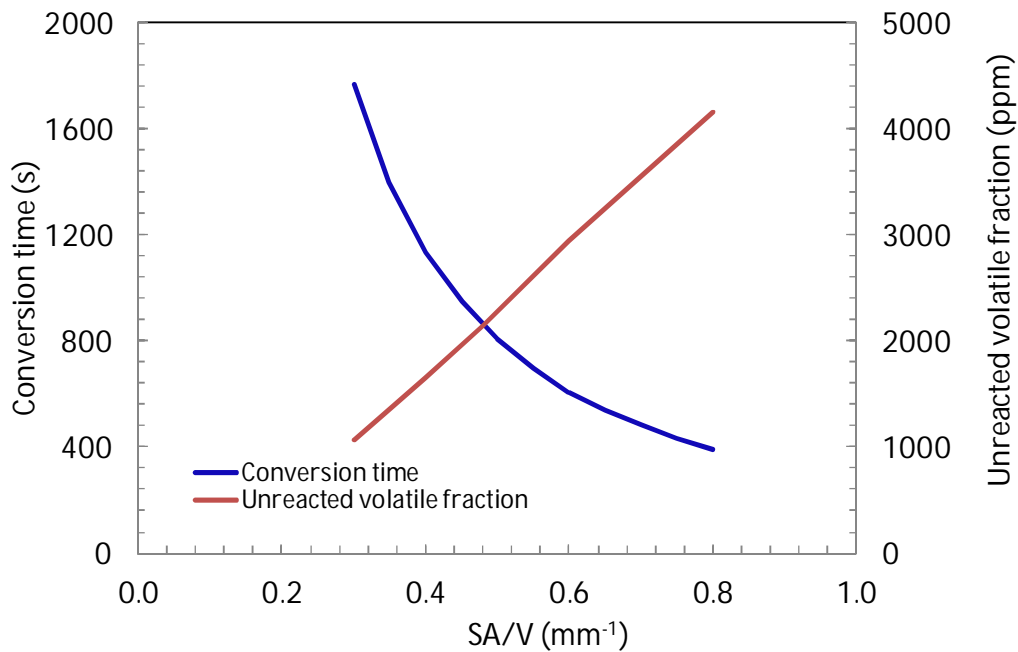
Fig 6.14 SA/V vs conversion time and unreacted volatile fraction

Data set for air mass flux is fixed at 0.105 kg/m^2-s, with varying particle size, with no moisture is presented in Fig 6.14. As the SA/V increases, the conversion time reduces, means smaller the particle (larger SA/V), conversion time is lower in compare with larger particle size (lower SA/V). It is found from Fig 6.14 that the conversion time varies with $(SA/V)^{-1.54}$. The time for pyrolysis is inversely proportional to the surface area, thus increase the surface area leads to increase the pyrolysis rate at the same temperature (Phuphuakrat *et al.* 2010). It is also important to mention that the pyrolysis of very small particle is mainly controlled by reaction kinetics, whereas for the larger particle, process mainly controlled by diffusion. Further, larger particle has

higher heat transfer resistance and hence, the actual temperature inside the particle is lower, leading to products of slow pyrolysis. However, in the case of smaller particles, it could transit to fast pyrolysis depending upon the temperature with products having larger fractions of volatiles. Simmons and Ragland (1986) reported that with the reduction of particle size, burning rate per unit mass increases linearly. Mason *et al.* (2015) observed as the aspect ratio increases; volatile burn time becomes quicker. The model estimation results analysis has a good agreement with the observations made in the literature. While the qualitative evaluation with supportive information from the literature has been used towards arriving the packed bed behaviour; further investigations is beyond the current scope.

6.7 Summary

Results from packed bed model reported in the study has been used to analyse, estimate the propagation rate, effective propagation rate, bed temperature, gas composition, unreacted volatile fractions in the bed. The model predictions compare well with the present experimental results, and also those found in the literature with respect to counter and co-current reactor configurations on the flame propagation and effective propagation rates. The propagation rate correlates with mass flux as $\dot{m}''^{0.883}$ during the increasing regimes of the front movement. It is also found that at an air mass flux of 0.235 kg/m^2-s, the front is receding, or moves towards the char bed. This phenomena also indicates that beyond this air mass flux (0.235 kg/m^2-s), reactor ceases to function due to reverse propagation of the front. The model and experimental measurement shows that the effective propagation rate increases with the increase in air mass flux. In case of peak temperature of the bed, model estimation and experimental measurement are quite close to each others. It is observed that as the air mass flux increases, peak bed temperature also increases. The model analysis provides a comprehensive understanding with respect to the packed reactor under gasification conditions addressing the dependence on mass flux on gas composition and propagation rate with experimental validation of the results.

Conclusions and future work

This thesis has contributed towards enhancing the fundamental understanding on the gasification process in a co-current downdraft reactor configuration. Identification of the optimal flame propagation front movement, bed movement and effective movement for a co-current configuration reactor has been the primary contribution. The study reports the performance of an open top down draft configuration and compares the results from literature; providing a scientific basis towards arriving at the performance of co-current gasifier system. Significance of the contribution arises from the fact that most of the reported works in the literature primarily focus on counter-current configurations for arriving at bed performance parameters like the propagation flame front and bed temperature. The current work bridges the gap in respect of co-current gasifier knowledge base.

The need and the status of the current understanding of different reactor configurations and their performance as packed bed reactors have been clearly addressed in the introduction. Most of the reported literature primarily reports results on flame propagation rate/ignition mass flux and temperature profiles under the combustion regime. Single particle analysis and importance with respect to the thermo-physical properties of the fuel have been established. Chapter one establishes the need to understand the co-current configuration with focus on the flame propagation rate towards enhancing the residence time of the process inside the reactor. Chapter two, three and four described with the experiments and analysis of the results using different capacity open top downdraft reactors, fuels of varying surface area/volume ratios; air mass flux, and its influence on tar generation, gas composition, propagation rate and other relevant parameters.

The study on particle physical properties depicts its influence on tar generation in a fixed bed gasification system and the importance of the heating rate and the surface area of the particle affecting the release of the volatile fraction is addressed. Studies with density variations between 357 kg/m^3 (wood flakes) to 1352 kg/m^3 (coconut shell) and the ratio of surface area to equivalent diameter (different shapes of biomass) in comparison to wood sphere of 1.88 to 1.97 m have established the significance of pyrolysis rate and the need to increase residence time required towards enabling thermal cracking of higher molecular weight compounds. These aspects have significant impact on the performance of packed bed reactors. Experimental results reveal that the amount of tar generated is in the range of 336 to 416 mg/m^3 in case of wood flakes, and for wood chips the values are in the range of 43 to 77 mg/m^3. The current work provides a scientific basis to address aspects related to generation of high tar in fixed bed gasification system for varying physical properties of fuel. Experimental studies suggest that improving the residence time of the gas in the reduction zone helps in reducing the tar. Gas residence time in the reduction zone can be controlled by appropriate proportioning of air between the top and the nozzle. Experimental results show that as the nozzle air flow to total air flow ratio reduces from 0.986 to 0.352, tar content in the gas drops from 1058 mg/m^3 to 47 mg/m^3. It can be concluded that increase in the residence time helps in reducing the amount of tar in the hot gases.

The present study, addresses the combined influence of flame front speed and biomass consumption rate in the form of *'effective propagation'*, a unique approach and term in case of co-current configuration systems. It is observed that the flame front speed increases with the increase of air mass flux, attains a peak value and then decreases at higher air mass flux. While the propagation rate decreases beyond a certain air mass flux, the bed movement continues to increases in a linear fashion with the air mass flux in the co-current configuration. The bed movement is the contribution of shrinkage due to pyrolysis and the char conversion process. The peak flame front propagation rates is 0.089 mm/s at air mass flux of 0.134 kg/m^2-s. On the

influence of biomass moisture content, it is observed that the flame front propagation rate decreases with an increase in fuel moisture content due to the endothermicity involved in drying of the moist wood.

Importance of surface area per unit volume of the particles in the packed bed has been recognized. The study observed that the high surface area per unit volume and the lower bulk density are the primary reasons for higher propagation rate in wood chips and pine shavings. Hence, the propagation flame front with thin particles is high compared to that for particle beds that consist of spherical or cubical particles. Effective propagation rate data from the present study and literature lie in a narrow band except for wood chips and pine shavings. These differences are argued to be so due to the high surface area per unit volume and the low bulk density of wood chips and pine shavings. Further, the normalized propagation rate or the propagation flame front flux or ignition mass flux depicts a better way to present the result to account for density variation in the packed bed. Finally, the physical properties of the fuel like particle shape and size (surface area per unit volume), bed density, particle density, energy content of fuel and moisture content together have an impact on propagation front movement.

The one-dimensional model developed is sufficiently versatile and predicts the experimental results of the current work and literature reported results for the counter current configuration with sufficient accuracy. The propagation rate correlates with mass flux as $\dot{m}''^{0.883}$ during the increasing regimes of the front movement. The extinction of flame propagation or the front receding has been established from the results; experimentally and from the model to be at an air mass flux of 0.235 kg/m^2-s. This phenomenon also indicates that beyond this air mass flux; reactor ceases to function due to reverse propagation of the front. The model analysis provides a comprehensive understanding with respect to the packed bed reactor under gasification conditions and addresses the dependence on air mass flux on gas

composition and propagation rate. The model also has the capability to predict the gas composition at varying air mass flux.

In summary, the scientific investigations carried out in the present study address the issues of solid fuel conversion under gasification regime and provide inputs towards the understanding the performance of packed bed reactors, while addressing the aero-thermochemistry issues linked to the fuel properties and air mass flux.

Future work

This study primarily focused on experimental work and modeling of the wood gasification system. While the work at Indian Institute of Science has indicated the capability of the open top down draft gasification to handle agro residue briquettes, additional experiments and modeling are required to handle the briquettes with varying ash content. Another important aspect is arriving at the sharing of air between the nozzles and the open top for varying thermo-physical properties of the fuel. This aspect coupled with computational fluid dynamic investigation would provide a complete solution to packed bed reactors.

Access to electricity through biomass gasification system

A.0 Introduction

Energy is one of the major inputs for the socio-economic development of the rural areas of any developing country. More than 600 million Africans and 300 million Indians are still without access to electricity (World Energy Outlook, 2014). Access to electricity is essential for economic growth, poverty elimination, employment generation and improvement of livelihood of the villages. In rural India, more than 44 per cent of the households do not have access to grid electricity (Census Report, 2011). In case of rural households, 43.2 % uses kerosene, and 55.3% uses electricity for lighting (Census Report, 2011). This study explore the use of biomass gasification system as a part of distributed power generation system to provide access to electricity in the remote villages as a part of sustainability of the technology package. This section[14] presents an analysis aimed at choosing between off-grid solar photovoltaic, biomass gasifier based power generation and conventional grid extension towards access to electricity in the remote villages. The model provides a relation between renewable energy systems capacity and economical distance limit from the existing grid point based on life cycle cost analysis. The CO_2 emissions from kerosene based lamps; modern bio-energy systems and solar photovoltaic are also studied. The fuel consumption is used to determine the CO_2 emissions for all the domestic lighting devices.

---

[14] *This work published in*

- *Mahapatra, S., Chanakya, H. N. Dasappa, S. Evaluation of various energy devices for domestic lighting in India: technology, economics and CO_2 emissions. Energy for Sustainable Development 2009; 13 (4): 271-279.*
- *Mahapatra, S., Dasappa, S. Rural electrification: optimising the choice between decentralised renewable energy sources and grid extension. Energy for Sustainable Development 2012; 16 (2): 146-154.*

A.1 Decentralized renewable energy based systems and grid extension

The study is focused on modeling off-grid renewable energy solutions using biomass gasifier based systems or photovoltaic systems and comparing them with grid extension for remote village electrification. The minimum load requirements for a rural household include power for domestic needs are lighting, fans, television, street lighting, and drinking water supply. Apart from this, small-scale industries like agro-processing are also required in villages. The approach is to formulate the relation between the renewable energy system capacity and the economical distance limit (EDL) from the existing grid point based on life cycle cost (LCC) analysis. The EDL is defined as the distance where the LCC of energy (Rs/kWh) of the renewable energy systems matches the LCC of energy from grid extension. This analysis is designed to predict the capacity of the renewable energy systems and corresponding optimal economical distance. The study also addresses sensitivity analysis of the critical parameters. The data used for the analysis is arrived at from case studies on various distributed power generation systems. The numbers considered in this study are indicative; it may vary as the cost changes with time, location and manufacturer.

A.2 The analysis

The competitiveness of biomass gasification and solar photovoltaic based power generation for rural electrification is assessed and compared with the conventional option of extending a state owned grid. The costs of biomass gasifiers and solar photovoltaic based systems are determined for different capacities. The cost incurred to extend the grid from the available grid point to the village is also determined. The LCC of energy generated at the end point (Rs/kWh) is used to compare these options. An exact and fair comparison between renewable energy systems and the conventional power grid is rendered difficult by the different operating situations. In this analysis, partial accounting of the environmental degradation is considered by using carbon trading benefit from these renewable energy based systems. Biomass price is considered constant in the entire project duration and inflation and the salvage value of the components are not considered for simplicity in calculations.

Although realistic costs have been used in the analysis, these parameters are indicative; the results are expected to vary slightly to account for different geographical locations. The cost of low tension transmission distribution lines within villages has been excluded, since it is the same in all the cases. The detailed cost analysis and input parameters are given in Mahapatra and Dasappa (2009) and Mahapatra and Dasappa (2012).

The costs of delivered energy from the biomass gasification and solar photovoltaic systems are calculated by the life cycle cost (LCC) analysis method. The LCC is calculated by considering the capital cost, fuel cost for the entire project life, present worth value of the operation and maintenance cost, component replacement cost etc, and also the total carbon trading benefits in the entire system life. The LCC of energy for each option is calculated by dividing the total LCC of the system by the total energy output in the system's life. The LCC values for different capacities of photovoltaic systems and biomass gasification systems are calculated by using the following relations.

$$LCC_{PV} = \frac{C_{PV} + C_B + (C_{PV} + C_B) \times \beta \times P(d,n) + C_R \times P(d,n_1) - C_C \times P(d.n)}{L \times h \times n} \quad (A.1)$$

$$C_C = (L \times h \times n \times C)$$

C_{PV} and C_B are the capital costs of the photovoltaic system, excluding the battery, and the battery respectively, β is the fraction of capital cost for annual operation and maintenance of the system, C_R is the component replacement cost, h is the annual operation hours, n_1 and n are the life of a specific component and the complete system, d is the discount rate, P is the present worth factor and C_C is the annual carbon benefit. L is the system capacity and C is the carbon emission benefit (Rs/kWh)[15].

$$LCC_{BG} = \frac{C_G + C_E + (C_F + C_M) \times P(d,n) + C_R \times P(d,n_1) - C_C \times P(d.n)}{L \times h \times n} \quad (A.2)$$

$$C_F = (S_C \times f_{con} \times h \times f_c)$$

---

[15] *Carbon emission benefit (Rs/kWh) is calculated by multiplying the grid emission factor (kg/kWh) and the carbon trading cost (Rs/tonne).*

$$C_M = (S_C \times h \times m_c)$$

$$C_C = (L \times h \times n \times C)$$

C_G and C_E are the capital costs of the gasifier system and engine, L is the gasification system capacity (kW), h is the annual operation hours, n_1 and n are the life of a specific component and the complete system, d is the discount rate, P is the present worth factor. C_F is the annual fuel cost, C_M is the annual maintenance cost, C_R is the component replacement cost and C_C is the annual carbon benefit. S_C is the gasifier rating (kg), f_{con} is the fuel consumption (kg/hr), f_c is the unit fuel cost (Rs/kg), m_c is the maintenance cost of the system (Rs/kWh) and C is the carbon emission benefit (Rs/kWh).

The grid extension cost depends on the distance of the village/load centre from the existing grid, cost of distribution transformer and operation and maintenance cost of the grid line. The cost of delivered electricity at the village or load centre depends on the cost of unit power generation (electricity cost at existing grid point), transmission and distribution losses, load demand and grid availability. So, the life cycle cost of grid extension depends on life cycle cost of electricity generation at the village load centre, capital cost for grid line depending on the distance of the village load centre from the existing grid point, cost of distribution transformer and operation and maintenance cost. The expression for calculation of LCC of energy (Rs/kWh) for grid extension can be written as

$$LCC_{GE} = \frac{LCC_{gen} + LCC_{grid} \times X}{L \times h \times n} \qquad (A.3)$$

$$LCC_{gen} = t_{gen} \times L \times h \times \left(\frac{1}{1-\delta_{t\&d}}\right) \times P \qquad (A.4)$$

$$LCC_{grid} = C_{grid} + C_t + (C_{grid} + C_t) \times \beta \times P \qquad (A.5)$$

$$P = \frac{d \times (1+d)^n - 1}{d \times (1+d)^n}$$

LCC_{GE}, LCC_{gen} and LCC_{grid} are the life cycle cost for grid extension, electricity generation and grid line (cable/conductor and transformer) cost respectively, X is the distance from the village load centre to the existing grid point. L is the load demand, h is the

annual operation hours, *d* is the discount rate and *n* is the life of the project. t_{gen} is the electricity generation cost, $\delta_{t\&d}$ is the transmission and distribution losses, *P* is the present worth factor, C_{grid} is the grid line cost, C_t is the distribution transformer cost, β is the fraction of capital cost for operation and maintenance of the grid. The economical distance limit (EDL) is calculated by considering the life cycle cost of the renewable energy systems and the distance at which this cost and the life cycle cost of grid extension match; this is similar to break even analysis. The following expression is used for the calculation of the economic distance limit (EDL).

$$\frac{LCC_{GE} \times EDL + LCC_{gen}}{L \times h \times n} - LCC_{BG/PV} = 0 \qquad (A.6)$$

EDL values are calculated for different capacities of renewable energy systems and for various operation hours of the renewable energy systems at various grid availability hours.

A.3 Results and discussion

A.3.1 Biomass gasification systems and grid extension

The critical distance of a load centre from the existing grid point above which the economic performance of grid extension matches that of local biomass gasification systems or photovoltaic systems, depicted as economical distance limit (EDL), has been calculated by using equation A.6 for different system capacities. Fig A.1 represents the EDL values for different gasification system capacities at different values of operation hours and grid availability. The EDL value varies from 4.2 km to 41.6 km for system capacities of 10 kW to 120 kW for daily operation with an availability of grid-based power of 6 hours.

The EDL values for 25 kW capacity systems with 6, 12 and 24 operation hours are 10.4 km, 5.9 km and 3.7 km respectively for 6 hours of availability of grid-based power. However, the EDL for the system increases for a particular value of operation hours as the availability of grid-based power increases. It is important to mention that in the conventional rural electrification programme through grid extension the quality and

availability of power is very poor in the villages. So, for the present study, 6 hours of availability of grid-based power can be considered a realistic approach. The life cycle cost of energy for grid extension and gasification systems for a village load of 25 kW, which is 10.5 km far from the existing grid, will be the same. With daily availability of grid-based power of 12 hours (though this is not very realistic in the present scenario) the EDL for a 25 kW system with 12 hours of operation is 12 km, whereas the EDL is 10.5 km for 6 hours of operation and availability of grid-based power. Hence, it can be concluded that the economics of a 25 kW biomass gasification system will be attractive if the village is approximately 12 km (considering 12 hours availability of grid-based power) away from the existing grid point. At the same time, as this biomass gasification based system is localized in the village, the reliability and quality of power from such a system is also very high.
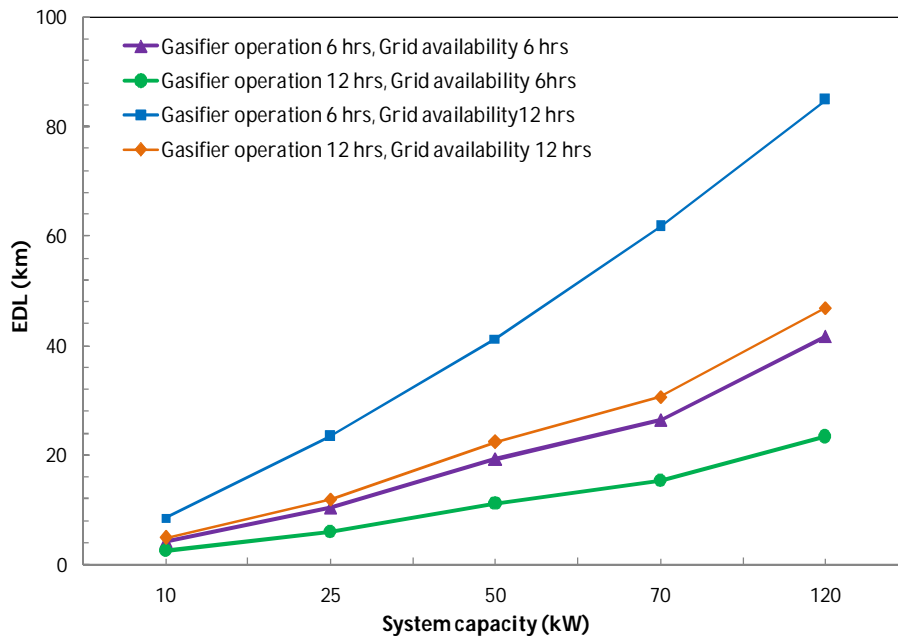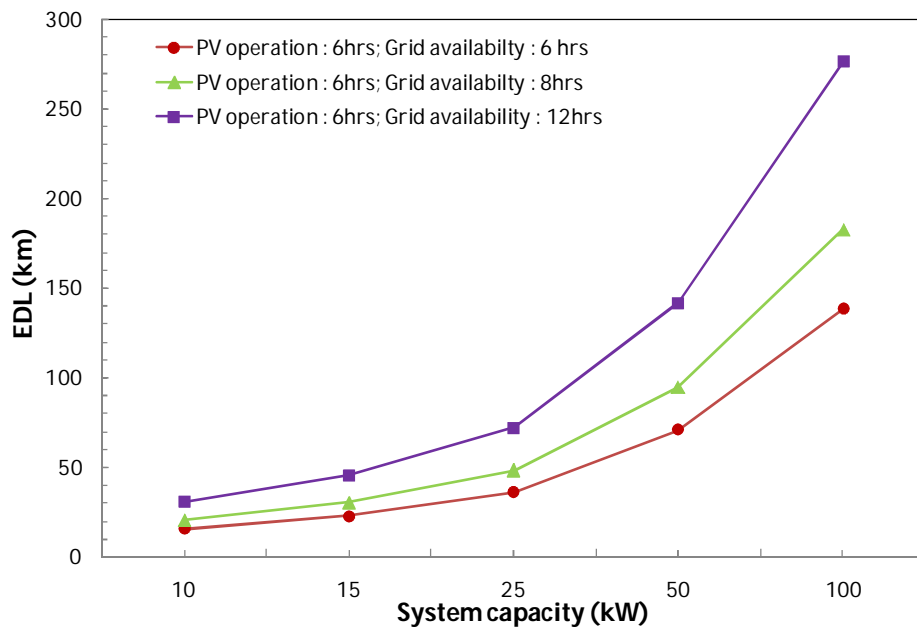

Fig A.1 Economic distance limit for biomass gasification systems

A.3.2 Photovoltaic systems and grid extension

The EDL for a photovoltaic system is calculated similarly to that for a gasification system. Fig A.2 represents the EDL for different capacities of photovoltaic systems for various availability of grid-based power. The life cycle cost of energy from a

photovoltaic system mainly depends on the capital cost of the system, whereas the operation cost is minimal as there is no fuel cost. It is observed from Fig A.2 that the EDL values increases with the increase in availability of grid-based power from 6 hours to 12 hours. The EDL values vary from 15 km to 138 km as the system capacity varies from 10 kW to 100 kW for daily system operation with an availability of grid-based power of 6 hours. For a system capacity of 25 kW, the EDL value varies from 36 km to 72 km as the availability of grid-based power varies from 6 hours to 12 hours. The electricity consumption pattern in a photovoltaic system is very different from that in a grid system or even in a biomass gasification system. Photovoltaic systems can provide a fixed amount of electricity per day whereas there is normally no such limitation for grid-connected or biomass gasification systems.

Fig A.2 Economic distance limit for photovoltaic systems

A.3.3 Comparison of biomass gasification systems, photovoltaic systems and grid extension

A comparative analysis of EDL for biomass gasification systems and photovoltaic systems has been done. The operation hours have been kept 6 hours for both the options and the grid availabilities are 6 hours, 8 hours and 12 hours respectively. Table A.1 represents the EDL comparison of biomass gasification and photovoltaic
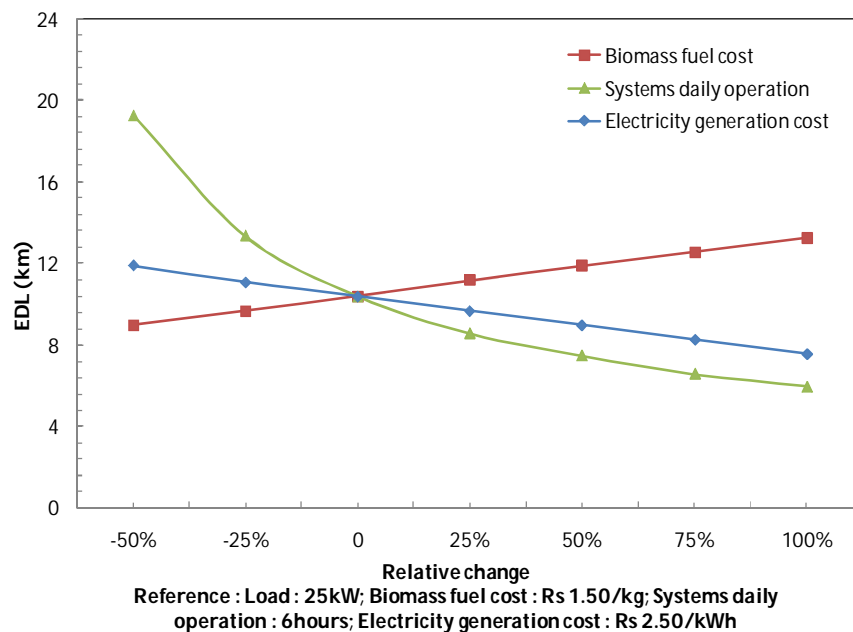
systems. It can be observed from Table A.1 that the EDL values for a photovoltaic system and a biomass gasification system are 36 km and 10.4 km respectively for a 25 kW system capacity with availability of grid-based power of 6 hours. Again, the EDL value for a photovoltaic system for availability of grid-based power of 12 hours increases to approximately 72 km for a 25 kW system capacity, whereas for the same capacity biomass gasification system it is 23 km. Hence, it can be concluded that biomass gasification systems are much more economically competitive compared to photovoltaic systems.

Table A.1 EDL comparisons of biomass gasifier and photovoltaic systems

Grid availability (hr)	Economic distance limit (km)					
	Photovoltaic systems			Biomass gasification systems		
	Load (kW)					
	10	25	50	10	25	50
6	15.2	36.0	70.9	4.2	10.4	19.3
8	20.2	48.0	94.5	5.0	13.9	25.8
12	30.4	72.0	141.8	8.4	23.4	41.2

It is evident from the analysis that the EDL values are dependent on LCC of energy. Again, LCC of energy is dependent on biomass fuel cost, system operation hours and electricity generation cost (existing grid point). Hence, it is important to check the sensitivity of the EDL with the relative change in system cost (gasification or photovoltaic), transmission line cost, biomass fuel cost, system operation hours and electricity generation cost. It is observed from the analysis that as the system cost (photovoltaic and gasification system) increases, the EDL also increases. However, as the transmission line cost increases the EDL comes down. This is expected trend as the transmission cost increases, means the grid extension cost increases, and hence the corresponding LCC for grid extension also increases. Fig A.3 represents the EDL sensitivity with the relative change in biomass fuel cost, operation hours and electricity generation cost for a 25 kW system capacity. It can be observed from Fig A.3 that the EDL varies from 9.0 km to 13.3 km as the fuel price relative change varies from -50% to 100% from its base price for a 25 kW biomass gasification system with daily operation and grid availability of 6 hours. It is also observed from the sensitivity

analysis that as the system operation hours increase, the EDL values come down. In the earlier analysis, the electricity cost at the existing grid point is considered to be Rs 2.50/kWh. However, this is a very conservative estimate. Hence, the LCC of grid extension has also been calculated by considering the relative change in electricity cost from -50% to 100%. As the electricity cost increases, the EDL value decreases from 10.4 km (at base price) to 9.6 km (at 100% increase in base price) at base biomass fuel cost and both daily operation and grid availability of 6 hours. So, it can be concluded that as the biomass fuel cost increases, the EDL value also increases; whereas, as the electricity cost increases, the EDL value comes down. It is observed that as the biomass cost increases to Rs 2.00/kg and the electricity cost increases to Rs 3.50/kWh, the EDL value changes from 10.4 to 10.3 km. So, it can be concluded that if both biomass price and electricity price increase simultaneously, there will not any significant effect on EDL.

Reference : Load : 25kW; Biomass fuel cost : Rs 1.50/kg; Systems daily operation : 6hours; Electricity generation cost : Rs 2.50/kWh

Fig A.3 Economic distance limit (EDL) sensitivity with biomass fuel cost, operation hours and electricity generation cost

Photovoltaic systems are designed for a certain load and operation hours and they cannot provide power longer durations or for increased loads. Unlike gasifier systems, where there is the flexibility of connecting other small scale agro-based industrial loads during the time when domestic loads are not in use, photovoltaic systems do not

have such flexibility. Hence, photovoltaic systems are suitable for the designed load and for the designed operation hours; whereas biomass gasification systems are suitable for the designed load with variable operation hours.

A.4 CO_2 emission analysis from energy devices for domestic lighting

Kerosene based lamps are predominantly used in the rural households. The light output of these lamps are very poor and in the combustion process, it also produce air pollutants, which are responsible for respiratory or eye infections etc. This section evaluates CO_2 emission based on fuel consumption rates of all the kinds of domestic lighting options. The best possible options are identified based on this calculation for providing good quality and reliable lighting in rural households. Kerosene lamps are inefficient and replacing them with electricity based lamps reduces the primary energy consumption, and also consequently reduces the CO_2 emissions. The CO_2 emissions from kerosene lamps are calculated both as CO_2 emitted per lumen-hours and as kg of CO_2/h to obtain a clear estimate of emissions per unit of illumination as well as total emissions. Table A.2 represents the annual CO_2 emissions associated with various kinds of devices for lighting systems. The emission reduction potential would be in choosing one alternative over another, e.g., solar photovoltaic CFL base systems over kerosene wick lamps.

Table A.2 CO$_2$ emissions in various lighting systems

Type of system	Fuel consumption	Luminous flux (lumen)	Gross CO$_2$ emission	Net CO$_2$ emission	Gross CO$_2$ emission [16] (g/lumen-h)	Net CO$_2$ emission (g/lumen-h)
Kerosene based lighting systems						
Kerosene wick lamp	21.6 (ml/hr)	76	0.055[17] (kg/h)	0.055 (kg/h)	0.728	0.728
Noorie	50 (ml/hr)	1250	0.128 (kg/h)	0.128 (kg/h)	0.102	0.102
Petromax	80 (ml/hr)	1300	0.205 (kg/h)	0.205 (kg/h)	0.158	0.158
Renewable energy based lighting systems						
Biogas mantle lighting systems	0.125 m³/hr	600	0.246[18] (kg/h)	Nil	0.409	Nil
Biogas based electricity	1m³ biogas and 80 ml diesel/kWh	81900 [19]	2.185 [20] (kg/kWh)	0.00537 (kg/kWh)	0.027	0.00007e
Biomass gasifier	1.4 kg wood/kWh	81900	2.684 [21] (kg/kWh)	0.00537 (kg/kWh)	0.033	0.00007
Grid electricity based lighting systems						
Grid electricity	--	81900	0.82 [22] kg/kWh	0.82 kg/kWh	0.010	0.010

---

[16] *Gross CO$_2$ emission considers all CO$_2$ emitted in combustion. Net CO$_2$ emission takes into account whether the fuel is renewable or not. Net CO$_2$ emission from biogas based electricity and biomass gasifier is due to the oxidation of the lubricant oil only, as otherwise these systems are carbon neutral. Here we assume that the biomass fuel input to the gasifier is renewable, i.e. does not lead to deforestation.*

[17] *One kg of kerosene contains 0.8669 kg of carbon; we considered this fraction of carbon oxidized fully during combustion. Now the CO$_2$ emission (kg/hour) from a kerosene based lamp will be:*

$$=SFC \left(\frac{litre}{hour}\right) \times Density \left(\frac{kg}{litre}\right) \times Carbon\ content\ \times \left(\frac{44}{12}\right)$$

Here we consider the density of kerosene to be 0.806 kg/litre.

[18] *We have considered that biogas contains 60% methane and 40% carbon dioxide. Methane is fully oxidized to form CO$_2$. Now the CO$_2$ emission (kg/hr) from a biogas based lighting system will be:*

$$= \frac{SFC \left(\frac{m^3}{hour}\right) \times \left(\frac{CH_4(\%)}{100} + \frac{CO_2(\%)}{100}\right) \times 44}{22.4}$$

[19] *In case of biogas based electricity and biomass gasifier based systems, we considered the fuel consumption per kWh. So the total illumination in each kW will be*

$$= \frac{1000\ (watt)}{Each\ lamp\ power\ rating\ (watt)} \times Each\ lamp\ lumen\ output\ (lumen)$$

[20] *In case of biogas electricity based lighting systems, we considered 2 ml lubricating oil is also oxidized during engine operation. We calculate the CO$_2$ emission from biogas as biogas mantle lighting systems and the CO$_2$ emission from diesel and lubricant oil as kerosene based lamps. We consider the density and carbon content of diesel and lubricant oil to be the same. The density is 0.850 kg/litre and carbon content is 0.8623. Gross CO$_2$ emission considers all CO$_2$ emitted in combustion. Net CO$_2$ emission takes into account whether the fuel is renewable or not. Net CO$_2$ emission from biogas based electricity and biomass gasifier is due to the oxidation of the lubricant oil only, as otherwise these systems are carbon neutral. Here we assume that the biomass fuel input to the gasifier is renewable, i.e. does not lead to deforestation.*

[21] *In case of biomass gasifier based lighting systems we also considered 2 ml lubricating oil is oxidized during engine operation. The wood is represented by $CH_{1.4}O_{0.6}$ and the CO$_2$ emission from one kg of wood is 1.9130 kg.*

[22] *The grid emission factor (combined margin for 2007-2008) in India is 0.82 tCO$_2$/ MWh (CEA, 2008).*

The CO_2 emissions have been found to be 0.73 and 0.10 g/lumen-h for kerosene wick lamp and Noorie respectively (while net emissions are 0.055 and 0.128 kg CO_2/h). There are 77 million rural households in India that use kerosene as fuel for lighting (Census, 2011). Assuming that each of these households uses two kerosene wick lamps for an average of 5h/day, the annual CO_2 emissions are estimated to be 15.46 million tons (MT). Electricity generation in India is dominated by coal based power plants, and therefore the emission factor is relatively high. India's emission factor for electricity generation was 0.82 tCO_2/MWh for 2007-2008 (CEA, 2009). The net CO_2 emission is 0.010 g/lumen-h from grid based electricity for a 11W CFL lamp. If, all the 77 million households using kerosene switch to using two 11W CFL lamps for 5 h/day, the annual emissions would be 2.54 MT CO_2.

The CO_2 emissions from renewable energy based lighting systems have also been estimated. In spite of an appreciable gross CO_2 emission from the biomass gasifier and biogas based systems, they are carbon neutral. Gross and net CO_2 emissions are estimated for all the different systems. The gross CO_2 emission in the case of biogas mantle lighting is 0.25 kg/h and for biogas based electricity it is 2.19 kg/kWh. The gross emission per lumen-hour in case of biogas mantle lighting systems is 0.409 g/lumen-h and for biogas based electricity and for biomass gasifier it is 0.027 g/lumen-h. However, since biogas is a renewable fuel, the net CO_2 emission in case of biogas mantle lighting systems is nil and biomass gasifier and biogas electricity systems it is 0.0054 kg/kWh. The small net emissions arise from the oxidation of the lubricating oil used in the engine. Thus, if all the 77 million households are using two 11W CFL lamps for 5h/day supplied by biomass gasifier or biogas based electricity, it would releases a net emission of 0.0166 MT CO_2/yr, for biomass gasifier or biogas based electricity. On the other hand, CO_2 emissions from solar photovoltaic based lighting systems are zero.

There is a great potential for CO_2 emission mitigation by switching over from inefficient kerosene wick lamps either to grid electricity or renewable energy based

lighting systems. Renewable energy based lighting systems could be of interest as they directly replace 15.29 MT of CO_2 emissions (the difference of emissions from kerosene based lamps and biomass or biogas electricity based systems) and 12.93 million tons of CO_2 emissions (the difference of emissions from kerosene based wick lamps and grid electricity based systems) from kerosene based lighting systems in 77 million households.

A.5 Summary

Access to electricity is a vital component for the socio-economic development, improvement in the livelihood of the rural villages in India. The other aspect of the concern is that even in the electrified households, people continue to depend mainly on kerosene as a backup for lighting due to poor quality and regular electric load-shedding. Decentralized renewable energy base system is an economical and convenient option towards access to electricity for rural village where grid extension is not feasible due to low load factor and long transmission and distribution lines. Electricity based lighting (from renewable such as solar photovoltaic, biogas and biomass gasifier or conventional grid based) has potential for providing good quality lighting compared to flame based lighting. Switching over from traditional kerosene based lighting systems to renewable energy systems based lighting will lead to significant energy conservation; avoidance of using a fossil fuel such as kerosene; and substantial reduction of CO_2 emissions while greatly improves the quality of life. This study reveals that decentralized power generation by biomass gasification and photovoltaic systems can be cost competitive, using life cycle cost analysis, for remote villages having low load demand. This study concludes that biomass gasification based systems are much more competitive than photovoltaic based systems or even grid extension for far away villages. The study provides a mathematical relation between renewable energy system capacity and economical distance from the existing grid point. This mathematical relation will be useful to predict the capacity of renewable energy systems and corresponding optimal economical distances.

References

Abatzoglou, N., Barker, N., Hasler, P., Konef, H. (2000). The development of a draft protocol for the sampling and analysis of particulate and organic contaminants in the gas from small biomass gasifiers. Biomass Bioenergy. 18 (1): 5-17.

Ahmed, I. I., Gupta, A. K. (2011). Particle size, porosity and temperature effects on char conversion. Applied Energy. 88 (12): 4667-4677.

Anis, S., Zainal, Z. A. (2011). Tar reduction in biomass producer gas via mechanical, catalytic and thermal methods: A review. Renewable and Sustainable Energy Reviews. 15(5): 2355-2377.

Antonopoulos, I. S., Karagiannidis, A., Gkouletsos, A., Perkoulidis, G. (2012). Modelling of a downdraft gasifier fed by agricultural residues. Waste Management. 32(4): 710-718.

Babu, B. V., Chaurasia, A. S. (2003). Modeling for pyrolysis of solid particle: kinetics and heat transfer effects. Energy Conversion and Management. 44(14): 2251–2275.

Babu, B. V., Chaurasia, A. S. (2004a). Heat transfer and kinetics in the pyrolysis of shrinking biomass particle. Chemical Engineering Science. 59(10): 1999-2012.

Babu, B. V., Chaurasia, A. S. (2004b). Pyrolysis of biomass: improved models for simultaneous kinetics and transport of heat, mass and momentum. Energy Conversion and Management. 45(9-10): 1297-1327.

Barman, N. S., Ghosh, S., De, S. (2012). Gasification of biomass in a fixed bed downdraft gasifier - A realistic model including tar. Bioresource Technology. 107: 505-511.

Baruah, D., Baruah, D. C. (2014). Modeling of biomass gasification: A review. Renewable and Sustainable Energy Reviews. 39: 806-815.

Blackwood, J. D., McGrory, F. (1958). The carbon steam reaction at high pressure. Australian Journal of Chemistry. 11(1): 16-23.

Bryden, K. M., Hagge, M. J. (2003). Modeling the combined impact of moisture and char shrinkage on the pyrolysis of a biomass particle. Fuel. 82(13): 1633-1644.

Buragohain, B., Mahanta, P., Moholkar, V. S. (2010). Thermodynamic optimization of biomass gasification for decentralized power generation and Fischer–Tropsch synthesis. Energy. 35 (6): 2557-2579.

CEA, 2008. Central Electricity Authority, Sewa Bhawan, RK Puram, New Delhi 110 066, Accessed on 01.06.2008.

Census Report 2011. Registrar General & Census Commissioner, Government of India, 2A Mansingh Road, New Delhi 110 011, India. Accessed on 01.06.2015

CGPL 2015, (Combustion, Gasification and Propulsion Laboratory), Indian Institute of Science, Bangalore, http://cgpl.iisc.ernet.in. Accessed on 01.06.2015

Dasappa, S., Paul, P. J., Mukunda, H. S., Shrinivasa, U. (1994). The gasification of wood-char spheres in CO_2-N_2 mixtures: Analysis and experiments. Chemical Engineering Science. 49(2): 223-232.

Dasappa, S., Paul, P. J., Mukunda, H. S., Shrinivasa, U. (1998). Wood-char gasification: Experiments and analysis on single particles and packed beds. Twenty-seventh Symposium (International) on Combustion. 1: 1335-1342.

Dasappa, S. (1999). Experimental and modeling studies on the gasification of wood-char. PhD Thesis, Indian Institute of Science, India.

Dasappa, S., Paul, P. J. (2001). Gasification of char particles in packed beds: analysis and results. International Journal of Energy Research. 25(12): 1053-1072.

Dasappa, S., Paul, P. J., Mukunda, H. S., Rajan, N. K. S., Sridhar, G., Sridhar, H. V. (2004). Biomass gasification technology – a route to meet energy demands. Current Science. 87(7): 908-915.

Devi, L., Ptasinski, K. J., Janssen, F. J. J. G. (2003). A review of the primary measures for tar elimination in biomass gasification processes. Biomass and Bioenergy. 24(2): 125-140.

Di Blasi, C. (2004). Modeling wood gasification in a counter current fixed-bed reactor. AIChE Journal. 50 (9): 2306-2319.

Di Blasi, C. (2009). Combustion and gasification rates of lignocellulosic chars. Progress in Energy and Combustion Science. 35(2): 121-140.

Dogru, M., Howarth, C. R., Akay, G., Keskinler, B., Malik, A. A. (2002). Gasification of hazelnut shells in a downdraft gasifier. Energy. 27(5): 415–427.

Dosanjh, S. S., Pagni, P. J., Fernandez-Pello, C. A. (1987). Forced cocurrent smoldering combustion. Combustion and Flame. 68(2): 131-142.

Enrico, G., Baldi, G. (2011). Analysis and modelling of wood pyrolysis. Chemical Engineering Science. 66(4): 650-660.

Fatehi, M., Kaviany, M. (1994). Adiabatic reverse combustion in a packed bed. Combustion and Flame. 99(1): 1-17.

Fatehi, H., Bai, X. S. (2014). A Comprehensive mathematical model for biomass combustion. Combustion Science and Technology. 186: 574–593.

Feng, Y., Xiao, B., Goerner, K., Naidu, R. (2011). Influence of particle size and temperature on gasification performance. Advanced Materials Research. 281: 78–83.

Friberg, R., Blasiak, W. (2002). Measurements of mass flux and stoichiometry of conversion gas from three different wood fuels as function of volume flux of primary air in packed-bed combustion. Biomass and Bioenergy. 23 (3): 189-208.

Gasification, 2015, All Power Labs. *http://www.allpowerlabs.com/info/gasification-basics/ gasification-explained,* Accessed on 01.06.2015

Ghassemi, H., Shahsavan-Markadeh, R. (2014). Effects of various operational parameters on biomass gasification process: a modified equilibrium model. Energy Conversion and Management. 79:18-24.

Gnanendra, P. M., Ramesha, D. K., Dasappa, S. (2012). Preliminary investigation on the use of biogas sludge for gasification. International Journal of Sustainable Energy. 31(4): 251-267.

Goldman, J., Xieu, D., Oko, A., Milne, R., Essenhigh, R. H. (1985). A comparison of prediction and experiment in the gasification of anthracite in air and oxygen-enriched steam mixtures. Symposium (International) on Combustion. 20(1): 1365-1372.

Gort, R. (1995). On the propagation of a reaction front in a packed bed, thermal conversion of municipal solid waste and biomass. PhD Thesis, University of Twente, Netherlands.

Gort, R., Brouwers, J. J. H. (2001). Theoretical analysis of the propagation of a reaction front in a packed bed. Combustion and Flame. 124(1–2): 1-13.

Green, D. W., Perry, R. H. (2007). Perry's Chemical Engineers' Handbook, Eighth Edition, McGraw-Hill Education, New York.

Groeneveld, M. J. (1980). The co-current moving bed gasifier. PhD Thesis, Twente University of Technology, Netherlands.

Han, J., Kim, H. (2008). The reduction and control technology of tar during biomass gasification/pyrolysis. Renewable and Sustainable Energy Reviews. 12(2): 397-416.

Hasler, P., Nussbaumer, T. (1999). Gas cleaning for IC engine applications from fixed bed biomass gasification. Biomass and Bioenergy. 16(6): 385-395.

Hasler, P., Nussbaumer, T. (2000). Sampling and analysis of particles and tars from biomass gasifiers. Biomass and Bioenergy. 18(1): 61-66.

Hernández, J. J., Aranda-Almansa, G., Bula, A. (2010). Gasification of biomass wastes in an entrained flow gasifier: Effect of the particle size and the residence time. Fuel Processing Technology. 91 (6): 681–692.

Hernández, J. J., Ballesteros, R., Aranda, G. (2013). Characterization of tars from biomass gasification: Effect of operating conditions. Energy. 50: 333-342.

Horttanainen, M. V. A., Saastamoinen, J. J., Sarkomaa, P. J. (2000). Ignition front propagation in packed beds of wood particles. IFRF Combustion Journal Article Number 200003.

Horttanainen, M., Saastamoinen, J., Sarkomaa, P. (2002). Operational limits of ignition front propagation against airflow in packed beds of different wood fuels. Energy & Fuels. 16(3): 676-686.

Howard, J. B. (1967). Combustion of carbon with oxygen. MIT Technical Report.

Janajreh, I., Shrah, A. M. (2013). Numerical and experimental investigation of downdraft gasification of wood chips. Energy Conversion and Management. 65:783-792.

Kaupp, A., Goss, J. R. (1984). Small scale gas producer engine systems. GATE, Germany.

Kinoshita, C. M., Wang, Y., Zhou, J. (1994). Tar formation under different biomass gasification conditions. Journal of Analytical and Applied Pyrolysis. 29(2): 169-181.

Klose, W., Wolki, M. (2005). On the intrinsic reaction rate of biomass char gasification with carbon dioxide and steam. Fuel. 84 (7-8): 885–892.

Knoef, H. A. M. (Ed.) (2012). Handbook Biomass gasification. Second Edition, Biomass Technology Group (BTG), Netherlands.

Koufopanos, C. A., Lucchesi, A., Maschio, G. (1989). Kinetic modelling of the pyrolysis of biomass and biomass components. Canadian Journal of Chemical Engineering. 67(1): 75-84.

Kucuk, M. M., Demirbas, A. (1997). Biomass conversion processes. Energy Conversion and Management. 38(2): 151-165.

Lu, H., Robert, W., Peirce, G., Ripa, B., Baxter, L. L. (2008). Comprehensive study of biomass particle combustion. Energy & Fuels. 22: 2826 - 2839.

Luo, S., Xiao, B., Hu, Z., Liu, S., Guan, Y., Cai, L. (2010). Influence of particle size on pyrolysis and gasification performance of municipal solid waste in a fixed bed reactor. Bioresource Technology. 101(16): 6517-6520.

Mahapatra, S., Chanakya, H. N., Dasappa, S. (2009). Evaluation of various energy devices for domestic lighting in India: technology, economics and CO_2 emissions. Energy for Sustainable Development. 13 (4): 271-279.

Mahapatra, S., Dasappa, S. (2012). Rural electrification: optimising the choice between decentralised renewable energy sources and grid extension. Energy for Sustainable Development. 16 (2): 146-154.

Mahapatra, S., Dasappa, S. (2014a). Experiments and analysis of propagation front under gasification regimes in a packed bed. Fuel Processing Technology. 121: 83-90.

Mahapatra, S., Dasappa, S. (2014b). Influence of surface area to volume ratio of fuel particles on gasification process in a fixed bed. Energy for Sustainable Development. 19: 122-129.

Mahapatra, S., Kumar, S., Dasappa, S. (2016). Gasification of wood particles in a co-current packed bed: experiments and model analysis. Fuel Processing Technology. 145: 76-89.

Mahmoudi, A. H., Markovic, M., Peters, B., Brem, G. (2015). An experimental and numerical study of wood combustion in a fixed bed using Euler-Lagrange approach (XDEM). Fuel. 150: 573-582.

Mason, P. E., Darvell, L. I., Jones, J. M., Pourkashanian, M., Williams, A. (2015). Single particle flame-combustion studies on solid biomass fuels. Fuel. 151: 21-30.

Melgar, A., Perez, J. F., Laget, H., Horillo, A. (2007). Thermochemical equilibrium modeling of a gasifying process. Energy Conversion and Management. 48(1): 59-67.

Mendiburu, A. Z., Carvalho, J. A., Coronado, C. J. R. (2014). Thermo chemical equilibrium modeling of biomass downdraft gasifier: Stoichiometric models. Energy. 66: 189-201.

Momeni, M., Yin, C., Kær, S. K., Hvid, S. L. (2013a). Comprehensive study of ignition and combustion of single wooden particle. Energy & Fuels. 27: 1061-1072.

Momeni, M., Yin, C., Kær, S. K., Hansen, T. B., Jensen, P. A., Glarborg, P. (2013b). Experimental study on effects of particle shape and operating conditions on combustion characteristics of single biomass particle. Energy & Fuels. 27: 507-514.

Mukunda, H. S., Paul, P. J., Shrinivasa, U., Rajan, N. K. S. (1984). Combustion of wooden spheres- Experiments and model analysis. Symposium (International) on Combustion. 1619-1628.

Mukunda, H. S., Paul. P. J., Dasappa, S., Shrinivasa, U., Sharan, H., Buehler, R., Hasler, P., Kaufmann, H. (1994). Results of an Indo-Swiss programme for qualification and testing of a 300 kW IISc-Dasag gasifier. Energy for Sustainable Development. 1(4), 46-49.

Mukunda, H. S. (2011). Understanding clean energy and fuels from biomass. Wiley India, New Delhi.

Murty, K. A. (1972). Thermal decomposition kinetics of wood pyrolysis. Combustion and Flame. 18, 75-83.

Namioka, T., Son, Y., Sato, M., Yoshikawa, K. (2009). Practical method of gravimetric tar analysis that takes into account a thermal reaction scheme. Energy & Fuels. 23(12): 6156-6162.

Nunes, S. M., Paterson, N., Herod, A. A., Dugwell, D. R., Kandiyoti, R. (2008). Tar formation and destruction in a fixed bed reactor simulating downdraft gasification: Optimization of conditions. Energy & Fuels. 22(3): 1955-1964.

Ohlemiller, T. J., Bellan, J., Rogers, F. (1979). A model of smoldering combustion applied to flexible polyurethane foams. Combustion and Flame. 36(1): 197-215.

Park, W. C., Atreya, A., Baum, H. R. (2010). Experimental and theoretical investigation of heat and mass transfer processes during wood pyrolysis. Combustion and Flame. 157: 481-494.

Patra, T. K., Sheth, P. N. (2015). Biomass gasification models for downdraft gasifier: A state of the art review. Renewable and Sustainable Energy Reviews. 50: 583-593.

Pattanotai, T., Watanabe, H., Okazaki, K. (2015). Effects of particle aspect ratio on pyrolysis and gasification of anisotropic wood cylinder. Fuel. 150:162-168.

Pérez, J. F., Melgar, A., Benjumea, P. N. (2012). Effect of operating and design parameters on the gasification /combustion process of waste biomass in fixed bed downdraft reactors: An experimental study. Fuel. 96: 487-496.

Phuphuakrat, T., Nipattummakul, N., Namioka, T., Kerdsuwan, S., Yoshikawa, K. (2010). Characterization of tar content in the syngas produced in a downdraft type fixed bed gasification system from dried sewage sludge. Fuel. 89(9): 2278-2284.

Plis, P., Wilk, R. K. (2011). Theoretical and experimental investigation of biomass gasification process in a fixed bed gasifier. Energy. 36(6): 3838-3845.

Porteiro, J., Patino, D., Collazo, J., Granada, E., Moran, J., Miguez, J. L. (2010). Experimental analysis of the ignition front propagation of several biomass fuels in a fixed-bed combustor. Fuel. 89 (1): 26-35.

Puig-Arnavat, M., Bruno, J. C., Coronas, A. (2010). Review and analysis of biomass gasification models. Renewable and Sustainable Energy Reviews. 14(9): 2841–2851.

Puig-Arnavat, M., Brun, J. C., Coronas, A. (2012). Modified thermodynamic equilibrium model for biomass gasification: A study of the influence of operating conditions. Energy & Fuels. 26(2): 1385-1394.

Ranzi, E., Corbetta, M., Manenti, F., Pierucci, S. (2014). Kinetic modeling of the thermal degradation and combustion of biomass. Chemical Engineering Science. 110:2-12.

REN 21, Renewable 2014, Global Status Report. http://www.ren21.net/status-of-renewables/global-status-report/, Accessed on 15.01.2014.

Reed, T. B., Markson, M. (1982). Biomass gasification reaction velocities, in : R.P. Overend, T. A. Milne, L. K. Mundge (Eds.), Fundamentals of Thermochemical Biomass Conversion, Elsevier Applied Science Publishers, England, pp. 951-965.

Reed, T. B. Graboski, M. S. Levie, B. (1988). Fundamentals, development and scale up of the air-oxygen stratified downdraft gasifier. The Biomass Energy Foundation Press.

Riaza, J., Khatami, R., Levendis, Y. A., Alvarez, L., Gil, M. V., Pevida, C., Rubiera, F., Pis, J. J. (2014). Combustion of single biomass particles in air and in oxy-fuel conditions. Biomass and Bioenergy. 64: 162-174.

Rönnbäck, M., Axell, M., Gustavsson, L., Thunman, H., Leckner, B. (2001). Combustion processes in a biomass fuel bed - Experimental results. Progress in Thermochemical biomass conversion. 743-757.

Ryu, C., Yang, Y. B., Khor, A., Yates, N. E., Sharifi, V. N., Swithenbank, J. (2006). Effect of fuel properties on biomass combustion: Part I experiments - fuel type, equivalence ratio and particle size. Fuel. 85 (7-8): 1039-1046.

Saastamoinen, J. J., Taipale, R., Horttanainen, M. V. A., Sarkomaa, P. J. (2000). Propagation of the ignition front in beds of wood particles. Combustion and Flame. 123 (1-2): 214-226.

Sandeep, K., Dasappa, S. (2015). Modified model for biomass gasification. CGPL Technical Report, Indian Institute of Science, Bangalore.

SERI, (1979). Generator Gas - The Swedish experience from 1938-1945 (translation). Solar Energy Research Institute, Colorado, NTIS/S 33-140.

Sharma, M., Attanoor, S., Dasappa, S. (2015). Investigation into co-gasifying Indian coal and biomass in a downdraft gasifier-Experiments and analysis. Fuel Processing Technology. 138: 435-444.

Shin, D., Choi, S. (2000). The combustion of simulated waste particles in a fixed bed. Combustion and Flame. 121(1-2): 167-180.

Simmons, W. W., Ragland, K. W. (1986). Burning rate of millimeter sized wood particles in a furnace. Combustion Science and Technology. 46(1): 1-15.

Tinaut, F. V., Melgar, A., Pérez, J. F., Horrillo, A. (2008). Effect of biomass particle size and air superficial velocity on the gasification process in a downdraft fixed bed gasifier: An experimental and modeling study. Fuel Processing Technology. 89 (11): 1076-1089.

Thunman, H., Leckner, B. (2001). Ignition and propagation of a reaction front in cross-current bed combustion of wet biofuels. Fuel. 80(4): 473-481.

Thunman, H., Leckner, B. (2003). Co-current and counter-current fixed bed combustion of biofuel- a comparison. Fuel. 82 (3): 275-283.

Thunman, H., Leckner, B. (2005). Influence of size and density of fuel on combustion in a packed bed. Proc. of the Combustion Institute. 30(II): 2939-2946.

Wan, K., Wang, Z., He, Y., Xia, J., Zhou, Z., Zhou, J., Cen, K. (2015). Experimental and modeling study of pyrolysis of coal, biomass and blended coal–biomass particles. Fuel. 139: 356-364.

Wang, Y., Kinoshita, M. C. (1993). Kinetic model of biomass gasification. Solar Energy. 51(1):19-25.

Ueki, Y., Torigoe, T., Ono, H., Yoshiie, R., Kihedu, J. H., Naruse, I. (2011). Gasification characteristics of woody biomass in the packed bed reactor. Proceedings of the Combustion Institute. 33(2): 1795-1800.

World Energy Outlook 2014. (2014). International Energy Agency (IEA). Paris, France.

Varunkumar, S., Rajan, N. K. S., Mukunda, H. S. (2011). Single particle and packed bed combustion in modern gasifier stoves - density effects. Combustion Science and Technology. 183(11): 1147-1163.

Yang, Y. B., Sharifi, V. N., Swithenbank, J. (2004). Effect of air flow rate and fuel moisture on the burning behaviours of biomass and simulated municipal solid wastes in packed beds. Fuel. 83 (11-12): 1553-1562.

Yang, Y. B., Ryu, C., Khor, A., Sharifi, V. N., Swithenbank, J. (2005). Fuel size effect on pinewood combustion in a packed bed. Fuel. 84(16): 2026-2038.

Yang, Y. B., Sharifi, V. N., Swithenbank, J. (2006). Substoichiometric conversion of biomass and solid wastes to energy in packed beds. AIChE Journal. 52(2): 809-817.

Yang, Y. B., Sharifi, V. N., Swithenbank, J., Ma, L., Darvell, L. I., Jones, J. M., Pourkashanian, M., Williams, A. (2008). Combustion of a single particle of biomass. Energy & Fuels. 22(1): 306-316.

Yin, R., Liu, R., Wu, J., Wu, X., Sun, C., Wu, C. (2012). Influence of particle size on performance of a pilot-scale fixed-bed gasification system. Bioresource Technology. 119: 15-21.

Yu, H., Zhang, Z., Li, Z., Chen, D. (2014). Characteristics of tar formation during cellulose, hemicellulose and lignin gasification. Fuel. 118: 250-256.